DEPARTMENT OF MATHEMATICS

THE TAYLOR-GALERKIN METHOD FOR THE SHALLOW WATER EQUATIONS ON THE SPHERE

by

A. Priestley

Numerical Analysis Report 9/91

UNIVERSITY OF READING

The Taylor-Galerkin Method for the Shallow Water Equations on the Sphere*

A. Priestley

Institute of Computational Fluid Dynamics,

Dept. of Mathematics,

University of Reading,

P.O. Box 220,

Reading,

U.K..

September 12, 1991

*The work reported here forms part of the research programme of the Reading/Oxford Institute for Computational Fluid Dynamics and was funded by the University of Reading's Research Endowment Fund.

List of Tables

List of Figures

Contents

.0 Abstract

In this paper we will attempt to solve the shallow water equations on the sphere using a method that has already proved its worth in other areas of Computational Fluid Dynamics (CFD), but has yet to make an impact in enviromental or meteorological type flows. This is the Taylor-Galerkin finite element method. This method offers the possibility of great flexibility in mesh refinement associated with the finite element method in general, together with the accuracy of the Lax-Wendroff method (although with fewer of the well-known problems of that method). Here the method will be formulated in a form suitable for solving advection problems on the sphere and its potential will be explored on two test problems. The problems will be solved in Cartesian geometry to avoid the usual singularities associated with the poles in the spherical polar transformation.

.1 Introduction

Although variational principles do exist for fluid flow problems, Sewell [32], the Bubnov-Galerkin, more usually just called the Galerkin, method has circumvented their use and freed finite element practitioners to tackle very wide classes of problems. The Galerkin method, though, is not terribly well-suited to the hyperbolic problems associated with fluid flow , see Strang & Fix [36], particularly when large gradients are present in the solution. This is partly because the Galerkin method is associated with best L_2 fits, which do not give good approximations to jumps, and partly because the Galerkin method conserves energy, for some hyperbolic systems, which is not true for all shocked flows and hence the method can never converge in these cases. There have been many attempts to remedy this situation. The Petrov-Galerkin method, see Morton & Parrott [25] for example, is a generalisation of the Galerkin method and has allowed upwind finite element schemes to be created with hyperbolic problems specifically in mind. It is not the intention of this paper to give an overview of this field but certain large classes of these schemes can be easily identified.

There are also the moving mesh methods which use a variety of criteria to move the nodes of the mesh to give a better solution, see Hawken, Gottlieb & Hansen [17] for a review of methods using both finite elements and finite differences. Included in this framework are the Lagrangian methods, perhaps the best known of the moving node methods, see Donea et al [12] for example. Other schemes, with a fixed mesh but still using the Lagrangian principles can be found in Morton, Priestley & Süli [26]. Mirroring the development of the

popular TVD finite difference schemes based upon characteristic decompostions of hyperbolic systems there is also the Euler Characteristic Galerkin method, see Childs & Morton [4]. Other successful algorithms are the streamwise-diffusion methods,see Johnson [20], least-squares methods, see Bruneau et al [3], and discontinuous Galerkin methods, see Cockburn et al [7, 6, 5]. Most of these methods owe their success, at least in part, to the introduction of some upwinding. As with finite differences the other option is to use a central scheme. The scheme we will be using here is of that ilk.

Finite differences and spectral methods are by far the more common numerical methods used in meteorology. Finite elements have been used on occasions though. From Wang et al [38] where a Galerkin method was used on a simplified problem to Cullen et al [9, 10] where the Galerkin method was used on problems of increasing realism. Staniforth & Mitchell [34] demonstrated that the finite element method could be written in a semi-implicit form to give a much more efficient time integration. The paper by Staniforth [33] gives a review of finite elements in meteorology. More recently there have been papers by Navon [27] and Steppeler et al [35] on the Numerov-Galerkin method. These last three papers all give many references in this field.

In the next section the Taylor-Galerkin method will be described and adapted for the terms that might be expected to be encountered in the context of this paper. In Section 3 two test problems from the meteorological literature will be described, the Taylor-Galerkin method will be described in some

detail for a typical momentum equation occuring in the shallow water equations on the sphere. Results for this method will be given. Finally, in Section 4, we will summarise the results and discuss the potential of the method.

.2 The Taylor-Galerkin Method

The Taylor-Galerkin method introduced by Donea [11] and further expounded by Donea et al [13, 14, 15], for example, has already proved to be a very powerful method. For example, see Löhner et al [21, 22, 23] and Peraire et al [28] for its application to high speed gas flows.

Basically the Taylor-Galerkin method is the finite element version of the Lax-Wendroff scheme. The Lax-Wendroff method is still popular despite its well-known misbehaviour at discontinuities. For smooth flows Lax-Wendroff is second order accurate in both space and time whilst at shocks artificial viscosity can help to give a reasonable solution. However, the finite element approach improves the phase accuracy, Donea et al [14], and although this does not eliminate the problems it does substantially reduce them. Together with mesh adaptivity to improve the resolution in regions of large gradients oscillations can be eliminated from all but the hardest cases where some artificial viscosity will still be needed, Morgan et al [24].

The shallow water equations on the sphere cannot, strictly speaking, be written in conservation form because of the presence of source terms.

However, depending on the variables used, some or many terms in the shallow water equations can be written in conservation form. As a starting point to deriving the method it is therefore useful to consider the single non-linear conservation law in one dimension,

$$u_t + F(u)_x = 0. \tag{.1}$$

Momentarily leaving aside the spatial discretization, a Taylor series in time for u is performed with of time-step of Δt. Assuming that we know the solution and its derivatives at the time-level n we can then write down the solution at the new time-level as

$$u^{n+1} = u^n + \Delta t u_t^n + \frac{1}{2}(\Delta t)^2 u_{tt}^n + \frac{1}{6}(\Delta t)^3 u_{ttt}^n + \ldots \quad . \tag{.2}$$

Into this semi-discretised equation we can now substitute for the temporal derivatives from the original differential equation (.1), i.e.,

$$\begin{aligned} u_t^n &= -F(u^n)_x \\ u_{tt}^n &= -F(u^n)_{xt} = -(a(u^n)u_t^n)_x = [a(u^n)F(u^n)_x]_x \end{aligned}$$

to second order, where $a(u) = \frac{\partial F(u)}{\partial u}$. More terms could be used if desired. Upon substitution into (.2) this then leads to the semi-discretised scheme

$$\frac{(u^{n+1} - u^n)}{\Delta t} = -F(u^n)_x + \frac{\Delta t}{2}(a(u^n)F(u^n)_x)_x. \tag{.3}$$

From this point we can apply whatever spatial approximation we like to the right-hand side of (.3). If we apply central differencing then we obtain the Lax-Wendroff method. Here, though, we will expand u in terms of some finite element basis functions and then take the weak form of equation (.3). That is we write

$$u^n(x) = \sum_{i=1}^{nodes} U_i^n \psi_i(x) \tag{.4}$$

where $\psi_i(x)$ is the finite element basis function and U_i^n is the nodal value. Throughout the rest of this paper we will assume $\psi_i(x)$ to be the usual piecewise linear 'hat' function, that is $\psi_i(x)$ is the piecewise linear function that satisfies the equation

$$\psi_i(x_j) = \delta_{i,j}, \tag{.5}$$

and is depicted in figure (1) for the two-dimensional case. Although these are the only elements that will be considered here there is no reason why higher order elements could not be used. The notation $\psi_e(x)$ will be used to represent the piecewise constant functions that take a value of 1 on element e and 0 everywhere else.

Substituting for $u(x)$, from (.4), into (.3) and then multiplying through by $\psi_j(x)$ and integrating over the entire domain we have the second order accurate Taylor-Galerkin scheme in one-dimension

$$\int_\Omega (U^{n+1} - U^n)\psi_j(x)d\Omega = -\Delta t \int_\Omega F(U^n)_x \psi_j(x) d\Omega$$

$$-\frac{\Delta t^2}{2}\left(\int_\Omega (\psi_j(x))_x a(U^n)F(U^n)_x d\Omega - \int_\Gamma \psi_j(x)a(U^n)F(U^n)d\Gamma\right) \quad \forall j.$$

Here we have denoted the solution domain by Ω and its boundary by Γ. The extension to multiple dimensions presents no difficulties.

The extension to a system is now quite straightforward. Letting $A(\underline{U}^n)$ denote the approximation to the Jacobian of $\underline{F}$, i.e.,

$$A = \frac{\partial \underline{F}}{\partial \underline{u}},$$

we can then write down the Taylor-Galerkin method for the system of conservation laws in multiple dimensions

$$\underline{u}_t + \frac{\partial \underline{F}_k}{\partial x_k} = 0,$$

where the usual notation has been used, as

$$\int_\Omega (\underline{U}^{n+1} - \underline{U}^n)\psi_j(\underline{x})d\Omega = -\Delta t \int_\Omega \frac{\partial \underline{F}_k^n}{\partial x_k}\psi_j(\underline{x})d\Omega$$

$$-\frac{\Delta t^2}{2}\int_\Omega A(\underline{U}^n)\frac{\partial \underline{F}_k^n}{\partial x_k}.\nabla\psi_j(\underline{x})d\Omega + \frac{\Delta t^2}{2}\int_\Gamma \underline{n}.A(\underline{U}^n)\frac{\partial \underline{F}_k^n}{\partial x_k}\psi_j(\underline{x})d\Gamma \quad \forall j, \qquad (.6)$$

$\underline{n}$ being the unit outward normal of the boundary Γ.

Just as the one-step Lax-Wendroff method is rarely used for systems because of the expense involved in calculating the matrix A and of then multiplying it by the vector $\frac{\partial \underline{F}_k}{\partial x_k}$, a two-stage version of the Taylor-Galerkin method

has been developed. This entirely mirrors the derivation of the two-stage Lax-Wendroff method, see Richtmyer & Morton [30]. In the finite difference scheme there are temporary values $u_{i+\frac{1}{2}}^{n+\frac{1}{2}}$ centred halfway in space and time. In the finite element version these quantities are still centred in space and time which means we need to introduce the piecewise constant representation

$$U^{n+\frac{1}{2}}(x) = \sum_{e=1}^{elements} U_e^{n+\frac{1}{2}} \psi_e(x),$$

where the $\psi_e(x)$ are the piecewise constant basis functions mentioned previously. This then leads to the two-stage Taylor-Galerkin scheme

$$\int_\Omega \underline{U}^{n+\frac{1}{2}} \psi_e(\underline{x}) d\Omega = \int_\Omega \underline{U}^n \psi_e(\underline{x}) d\Omega - \frac{\Delta t}{2} \int_\Omega \frac{\partial \underline{F}_k^n}{\partial x_k} \psi_e(\underline{x}) d\Omega \quad \forall e \tag{.7}$$

$$\int_\Omega (\underline{U}^{n+1} - \underline{U}^n) \psi_j(\underline{x}) d\Omega = \Delta t \int_\Omega \underline{F}^{n+\frac{1}{2}} \frac{\partial \psi_j(\underline{x})}{\partial x_k} d\Omega -$$

$$\Delta t \int_\Gamma \underline{F}^n \psi_j(\underline{x}) d\Gamma - \Delta t \int_\Gamma (\underline{F}_n^{n+\frac{1}{2}} - \overline{F}_n^n) \psi_j(\underline{x}) d\Gamma \quad \forall j, \tag{.8}$$

where $\underline{F}_n$ denotes the outward normal flux and the overbar represents an element averaged quantity.

This could be considered the classical derivation of the two-stage Taylor-Galerkin method. For use on the sphere we can specialize the scheme. Firstly, there are no boundary terms for advection problems on the sphere and so eq. (.8) immediately simplifies. We note that in three-dimensional models of the atmosphere this would not be the case. In this application area, unlike gas

dynamics for example, all the terms in the differential equation will not be in conservation form. Nor may we wish to write the terms in conservation form. Terms not involving derivatives, the Coriolis terms for example, are easily integrated. To see how to treat the other derivative terms consider the advection equation

$$u_t + \underline{a}.\underline{\nabla}u.$$

The velocity field, $\underline{a}$, will be a function of position, $\underline{x}$, alone in the first example to be treated later, but will generally be a function of the solution u. Hence we consider $\underline{a} = \underline{a}(\underline{x}, u)$. The first step, eq. (.7), goes through as before. In the second step of the Taylor-Galerkin method, eq. (.8), the term that needs to be treated slightly differently is the one where the derivative of the flux function, at this stage represented by piecewise constants and therefore undifferentiable, is put onto the piecewise linear basis function by integration by parts. Now these terms are treated in the following way:-

$$\begin{aligned}
\int_{Element=E} \underline{a}(\underline{x}, U_E^{n+\frac{1}{2}})\underline{\nabla}U_E^{n+\frac{1}{2}}\psi_j(\underline{x})dE = \quad & -\int_E U_E^{n+\frac{1}{2}}\underline{\nabla}.(\psi_j(\underline{x})\underline{a}(\underline{x}, U_E^{n+\frac{1}{2}}))dE \\
= \quad & -U_E^{n+\frac{1}{2}}\int_E \underline{\nabla}.(\psi_j(\underline{x})\underline{a}(\underline{x}, U_E^{n+\frac{1}{2}}))dE \\
= \quad & -U_E^{n+\frac{1}{2}}\int_S \psi_j(\underline{x})\underline{a}(\underline{x}, U_E^{n+\frac{1}{2}}).d\underline{S} \quad \forall E,
\end{aligned}$$

where S is the surface of the element and $d\underline{S} = \underline{n}dS$, where $\underline{n}$ is again the outward normal. Given that $\psi_j(x)$ is a linear function on each element and that $\underline{a}(\underline{x}, U_E^{n+\frac{1}{2}})$ is a piecewise constant function on each element (if a function of $U^{n+\frac{1}{2}}$) or a piece-

wise linear function (if a function of $\underline{x}$), the surface integral is then very simple to evaluate exactly and cheaply as the normal vectors only need to be calculated the once.

.2.1 Taylor-Galerkin on the Sphere

A triangular grid used previously for calculations on the sphere is the spherical goedisic grid. This has been used for finite element calculations, see Cullen [9], and finite difference calculations, see Williamson [40]. Although there is no reason why this grid could not be used in the context of this method, another, very similar, approach has been used here. A first grid is defined consisting of a node at each pole and six equi-spaced points around the equator. This then gives a grid of 12 equilateral triangles (as viewed in 3-D cartesian space). Successive refinements are then made by dividing each existing equilateral triangle into 4 equal sized triangles. The nodes of the triangles are then projected onto the surface of the sphere. This leads to a grid where each node has six elements attached to it except for the original six nodes on the equator where only four elements meet. The n^{th} grid then refers to the grid produced by the n^{th} refinement of the original grid. In this paper we will not examine the possibilities of grid refinement but in order to demonstrate that we are by no means restricted to uniform grids the grids are then "smoothed". The word smoothing is used in inverted commas because although it is a simple grid smoothing algorithm, that aims to place each node at the centre of all its neighbours, and gives aesthetically pleasing grids, see figures (4) and (5), we see that it also introduces some asymmetry on the coarser

mesh, figure (3), where the grids on the northern and southern hemispheres no longer overlap. More importantly, we see from table (i) that there is now a large range of element sizes. Before the smoothing all element sizes were very close to being the average value. This procedure does have an adverse effect on the time-step that can be taken but we hope goes some way to showing the prospective flexibility of the method.

One great advantage of using a cartesian co-cordinate system is that the equations are well defined everywhere, there is no singularity present due to the transformation of co-ordinates and there is no ambiguity in the definition of velocities and derivatives at the poles. (The reader may be interested in Swarztrauber [37] at this point where these points are addressed whilst still using spectral methods.) However, using a finite element method, unlike spherical harmonic based methods or most finite difference schemes, we can discretize directly onto a surface in 3-dimensional cartesian space. This means that we have the three velocities (u, v, w), instead of the usual two $(\dot{\lambda}, \dot{\theta})$, and three 'independent' directions (x, y, z) instead of just (λ, θ). Clearly only two of the velocities are truly independent, the third being defined by the need for the velocity to be tangential to the sphere, i.e.,

$$\underline{r}.\underline{u} = 0, \tag{.9}$$

where $\underline{u} = (u, v, w)$ and $\underline{r}$ is the normal vector to the sphere. Similarly only two directions are truly independent and hence only two derivatives can be calculated on the sphere. The third is obtained through the relation

$$\underline{r}.\underline{\nabla} f = 0 \quad \forall \text{ differentiable functions } f. \tag{.10}$$

Both indentities (.9) and (.10) will be used extensively in the following. Explicitly then, for example, eq. (.9) can be used to recover the velocity in the vertical direction given the x and y velocities,

$$w = \frac{-(xu + yv)}{z}$$

and the derivative in this direction is then given as

$$\frac{\partial f}{\partial z} = \frac{-\left(x\frac{\partial f}{\partial x} + y\frac{\partial f}{\partial y}\right)}{z}.$$

Clearly for z close to 0 it would be unwise to use these formulae. In practice the largest, in absolute value, of x, y or z is used to determine which velocity and derivative is to be recovered from (.9) and (.10). In the following we will assume that $|z|$ is the largest. Entirely analogous results follow if the other co-ordinate directions are chosen.

The calculation of the x and y derivatives can be approached from many angles; here we just present one way.

In the plane (x', y') the two derivatives, $\frac{\partial}{\partial x'}$ and $\frac{\partial}{\partial y'}$, are easily calculated, for piecewise linear functions, as

$$\frac{\partial U}{\partial x'} = \frac{1}{J}\left[(U_1 - U_3)(y_2' - y_3') - (U_2 - U_3)(y_1' - y_3')\right]$$

$$\frac{\partial U}{\partial y'} = \frac{-1}{J}\left[(U_1 - U_3)(x'_2 - x'_3) - (U_2 - U_3)(x'_1 - x'_3)\right],$$

where

$$J = (x'_1 - x'_3)(y'_2 - y'_3) - (x'_2 - x'_3)(y'_1 - y'_3)$$

is the element Jacobian and can either be stored or calculated when needed. The subscripts refer to the three nodes of the element with the usual anti-clockwise numbering convention. We may define x' and y' how we please but perhaps the simplest is

$$\begin{aligned} x' &= x \\ y' &= y. \end{aligned}$$

The chain rule tells us that

$$\frac{\partial u}{\partial x'} = \frac{\partial x}{\partial x'}\frac{\partial u}{\partial x} + \frac{\partial y}{\partial x'}\frac{\partial u}{\partial y} + \frac{\partial z}{\partial x'}\frac{\partial u}{\partial z}$$

$$\frac{\partial u}{\partial y'} = \frac{\partial x}{\partial y'}\frac{\partial u}{\partial x} + \frac{\partial y}{\partial y'}\frac{\partial u}{\partial y} + \frac{\partial z}{\partial y'}\frac{\partial u}{\partial z}.$$

We can substitute in for the z derivative from eq. (.10). The derivatives of z with respect to the new variables x' and y' can be obtained by noting that, where a is

the radius of the earth,

$$\begin{aligned} z^2 &= a^2 - x^2 - y^2 \\ &= a^2 - x'^2 - y'^2 \end{aligned}$$

and hence

$$\frac{\partial z}{\partial x'} = -\frac{x'}{z}$$

and

$$\frac{\partial z}{\partial y'} = -\frac{y'}{z}.$$

Inverting the resultant matrix then gives us the derivatives we require,

$$\begin{pmatrix} \dfrac{\partial u}{\partial x} \\ \\ \dfrac{\partial u}{\partial y} \end{pmatrix} = \frac{1}{a^2} \begin{pmatrix} z^2 + y^2 & -xy \\ \\ -xy & z^2 + x^2 \end{pmatrix} \begin{pmatrix} \dfrac{\partial u}{\partial x'} \\ \\ \dfrac{\partial u}{\partial y'} \end{pmatrix}.$$

This has dealt with all the terms created by the right-hand sides of equations (.7,.8). This now leaves us with a system of equations to solve

$$M(\underline{U}^{n+1} - \underline{U}^n) = \underline{b}, \tag{.11}$$

where M is the mass matrix whose elements are given by

$$M_{i,j} = \int_{\Omega} \psi_i(\underline{x})\psi_j(\underline{x})d\Omega.$$

This, of course, is not just a product of the Taylor-Galerkin method but of any Galerkin method using non-orthogonal basis functions. Fortunately the mass matrix, M, can be inverted accurately and cheaply. Wathen [39] showed that with diagonal pre-conditioning the eigenvalues of M were all contained in the region $[\frac{1}{2}, 2]$ for the linear elements on triangles to be used here. Similar results hold for other types of element. This then implies that the conjugate gradient (CG) method, see Golub & Van Loan [16] for example, would be particularly efficient in the sense that very few iterations are needed. Typically we found one CG iteration sufficient to reduce the norm of the initial residual vector by a factor of 10^{-10}. In some of the examples with very large time-steps three iterations were required. If a vector machine is available then each iteration can also be made extremely fast, see Axelsson & Barker [1] and Howard et al [19].

.3 Test Problems and Results

.3.1 A Linear Problem

The first test problem is that due to Ritchie [31]. This involves the advection of a Gaussian hill around the sphere, completing one revolution in 20 days. The velocity field is defined as giving constant angular velocity around the point $(\lambda_0, \theta_0) = (0^o, 45^o)$. The Gaussian hill is centred on the point $(0^o, 0^o)$ and is

given by

$$G(r) = 100e^{-\left(\frac{\pi^2 r^2}{L^2}\right)},$$

where r is the distance from the centre of the hill as measured in the plane generated by the stereographic projection true at $(0^o, 0^o)$ and L is the wave length of the field and takes values of 10,000km., 5,000km. and 2,500km.. Full specifications of the problem can be found in Ritchie [31]. Due to the definition of the velocity field and the positioning of the initial data the cone passes directly over the north pole after 10 days. This can prove to be a problem for some schemes but in the cartesian co-ordinate system with the grids described previously this is not the case.

The results are all taken after a full 20 day rotation. The maxima and minima are given to indicate the sucess of the solution and an l_2 error provides a more objective, comparative measure. The maximum and minimum should remain 100 and 0. No pictures are given of the results as they only confirm the impression gained from looking at the extrema, i.e. the solution was obviously degraded or clearly doing very well. There was no noticeable phase error and no increase in the rate of error growth occured in transversing the pole. Results are given for various time-steps and meshes and with various values of L to assess the temporal and spatial accuracy. Tables (ii-iv) give the results for the $3^{rd}, 4^{th}$ and 5^{th} grids for L = 10,000km.. Tables (v-vii) give the same results for L = 5,000km. and tables (viii-x) for L = 2,500km..

From Table (ii) we see that there is no point reducing the time-step

below 1,000 seconds as the results have time-converged at that point and to take more time-steps is to invite more projection error to creep in, as indeed happens. If we subtract off the purely spatial error, i.e. that error that remains in the time-converged solution, then we can calculate the temporal orders of convergence to be 2.2 and 2.19. Similarly on the 4^{th} grid in table (iii), if we subtract off what is assumed to be the time-converged solution, we can calculate the order of convergence to be 1.955, 1.38, 1.37 and 1.7. It is worth noting here that the 4^{th} grid has resolved the Gaussian hill much more adequately than the previous grid. This is shown by the vast improvements, apart from with the very large time-steps, in the maximum and minimum values. If a strictly non-negative quantity needs transporting, for example humidity, then it is clear from these results that, provided the mesh is capable of representing the solution and a moderate time-step is chosen, then very little post-processing of the solution will need to be done to maintain positivity. The final grid in the sequence is the 5^{th} and its results are in table(iv). These results show only a modest improvement over those obtained on the 4^{th} grid. This is due to the fact that most of the wavelengths present could be adequately resolved on the 4^{th} grid. It is not possible to give figures for the spatial convergence rate due to restricted number of grids we were able to use.

Now looking at the steeper Gaussians we, not surprisingly, see that the 3^{rd} mesh with just 768 elements fails to resolve these cones, see tables (v) and (viii). The other two meshes both make a good job of the 5,000km. cone, tables (vi) and (vii), although now the 5^{th} grid is showing itself to be superior. For the final case of L = 2,500km., tables (ix) and (x), again the 5^{th} grid does well whilst

the 4^{th} grid is showing signs of deterioration.

Overall then we have shown that the Taylor-Galerkin finite element method copes reasonably well with this test problem. On a fixed mesh it would be difficult for a finite element method based on piecewise linear elements to compete with the high accuracy semi-Lagrangian schemes. The real benefits of the finite element method will show through when adaptive meshing is used enabling the resolution of the 5^{th} grid to be obtained with a mesh of significantly fewer elements. This is particularly true of the current example where the vast majority of the mesh is doing nothing. It is beyond the scope of this paper to look at the various ways mesh adaptation could be implemented.

.3.2 A Non-Linear Problem

The radius of the earth, a, the rotation rate of the earth, Ω, and the acceleration due to gravity, g, are defined to have the following values:-

$$a = 6.37122 \times 10^6 m$$

$$\Omega = 7.292 \times 10^{-5} s^{-1}$$

$$g = 9.80616 m s^{-2}.$$

Following Côté [8], for example, we write the shallow water equations on a sphere as

$$\frac{d\underline{V}}{dt} = \underline{F} - \left(\frac{1}{a^2}\right)\underline{V}.\underline{Vr} \tag{.12}$$

$$\frac{d\phi}{dt} + \phi\underline{\nabla}.\underline{V} = 0,$$

where

$$\underline{V} = (u, v, w)^T$$

$$\underline{r} = (x, y, z)^T$$

$$\frac{d}{dt} = \frac{\partial}{\partial t} + u\frac{\partial}{\partial x} + v\frac{\partial}{\partial y} + w\frac{\partial}{\partial z}$$

and

$$\underline{F} = -\frac{1}{a}f\underline{r} \times \underline{V} - \underline{\nabla}\phi$$

with

$$f = \frac{2\Omega z}{a}.$$

We will now look in some detail at the treatment of the first component of eq. (.12), the velocity in the x direction. Expanded, the equation becomes,

$$\frac{\partial u}{\partial t} + u\frac{\partial u}{\partial x} + v\frac{\partial u}{\partial y} + w\frac{\partial u}{\partial z} + \frac{x}{a^2}(u^2 + v^2 + w^2) + \frac{\partial \phi}{\partial x} + \frac{2\Omega z}{a^2}(-zv + yw) = 0.$$

The equations for v and w are entirely similar. As only the one element will be considered subscripts refering to elements will be dropped. Instead the subscripts will refer to the local numbering on the element. Temporal superscripts will also be dropped for simplicity where possible. This is illustrated in figure (2). A subscript c will be used to denote the value of a quantity at the centroid of an element. For a linear function this is just

$$f_c = \frac{f_1 + f_2 + f_3}{3}$$

and is hence equal to the integral of the function f over the element, when multiplied by the element area. Geometric quantities will be assumed to be constants over the element and will take the value at the centroid. The integral of the quadratic terms was performed in two ways. It was evaluated exactly and by the centroid quadrature. No difference could be detected in the results and so we just present the method with the centroid quadrature used. The derivatives are calculated as discussed in the previous section and are treated as constants on the element. The constant approximation to u on this element at the half time-level is then given by

$$u^{n+\frac{1}{2}} = u_c - \frac{\Delta t}{2}\left(u_c\frac{\partial u}{\partial x} + v_c\frac{\partial u}{\partial y} + w_c\frac{\partial u}{\partial z} + \frac{x_c}{a^2}\left(u_c^2 + v_c^2 + w_c^2\right) + \frac{\partial \phi}{\partial x} + \frac{2\Omega z_c}{a^2}\left(-z_c v_c + y_c w_c\right)\right).$$

Having now calculated $u^{n+\frac{1}{2}}, v^{n+\frac{1}{2}}, w^{n+\frac{1}{2}}$ and $\phi^{n+\frac{1}{2}}$ on this element it now remains to calculate the contributions this element makes towards the nodal equations locally termed 1,2 and 3. We drop the superscript $n+\frac{1}{2}$. Denoting the contributions to the equations as Δu_i and the normal vectors $\underline{n}_i$, see figure (2), as

$(x_{n_i}, y_{n_i}, z_{n_i})$ we have, assuming the vector to have been normalized to have length $\sqrt{(x_1-x_2)^2+(y_1-y_2)^2+(z_1-z_2)^2}$ in the case of $\underline{n}_1$ for example,

$$\begin{aligned}\Delta u_1 &= \Delta t\left\{\frac{u}{2}\left[u(x_{n_1}+x_{n_3})+v(y_{n_1}+y_{n_3})+w(z_{n_1}+z_{n_3})\right]+\frac{\phi}{2}(x_{n_1}+x_{n_3})\right.\\ &- \left.\frac{area(\triangle)}{3}\left[\frac{x_c}{a^2}(u^2+v^2+w^2)-\frac{2\Omega z_c}{a^2}(-z_c v+y_c w)\right]\right\}\end{aligned}$$

$$\begin{aligned}\Delta u_2 &= \Delta t\left\{\frac{u}{2}\left[u(x_{n_1}+x_{n_2})+v(y_{n_1}+y_{n_2})+w(z_{n_1}+z_{n_2})\right]+\frac{\phi}{2}(x_{n_1}+x_{n_2})\right.\\ &- \left.\frac{area(\triangle)}{3}\left[\frac{x_c}{a^2}(u^2+v^2+w^2)-\frac{2\Omega z_c}{a^2}(-z_c v+y_c w)\right]\right\}\end{aligned}$$

$$\begin{aligned}\Delta u_3 &= \Delta t\left\{\frac{u}{2}\left[u(x_{n_2}+x_{n_3})+v(y_{n_2}+y_{n_3})+w(z_{n_2}+z_{n_3})\right]+\frac{\phi}{2}(x_{n_2}+x_{n_3})\right.\\ &- \left.\frac{area(\triangle)}{3}\left[\frac{x_c}{a^2}(u^2+v^2+w^2)-\frac{2\Omega z_c}{a^2}(-z_c v+y_c w)\right]\right\},\end{aligned}$$

where $area(\triangle)$ is just the area of the element in question. We note that many of the terms are common between these three contributions and there are more common components with terms in the equations for v and w. This means that a lot of time can be saved in the calculation of these integrals.

The test problem is that due to Phillips [29]. It involves the evolution of a Rossby-Haurwitz wave. The initial velocity field is given by the stream function,

$$\psi = a^2\left(-\omega\sin(\theta)+K\cos^R(\theta)\sin(\theta)\cos(R\lambda)\right), \qquad (.13)$$

where ω, K and R are constants. The longitudinal and latitudinal velocities can now be defined from the streamfunction (.13) as

$$\tilde{u} = a\dot{\lambda}\cos(\theta) = -a^{-1}\frac{\partial\psi}{\partial\theta} = a\omega\cos(\theta) + aK\cos^{R-1}(\theta)\left(R\sin^2(\theta) - \cos^2(\theta)\right)\cos(R\lambda)$$

$$\tilde{v} = a\dot{\theta} = (a\cos(\theta))^{-1}\frac{\partial\psi}{\partial\lambda} = -aKR\cos^{R-1}(\theta)\sin(\theta)\sin(R\lambda),$$

where the ˜'s have just been used to distinguish these velocities from their cartesian counterparts. The cartesian velocities can now be obtained from the relations

$$u = -\tilde{u}\sin(\lambda) - \tilde{v}\cos(\lambda)\sin(\theta)$$

$$v = \tilde{u}\cos(\lambda) - \tilde{v}\sin(\lambda)\sin(\theta)$$

$$w = \tilde{v}\cos(\theta).$$

Haurwitz [18] showed that in a non-divergent barotropic model the wind field defined by eq. (.13) moves from west to east with angular velocity

$$\nu = \frac{R(3+R)\omega - 2\Omega}{(1+R)(2+R)} \tag{.14}$$

without distortion. The shallow water equations do not have a known solution for this problem but for stable waves this solution proves to be very accurate. The initial height field is obtained analytically from the streamfunction by solving the balance equation, see Phillips [29]. This means that not only is the divergence

of the velocity field zero, from its definition, but also the initial tendency of the divergence is zero. The height is then given in [29] as

$$gh = gh_0 + a^2 \left(A(\theta) + B(\theta)\cos(R\lambda) + C(\theta)\cos(2R\lambda)\right)$$

where

$$A(\theta) = \frac{\omega}{2}(2\Omega+\omega)\cos^2(\theta) + \frac{1}{4}K^2\cos^{2R}(\theta)\left[(R+1)\cos^2(\theta) + \left(2R^2 - R - 2\right)\right.$$

$$\left. -2R^2\cos^{-2}(\theta)\right]$$

$$B(\theta) = \frac{2(\Omega+\omega)K}{(R+1)(R+2)}\cos^R(\theta)\left[(R^2+2R+2) - (R+1)^2\cos^2(\theta)\right]$$

$$C(\theta) = \frac{1}{4}K^2\cos^{2R}(\theta)\left[(R+1)\cos^2(\theta) - (R+2)\right].$$

The problem is then fully defined by choosing

$$h_0 = 8 \times 10^3 \text{m.},$$

$$\omega = 7.848 \times 10^{-6}\text{sec}^{-1},$$

$$K = 7.848 \times 10^{-6}\text{sec}^{-1},$$

$$R = 4.$$

A contour plot of the height field and a representation of the wind field is given for the initial data, on the 3^{rd} grid, in figures (6,7). Figure (6) is an equatorial projection and figure (7) is a polar projection.

With the choice of parameters defined above this gives an angular velocity of the solution, from eq. (.14), of 2.4635×10^{-6}rad $\sec^{-1}$ or 0.2128rad day^{-1} or 12.2^{o} per day.

Results are given for the three grids at daily intervals up to the seventh day. Wind arrows are not included in the results for the 5^{th} grid. An equatorial and polar projection are provided for each grid for each day. It was found easier to estimate the angular velocity of the solution from the polar projections whereas the equatorial projection would provide a better indication of the overall acceptability of the solution. Figures (8–21) are the results for the 3^{rd} grid, figures (22–35) relate to the 4^{th} grid and figures (36–49) are for the 5^{th} grid.

The grids all give the same basic answer revolving the solution without any great distortion. This distortion becomes less on the finer grids, as we would expect, but even on the coarsest grid the breakup is very limited. Considering that only 768 elements are used on this grid and that they are not equi-distributed the method performs remarkably well. On the 4^{th} grid the solution improves with there now only being a slight distortion of the 'highs' revolving around the equator. On the 5^{th} grid this has all but disappeared.

.4 Summary

We have taken one of the simplest specialist hyperbolic finite element methods and applied it to the shallow water equations on the sphere. The results would

appear to be very good, with a good resolution being obtained on a quite coarse grid. The grids used had elements that varied greatly in size demonstrating very clearly that regular grids are not needed. The results were obtained with no artificial diffusion or any filters and the geopotential was conserved as a direct property of the scheme.

The major disadvantage of the scheme is its explicit time-step. This means that the time-step is limited by the fastest moving waves which are the gravity waves, $u \pm \sqrt{\phi}$, and the smallest Δx. Although in the cases reported here we did make the Δx smaller than we need have in order to demonstrate that the method did not need a regular grid, the main problem is the gravity waves. Other schemes have used a semi-implicit approach to overcome this problem and this has also been done for the finite element method by Staniforth & Mitchell [34]. This approach is widely regarded as being very efficient and it is hoped that together with the conjugate gradient method as a very efficient matrix inverter that it might prove to be even more so in the context we have developed here.

Another paper we could do well to learn from is that of Steppeler et al [35]. Here we achieved conservation of geopotential but there are many other conserved quantities, total energy, vorticity, divergence and potential enstrophy for example. In [35] the question of integral invariants within a finite element method was addressed with particular reference to the conservation of energy. This was found to increase the non-linear stability for long-term integrations and to improve the accuracy of their scheme. It is hoped that this might have the

same effect on the algorithm described here. Again the constrained conjugate gradient method could be put to good use to ensure an efficient solution of the resulting implicit equations. It has already proved to be effective in other application areas, Baines et al [2].

In conclusion then we have shown the Taylor-Galerkin method to be capable of solving problems of meteorological interest. What remains to be shown is that the method is also efficient. Although we showed here that the calculations needed to update the solution at each time-step were modest, a semi-implicit version is really needed so that reasonable time-steps may be taken. Conserving the values of integral invariants may also aid the length of time-step that could be taken and should also increase the accuracy of the method. Both future improvements should fit nicely into the algorithm used in this paper.

References

[1] Axelsson, O. & Barker, V.A., 1984: *"Finite Element Solution of Boundary Value Problems."* Academic Press Inc..

[2] Baines, M.J., Birkett, N.R.C. & Sweby, P.K., 1990: *"Non-Linear Diffusion in Process Modelling."* Int. J. of Numer. Modelling: Elec. Networks, Devices and Fields, Vol. 3, pp. 79-90.

[3] Bruneau, C.H., Chattot, J.J., Laminie, J. & Guiu-Roux, J., 1982: *"Finite Element Least-Squares method for Solving Full Steady Euler Equations in a plane nozzle."* 8^{th} ICNMFD, Aachen 1982, Lecture Notes in Physics 170.

[4] Childs, P.N. & Morton, K.W., 1990: *"Characteristic Galerkin Methods for Scalar Conservation Laws in One-Dimension."* SIAM J. Numer. Anal., Vol. 27, No. 3, pp. 553-594.

[5] Cockburn, B., Hou, S. & Shu, C.W., 1990: *"TVB Runge-Kutta Local Projection Discontinuous Galerkin Finite Element Method for Conservation Laws IV: The Multidimensional Case."* Math. Comp., Vol. 54, pp. 545-581.

[6] Cockburn, B., Lin S.Y. & Shu, C.W., 1989: *"TVB Runge-Kutta Local Projection Discontinuous Galerkin Finite Element Method for Conservation Laws*

III: One Dimensional Systems." J.C.P., Vol. 84, pp. 90-113.

[7] Cockburn, B. & Shu, C.W., 1989: *"TVB Runge-Kutta Local Projection Discontinuous Galerkin Finite Element Method for Conservation Laws II: General Framework."* Math. Comp., Vol. 52, pp. 411-435.

[8] Côté, J., 1988: *"A Lagrange Multiplier Approach for the Metric Terms of Semi-Lagrangian Models on the Sphere."* Quart. J. R. Met. Soc., Vol. 114, pp. 1347-1352.

[9] Cullen, M.J.P., 1974: *"Integrations of the primitive equations on a sphere using the finite element method."* Quart. J. R. Met. Soc., Vol. 100, pp. 555-562.

[10] Cullen, M.J.P. & Hall, C.D., 1979: *"Forecasting and general circulation results from finite element models."* Quart. J. R. Met. Soc., Vol. 105, pp. 571-592.

[11] Donea, J., 1984: *"A Taylor-Galerkin method for convective transport problems."* Int. J. for Num. Meths. in Eng., Vol. 20, pp. 101-118.

[12] Donea, J., Guiliani, S. & Halleux, J.P., 1982: *"An Arbitrary Lagrangian Eulerian Finite Element Method for Transient Dynamic Fluid Structure Interactions."* Comput. Meths. Appl. Mech. Eng., Vol. 33, pp. 689-723.

[13] Donea, J., Guiliani, S., Laval, H. & Quartapelle, L., 1984: *"Time-accurate solution of advection-diffusion problems by Finite Elements"*. Comp. Meths. in Appl. Mech. and Eng., Vol. 45, pp.123-145.

[14] Donea, J., Quartapelle, L. & Selmin, V., 1987: *"An analysis of time discretization in the Finite Element solution of hyperbolic problems."* JCP, Vol. 70, pp. 463-499.

[15] Donea, J., Selmin, V. & Quartapelle, L., 1988: *"Recent developments of the Taylor-Galerkin method for the numerical solution of hyperbolic problems."* Numerical Methods for Fluid Dynamics III (Eds. K.W. Morton and M.J. Baines), Oxford University Press, pp. 171-185.

[16] Golub, G.H. & Van Loan, C.F., 1989: *"Matrix Computations."* Second Edition, The John Hopkins University Press, Baltimore and London.

[17] Hawken, D.F., Gottlieb, J.J. & Hansen, D.F., 1991: *"Review of some Adaptive Node-Movement Techniques in Finite-Element and Finite-Difference So-*

lutions of Partial Differential Equations." J.C.P., Vol. 95, pp. 254-302.

[18] Haurwitz, B., 1940: *"The Motion of Atmospheric Disturbances on the Spherical Earth."* J. Marine Res., Vol. 3, pp. 254-267.

[19] Howard, D., Connolley, W.M. & Rollett, J.S., 1989: *"Unsymmetric Conjugate Gradient Methods and Sparse Direct Methods in Finite Element Flow Simulation."* Oxford University Computing Laboratory Report no. 89/2. O.U.C.L., 8-11 Keble Road, Oxford, U.K..

[20] Johnson, C., 1987: *"Numerical Solution of Partial Differential Equations by the Finite Element Method."* Cambridge University Press.

[21] Löhner, R., Morgan, K., Peraire, J., Zienkiewicz, O.C. & Kong, L., 1986: *"Finite Elements for compressible flow."* Numerical Methods for Fluid Dynamics II (Eds. K.W. Morton and M.J. Baines), Oxford University Press, pp. 27-53.

[22] Löhner, R., Morgan, K. & Zienkiewicz, O.C., 1984: *"The use of Domain Splitting with an Explicit Hyperbolic Solver."* Comput. Meths. Appl. Mech. Eng., Vol. 45, pp. 313-329.

[23] Löhner, R., Morgan, K. & Zienkiewicz, O.C., 1985: *"An Adaptive Finite Element procedure for Compressible High speed Flows."* Comput. Meths. Appl. Mech. Eng., Vol. 51, pp. 441-464.

[24] Morgan, K., Peraire, J & Löhner, R., 1988: *"Adaptive Finite Element Flux Corrected Transport Techniques for CFD."* in Finite Elements Theory and Application, Eds. D.L. Dwoyer, M.Y. Hussaini & R.G. Voigt, Proceedings of the ICASE Finite Element Theory and Application Workshop July 1986, Hampton Virginia. Springer-Verlag, New York, pp. 165-175.

[25] Morton, K.W. & Parrott, A.K., 1980: *"Generalised Galerkin Methods for First-Order Hyperbolic Equations."* JCP Vol. 36, No. 2, pp. 249-270.

[26] Morton, K.W., Priestley, A. & Süli, E.E., 1988: *"Stability of the Lagrange-Galerkin Method with non-exact Integration."* RAIRO M^2AN Vol. 22, No. 4, pp. 625-653.

[27] Navon, I.M., 1987: *"FEUDX: A two-stage, high-accuracy, Finite-Element Fortran program for solving Shallow-Water equations."* Comp. & Geosciences, Vol. 13, No. 3, pp. 255-285.

[28] Peraire, J., Vahdati, M., Morgan, K. & Zienkiewicz, O.C., 1987: *"Adaptive Remeshing for Compressible Flow Computations."* J.C.P., Vol. 72, pp. 449-

466.

[29] Phillips, N.A., 1959: *"Numerical Integration of the Primitive Equations on the Hemisphere."* Mon. Weath. Rev., Vol. 87, pp. 333-345.

[30] Richtmyer, R.D. & Morton, K.W., 1967: *"Difference Methods for Initial-Value Problems."* Second edition, Interscience Publishers.

[31] Ritchie, H., 1987: *"Semi-Lagrangian advection on a Gaussian grid."* Mon. Weath. Rev., Vol. 115, pp. 608-619.

[32] Sewell, M.J., 1963: *" On Reciprocal Variational Principles for Perfect Fluids."* J. Math. Mech., Vol. 12, pp. 495-504.

[33] Staniforth, A.N., 1984: *"The application of the finite-element method to meteorological simulations –a review."* Int. J. Numer. Meth. in Fluids, Vol. 4, pp. 1-12.

[34] Staniforth, A.N. & Mitchell, H.L., 1977: *"A Semi-Implicit Finite-Element Barotropic Model."* Mon. Weath. Rev., Vol. 105, pp. 154-169.

[35] Steppeler, J., Navon, I.M. & Lu, H.I., 1990: *"Finite-Element Schemes for Extended Integrations of Atmospheric Models."* JCP, Vol. 89, pp. 95-124.

[36] Strang, G. & Fix, G.J., 1973: *"An Analysis of the Finite element Method."* Prentice-Hall, Inc., New Jersey.

[37] Swarztrauber, P.N., 1981: *"The approximation of vector functions and their derivatives on the sphere."* SIAM J. Numer. Anal., Vol. 18, pp. 191-210.

[38] Wang, H.H., Halpern, P. Douglas, J. & Dupont, T., 1972: *"Numerical solutions of the one-dimensional primitive equations using Galerkin approximations with localized basis functions."* Mon. Weath. Rev., Vol. 100, pp.738-746.

[39] Wathen, A.J., 1987: *"Realistic Eigenvalue Bounds for the Galerkin Mass Matrix."* I.M.A. J. Numer. Anal., Vol. 7, pp. 449-457.

[40] Williamson, D.L., 1970: *"Integration of the primitive barotropic model over a spherical geodesic grid."* Mon. Weath. Rev., Vol. 98, pp. 512-520.

Grid	No. of elements	No. of nodes	mean area km^2	min. area	max. area
3^{rd}	768	386	658569	77066	1712100
4^{th}	3072	1538	165694	15382	218084
5^{th}	12288	6146	41490	3161	49830

Table i: Details of the grids used.

Δt (secs)	Max.	Min.	l_2 error
8000	61.33	-106.5	0.699
4000	72.24	-28.69	0.289
2000	79.28	-12.80	0.2
1000	83.62	-7.87	0.175
500	86.29	-7.52	0.176
250	87.87	-10.2	0.185
125	88.74	-11.95	0.195

Table ii: Results for 3^{rd} grid with L=10000km.

Δt (secs)	Max.	Min.	l_2 error
1000	91.59	-39.28	0.144
500	95.37	-9.74	0.0409
250	97.61	-3.93	0.0189
125	98.79	-1.85	0.01043
62.5	99.4	-0.963	0.00672
31.25	99.69	-0.507	0.00508

Table iii: Results for 4^{th} grid with L=10000km.

Δt (secs)	Max.	Min.	l_2 error
125	98.77	-6.77	0.01135
62.5	99.39	-2.39	0.00482
31.25	99.71	-1.04	0.00252

Table iv: Results for 5^{th} grid with L=10000km.

Δt (secs)	Max.	Min.	l_2 error
8000	26.891	-38.036	0.4462
4000	34.153	-15.573	0.3155
2000	38.662	-11.669	0.2903
1000	41.830	-9.851	0.2929
500	44.516	-12.332	0.3159
250	46.533	-19.617	0.3506
125	47.794	-25.532	0.3827

Table v: Results for 3^{rd} grid with L=5000km.

Δt (secs)	Max.	Min.	l_2 error
1000	106.767	-77.097	0.2061
500	80.724	-12.926	0.04711
250	85.717	-2.840	0.030931
125	88.507	-3.2507	0.027813
62.5	89.977	-3.777	0.0276
31.25	90.7362	-4.0714	0.027923

Table vi: Results for 4^{th} grid with L=5000km.

Δt (secs)	Max.	Min.	l_2 error
125	95.389	-5.152	0.0075188
62.5	97.556	-1.871	0.004036
31.25	98.72	-1.255	0.0025215

Table vii: Results for 5^{th} grid with L=5000km.

Δt (secs)	Max.	Min.	l_2 error
8000	10.462	-13.102	0.2705
4000	11.62	-6.359	0.2453
2000	13.349	-5.195	0.2414
1000	15.103	-5.279	0.2434
500	17.657	-9.307	0.2556
250	20.286	-15.259	0.2808
125	22.298	-19.631	0.3101

Table viii: Results for 3^{rd} grid with L=2500km.

Δt (secs)	Max.	Min.	l_2 error
1000	158.225	-143.286	0.2734
500	42.039	-17.83	0.070526
250	46.948	-10.174	0.0630852
125	49.865	-11.777	0.066177
62.5	51.447	-12.962	0.070369
31.25	52.258	-13.906	0.073764

Table ix: Results for 4^{th} grid with L=2500km.

Δt (secs)	Max.	Min.	l_2 error
125	77.268	-8.742	0.01319
62.5	82.367	-5.389	0.0097691
31.25	85.280	-6.58	0.009673

Table x: Results for 5^{th} grid with L=2500km.

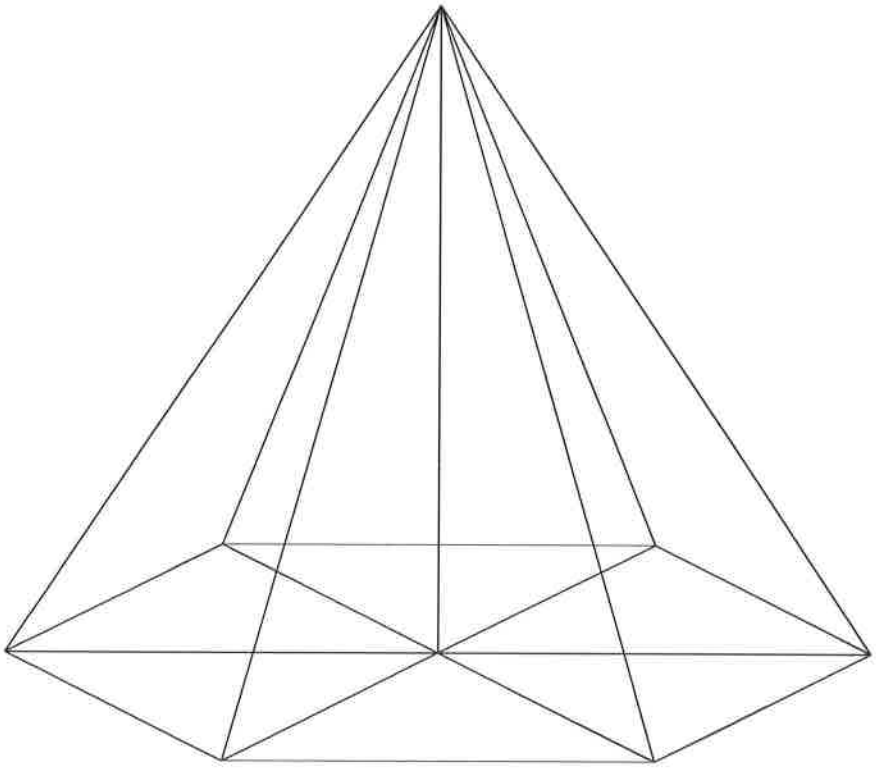

Figure 1: Piecewise linear basis function.

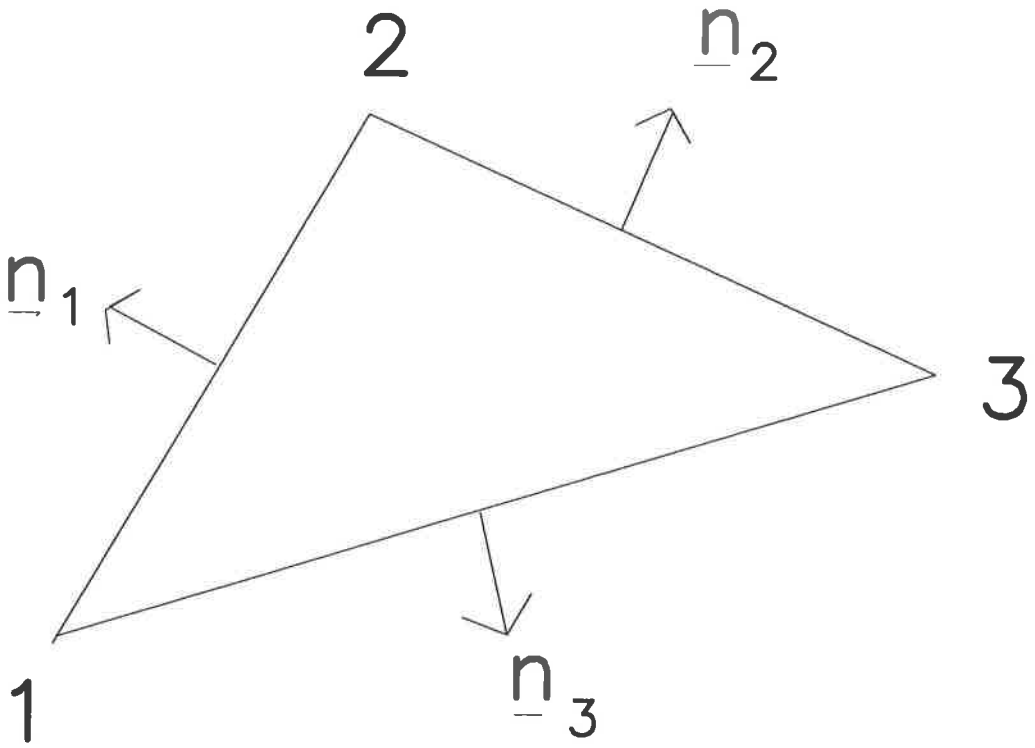

Figure 2: Local element numbering.

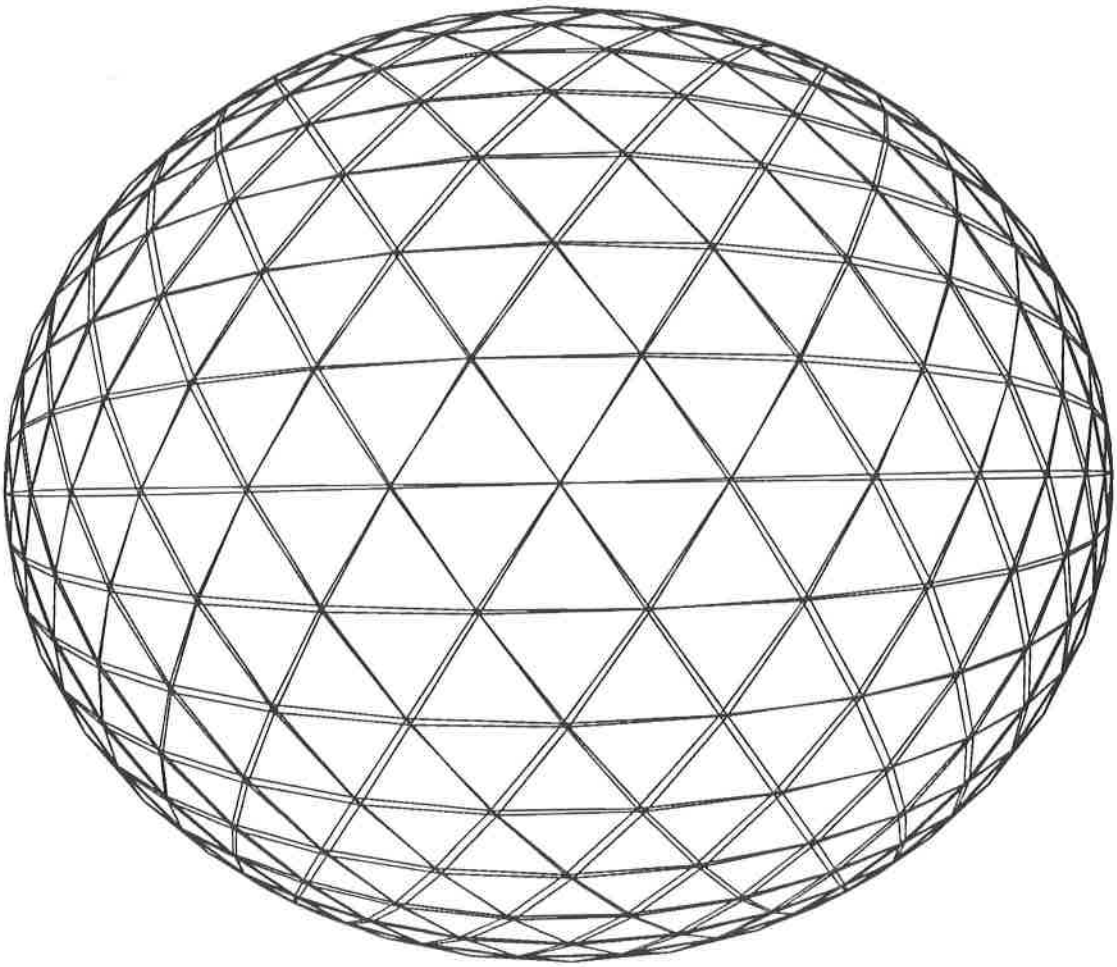

Figure 3: Grid generated by the 3^{rd} refinement.

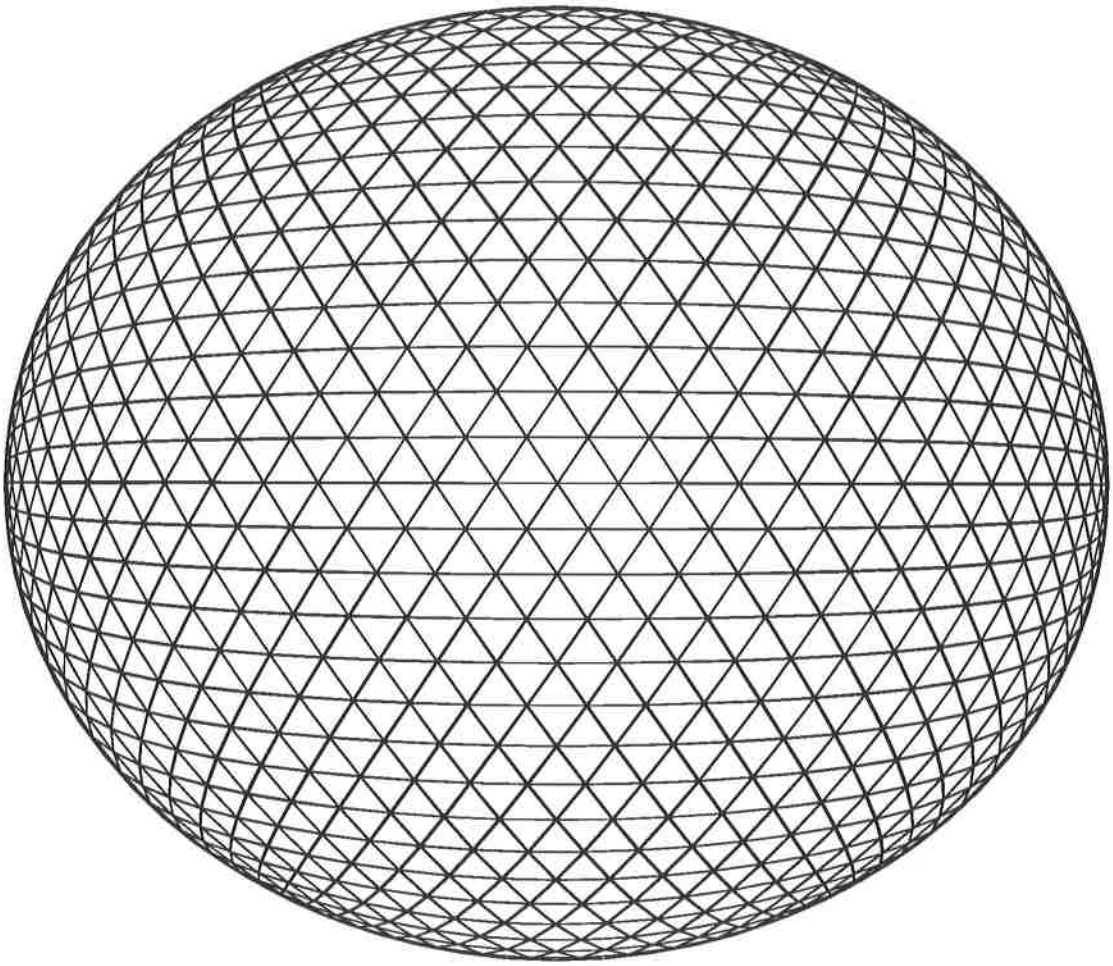

Figure 4: Grid generated by the 4^{th} refinement.

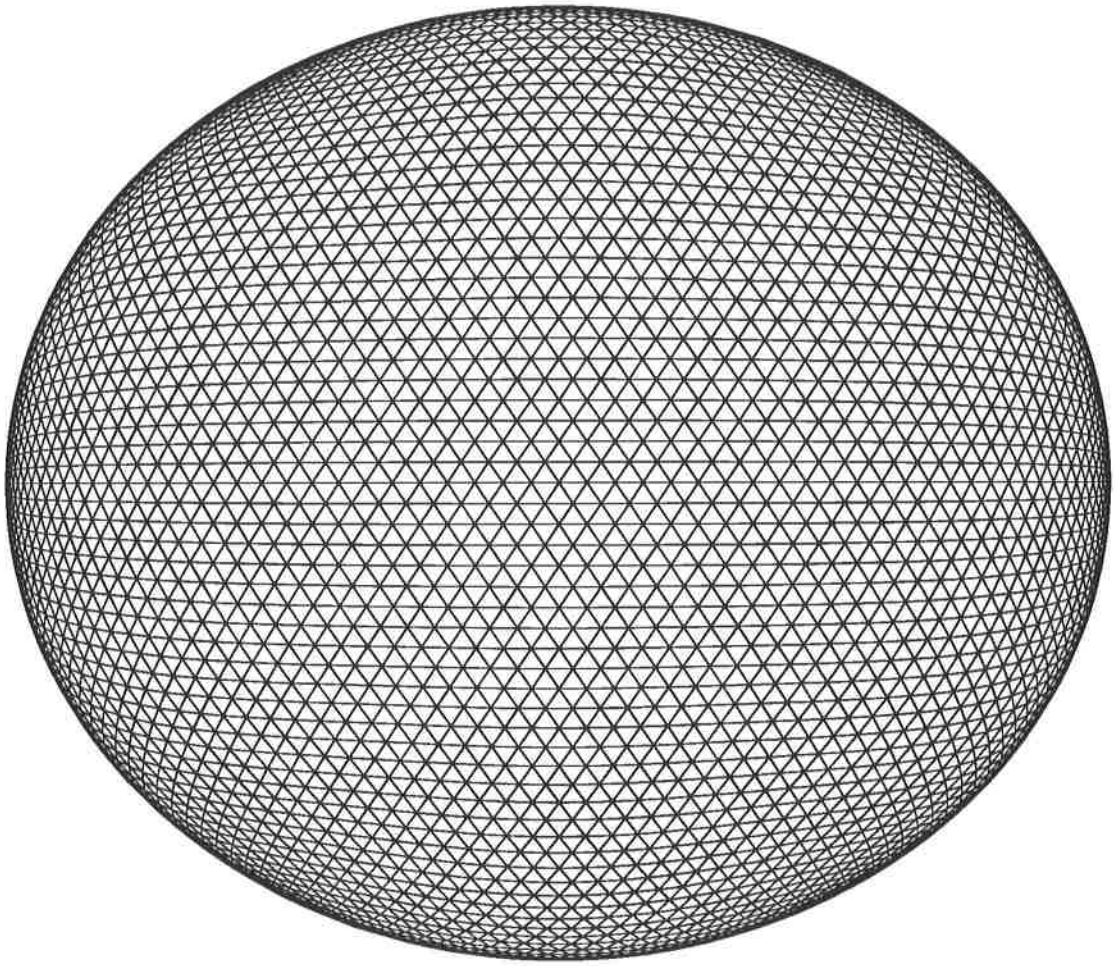

Figure 5: Grid generated by the 5^{th} refinement.

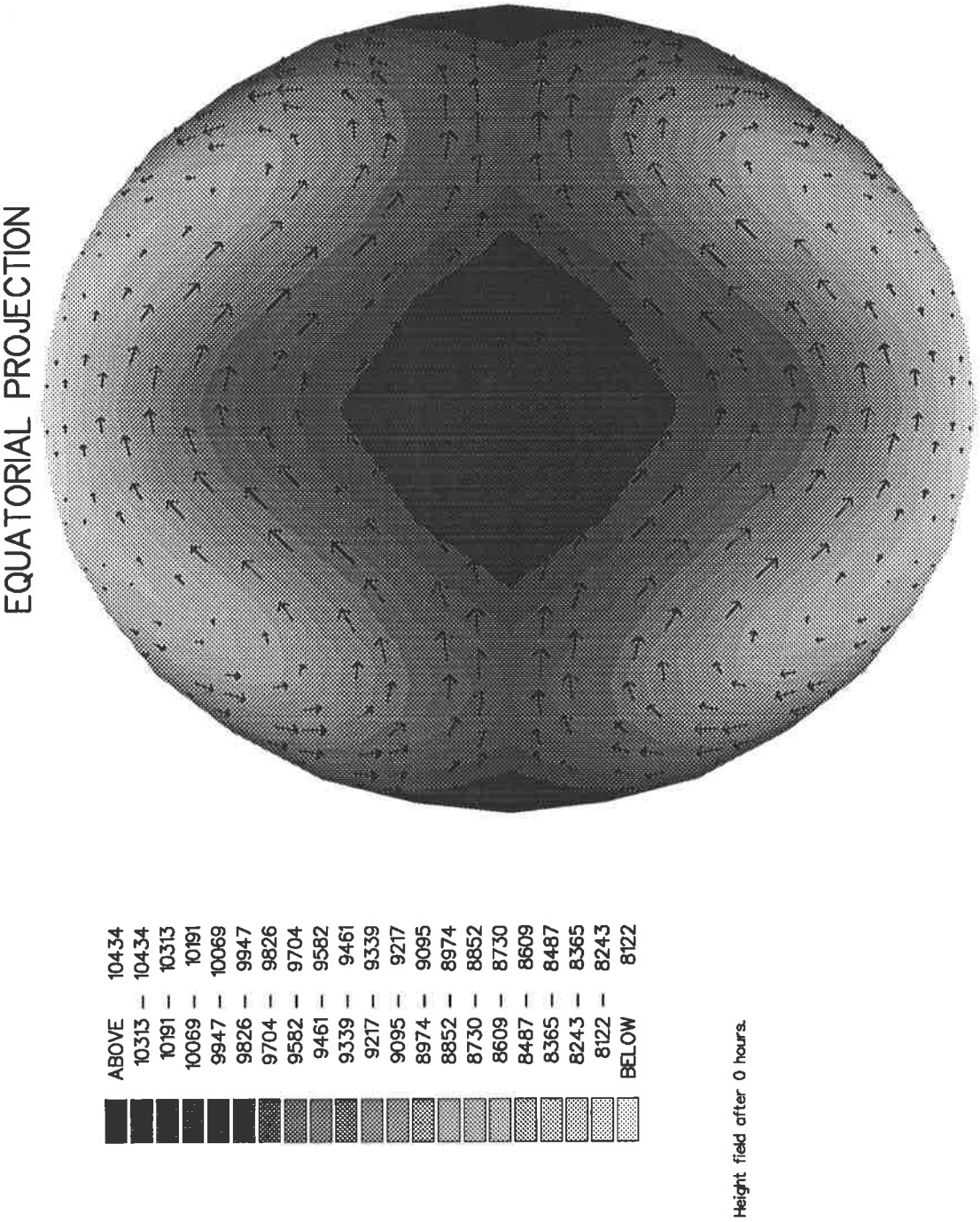

Figure 6: Equatorial projection of the initial height field and winds on the 3^{rd} grid.

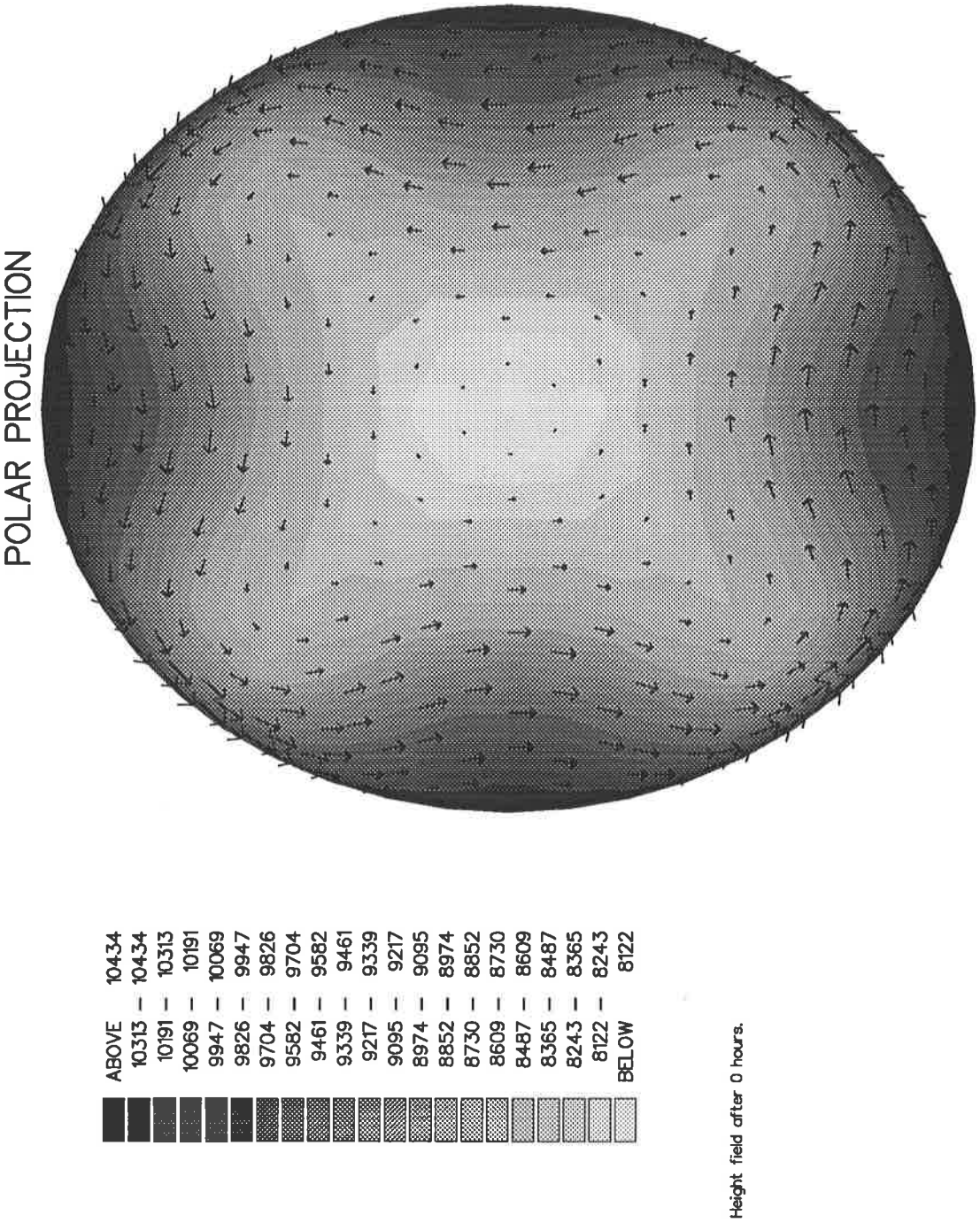

Figure 7: Polar projection of the initial height field and winds on the 3^{rd} grid.

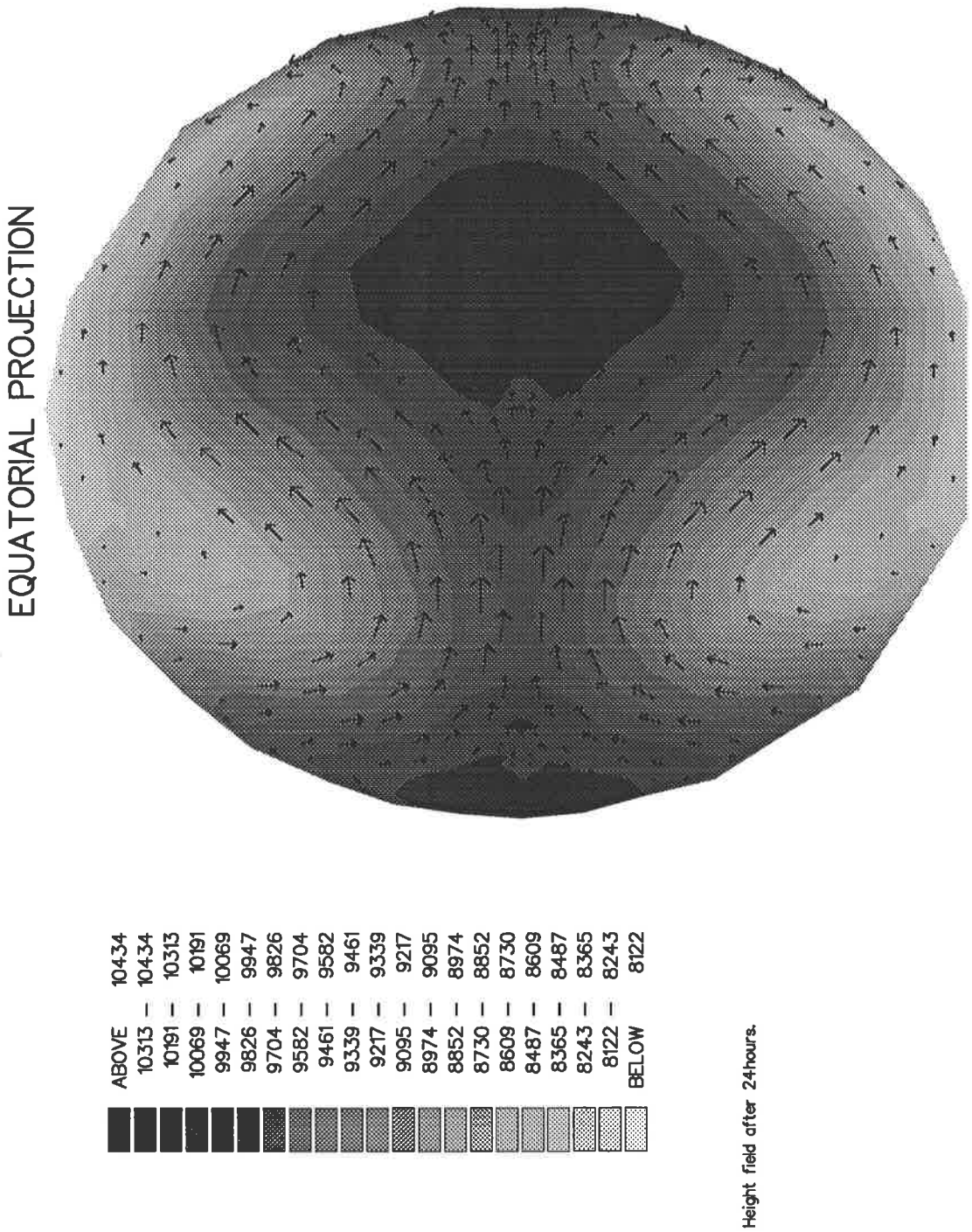

Figure 8: Equatorial projection of the height field and winds on the 3^{rd} grid after 1 day.

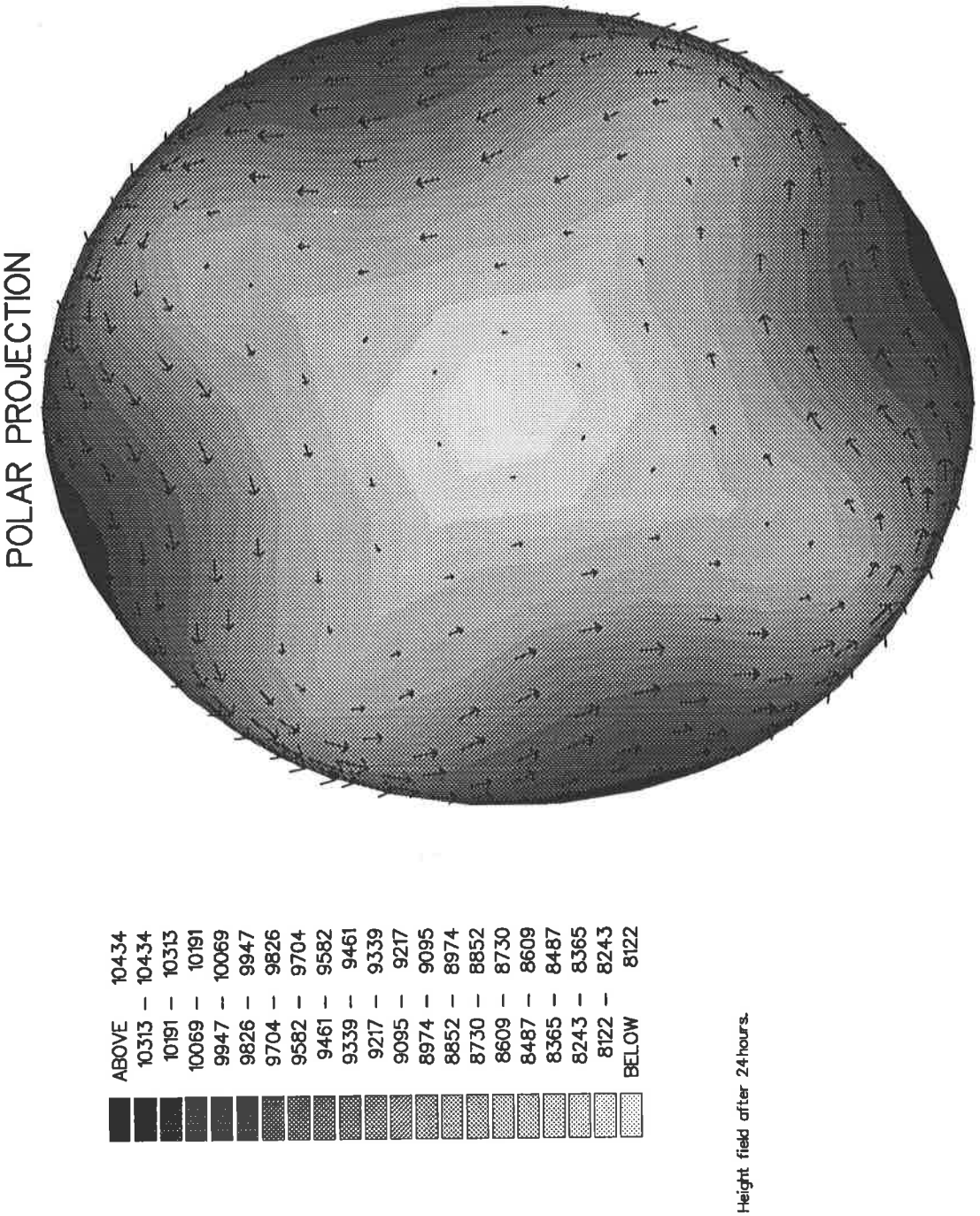

Figure 9: Polar projection of the height field and winds on the 3^{rd} grid after 1 day.

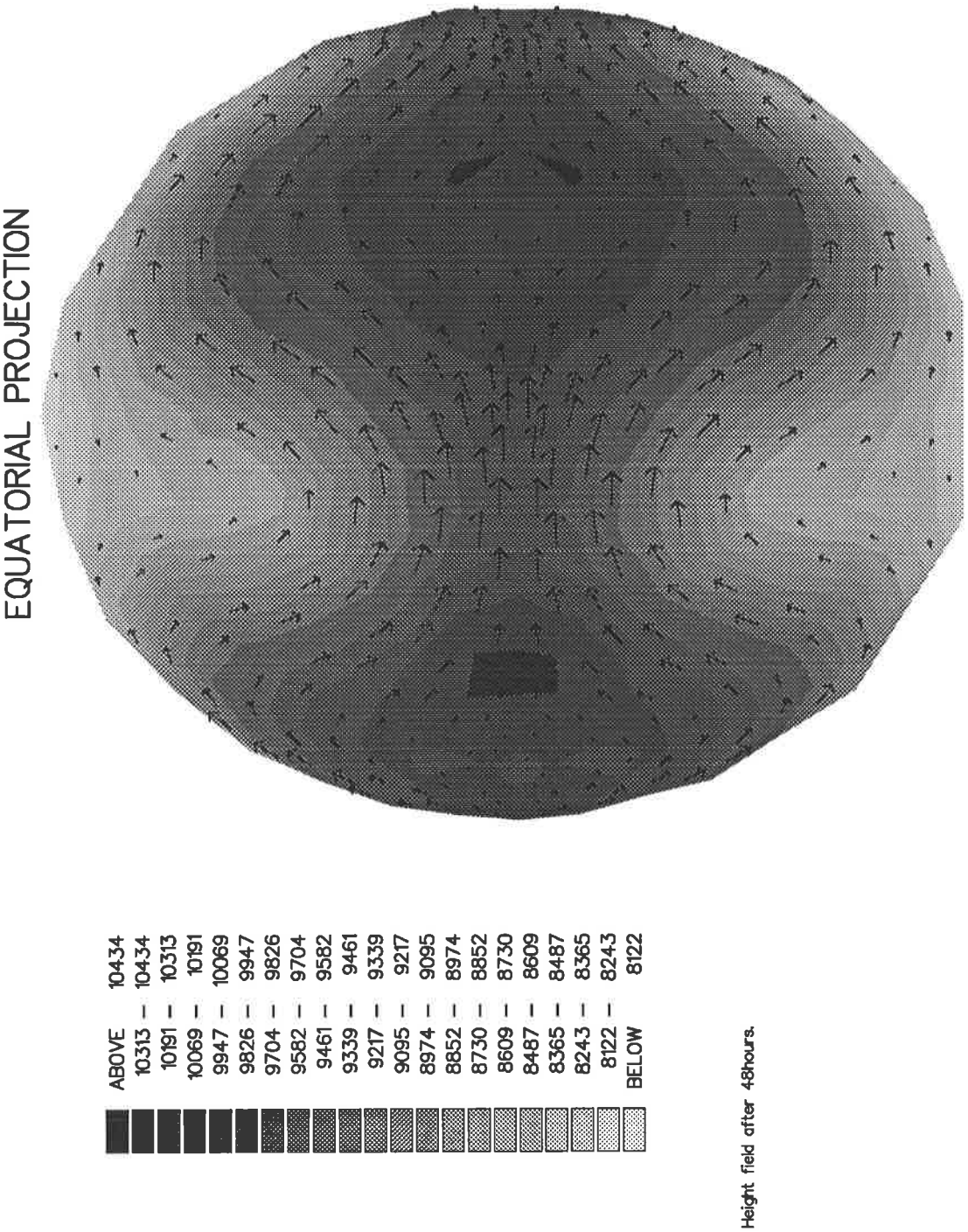

Figure 10: Equatorial projection of the height field and winds on the 3^{rd} grid after 2 days.

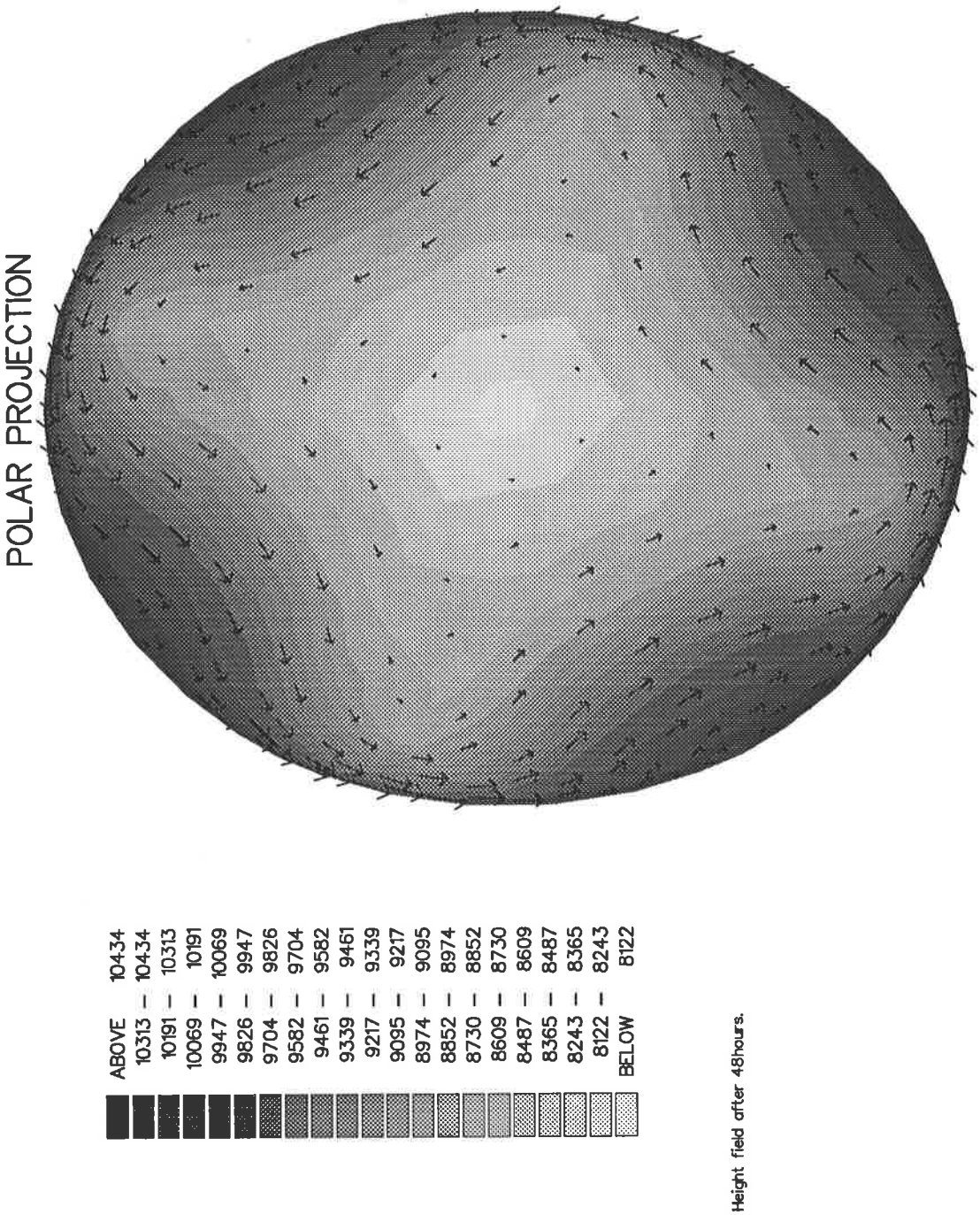

Figure 11: Polar projection of the height field and winds on the 3^{rd} grid after 2 days.

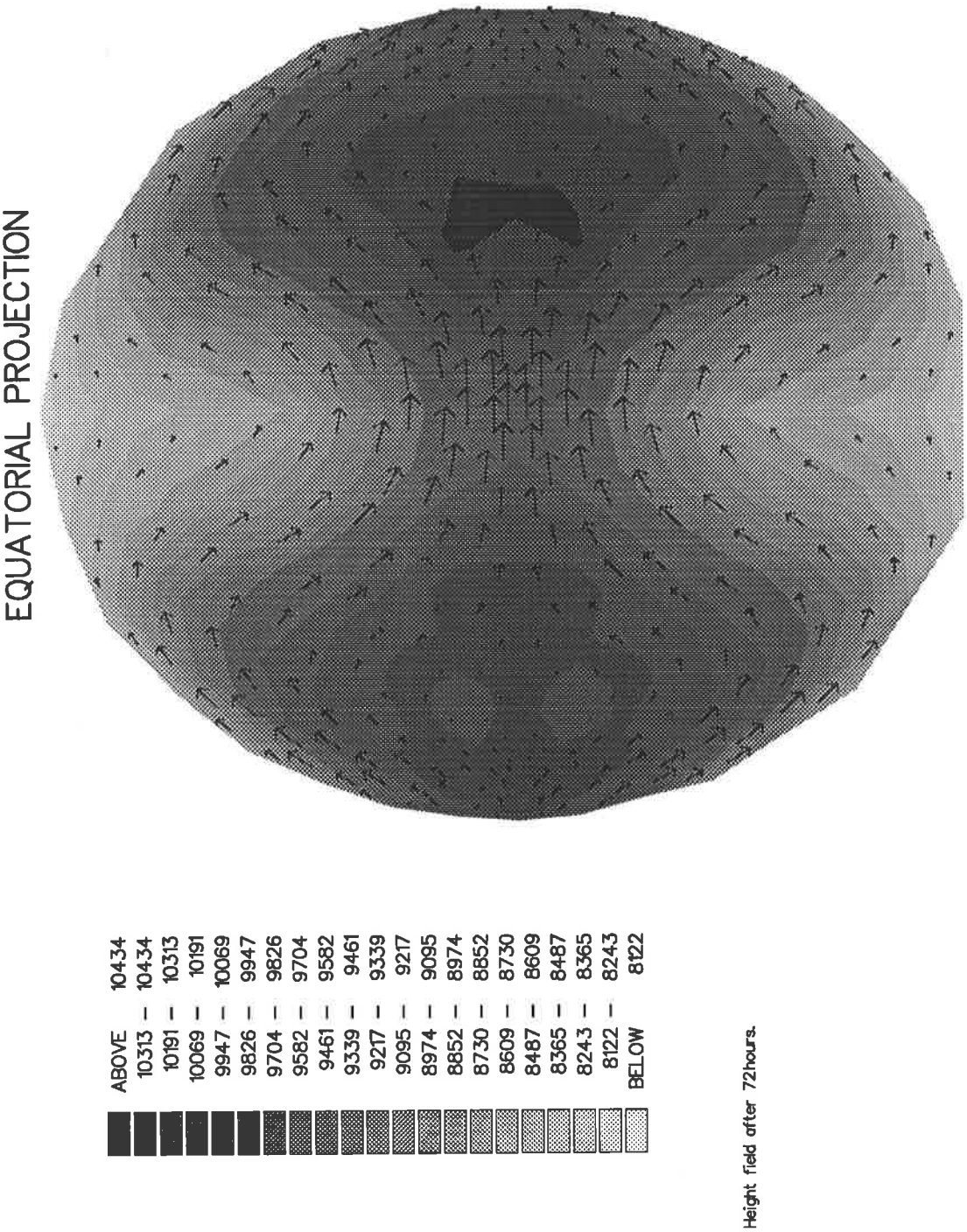

Figure 12: Equatorial projection of the height field and winds on the 3^{rd} grid after 3 days.

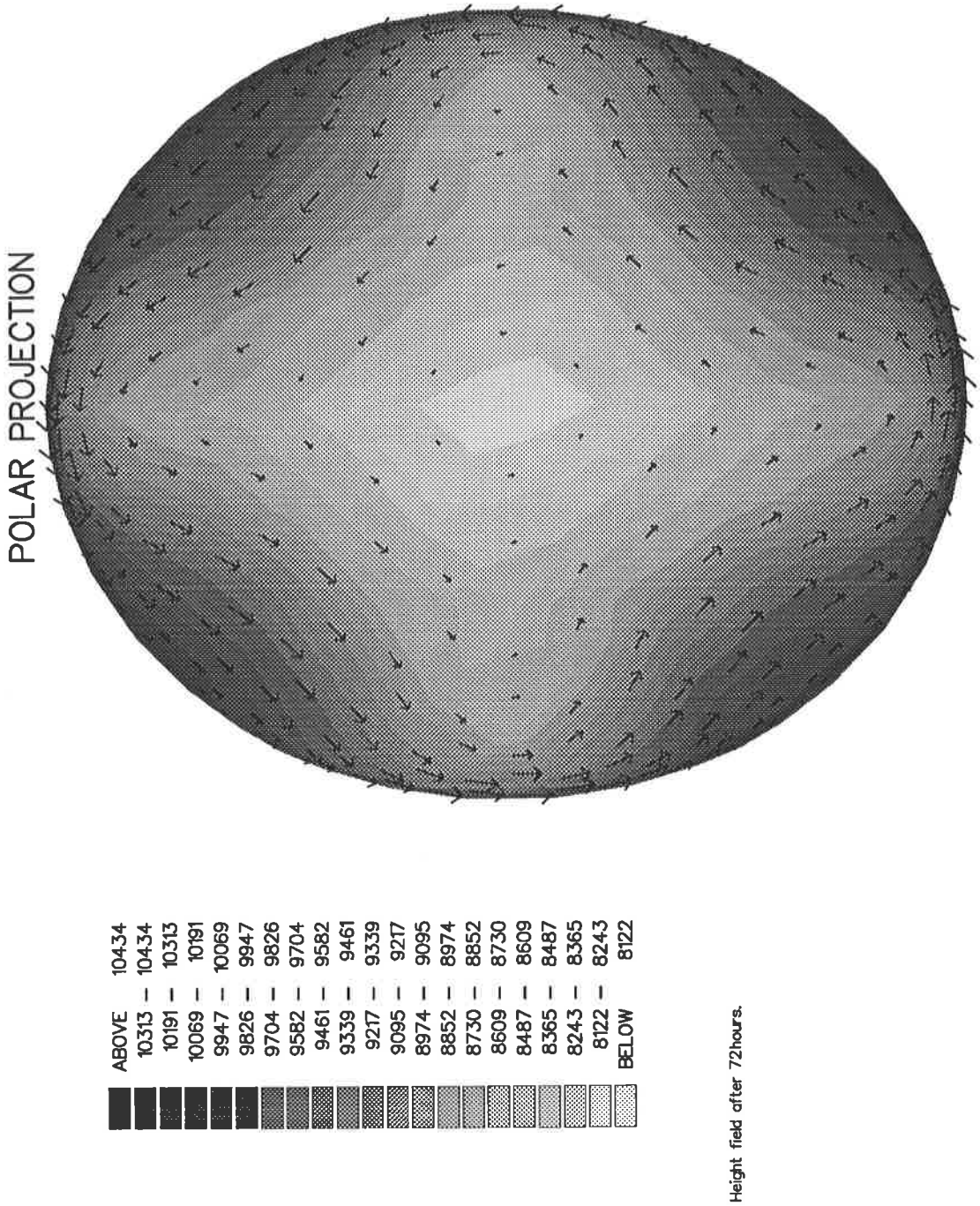

Figure 13: Polar projection of the height field and winds on the 3^{rd} grid after 3 days.

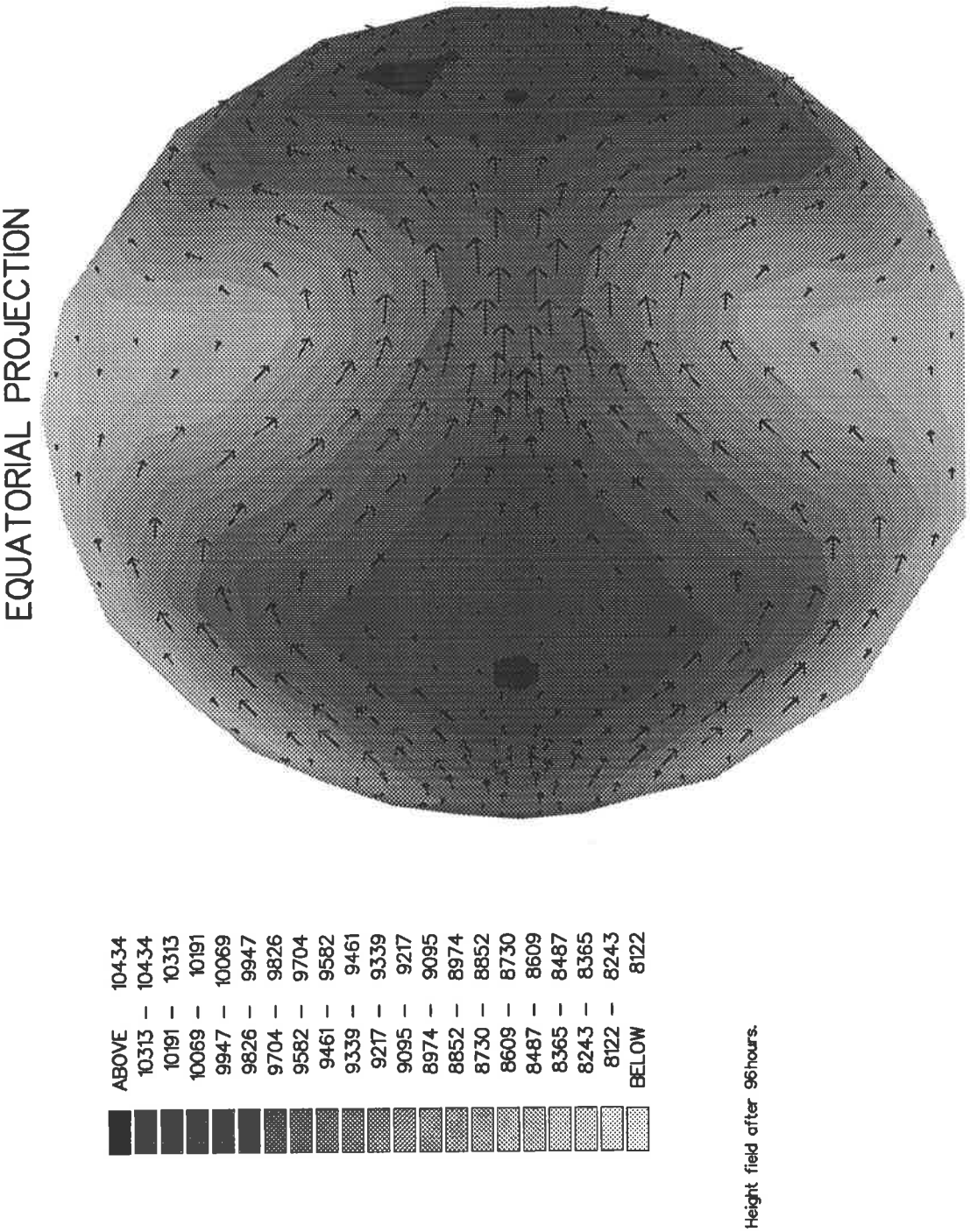

Figure 14: Equatorial projection of the height field and winds on the 3^{rd} grid after 4 days.

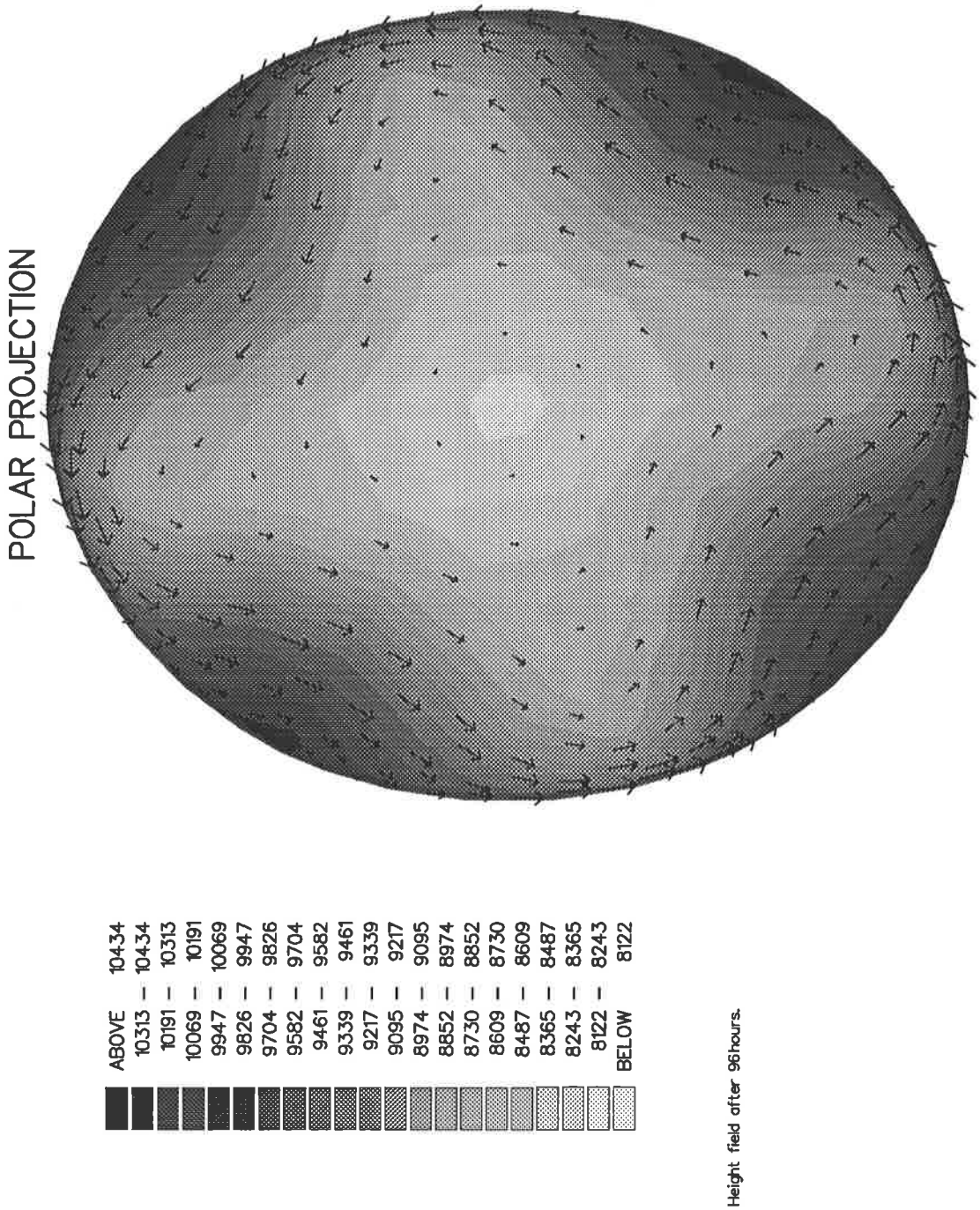

Figure 15: Polar projection of the height field and winds on the 3^{rd} grid after 4 days.

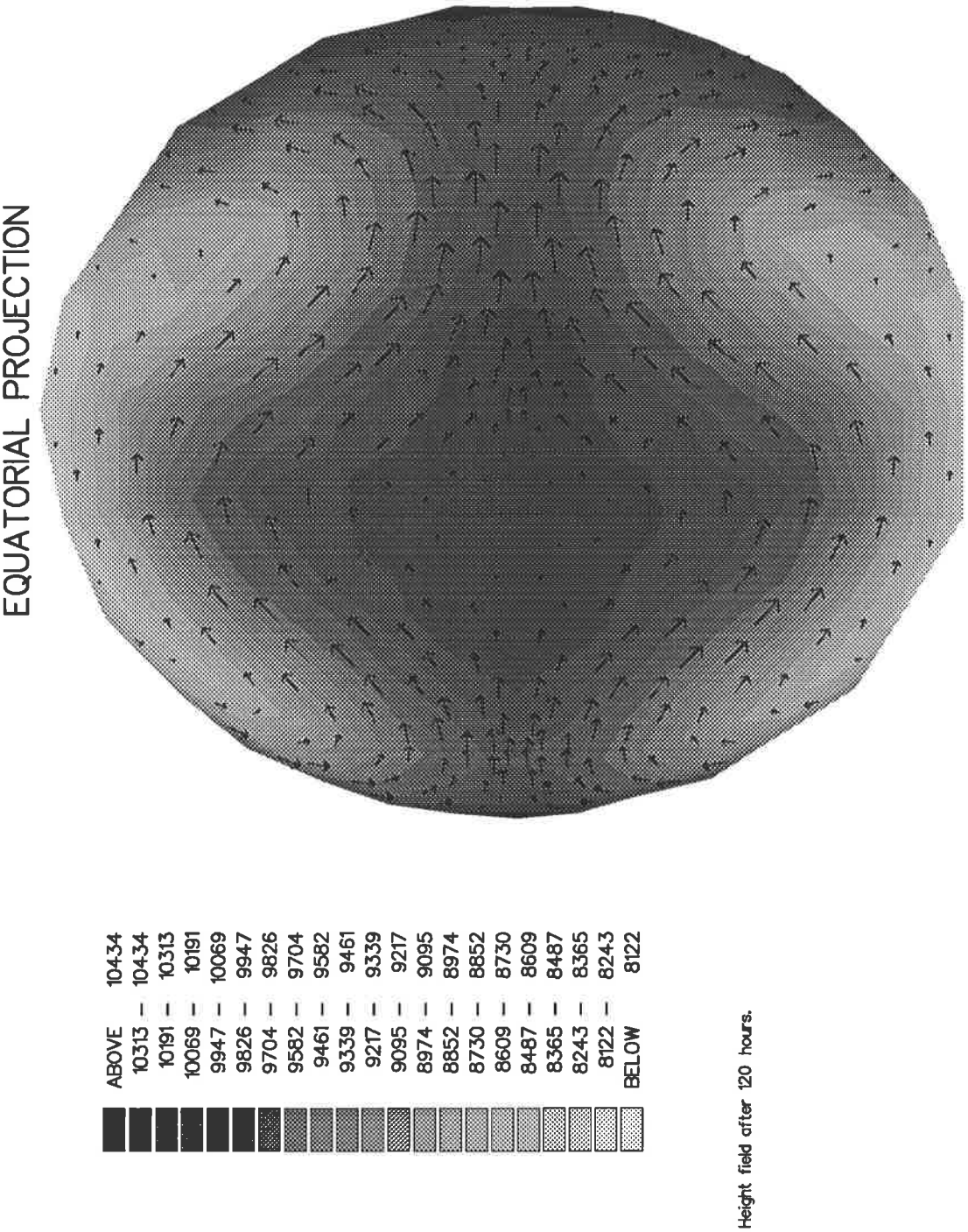

Figure 16: Equatorial projection of the height field and winds on the 3^{rd} grid after 5 days.

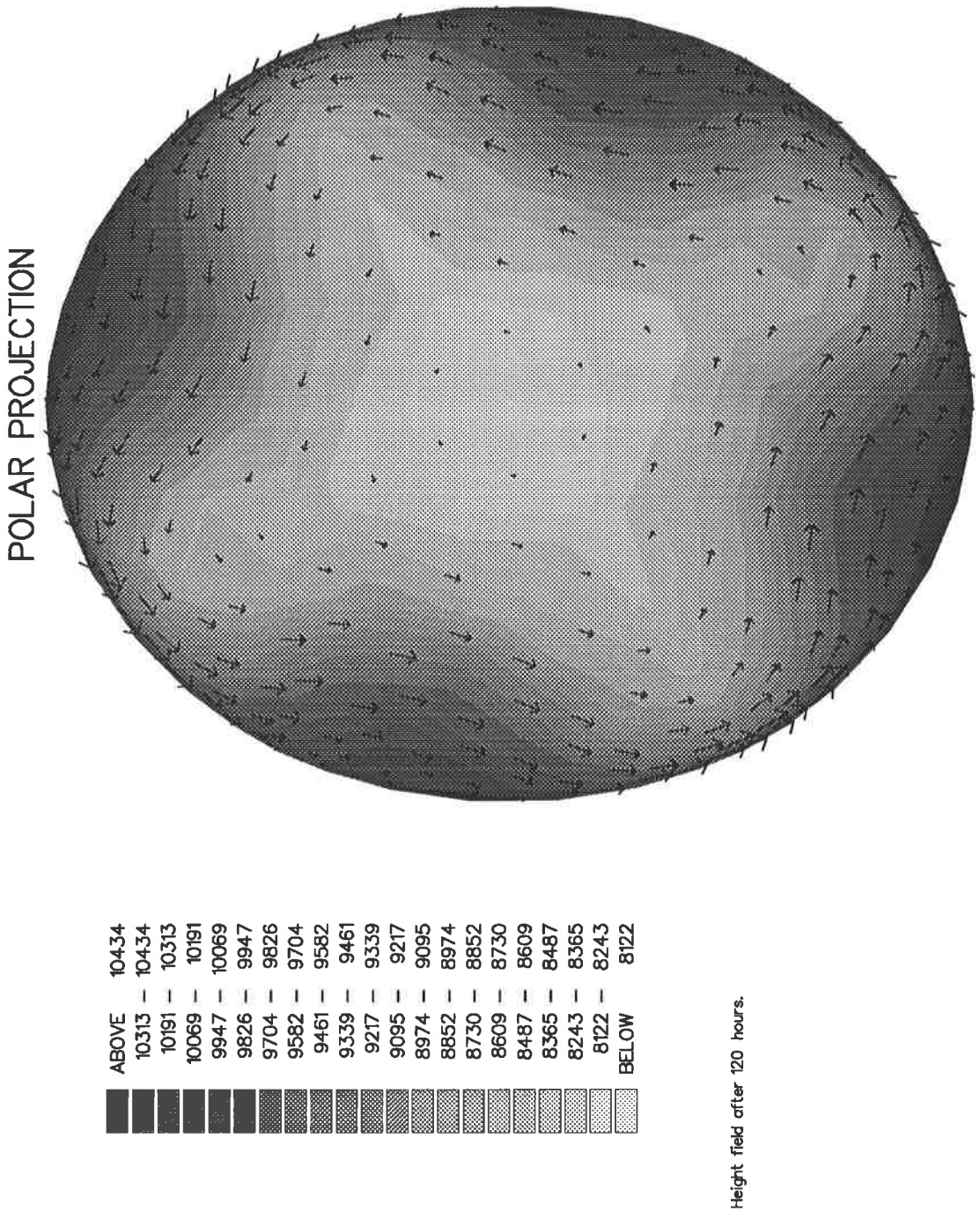

Figure 17: Polar projection of the height field and winds on the 3^{rd} grid after 5 days.

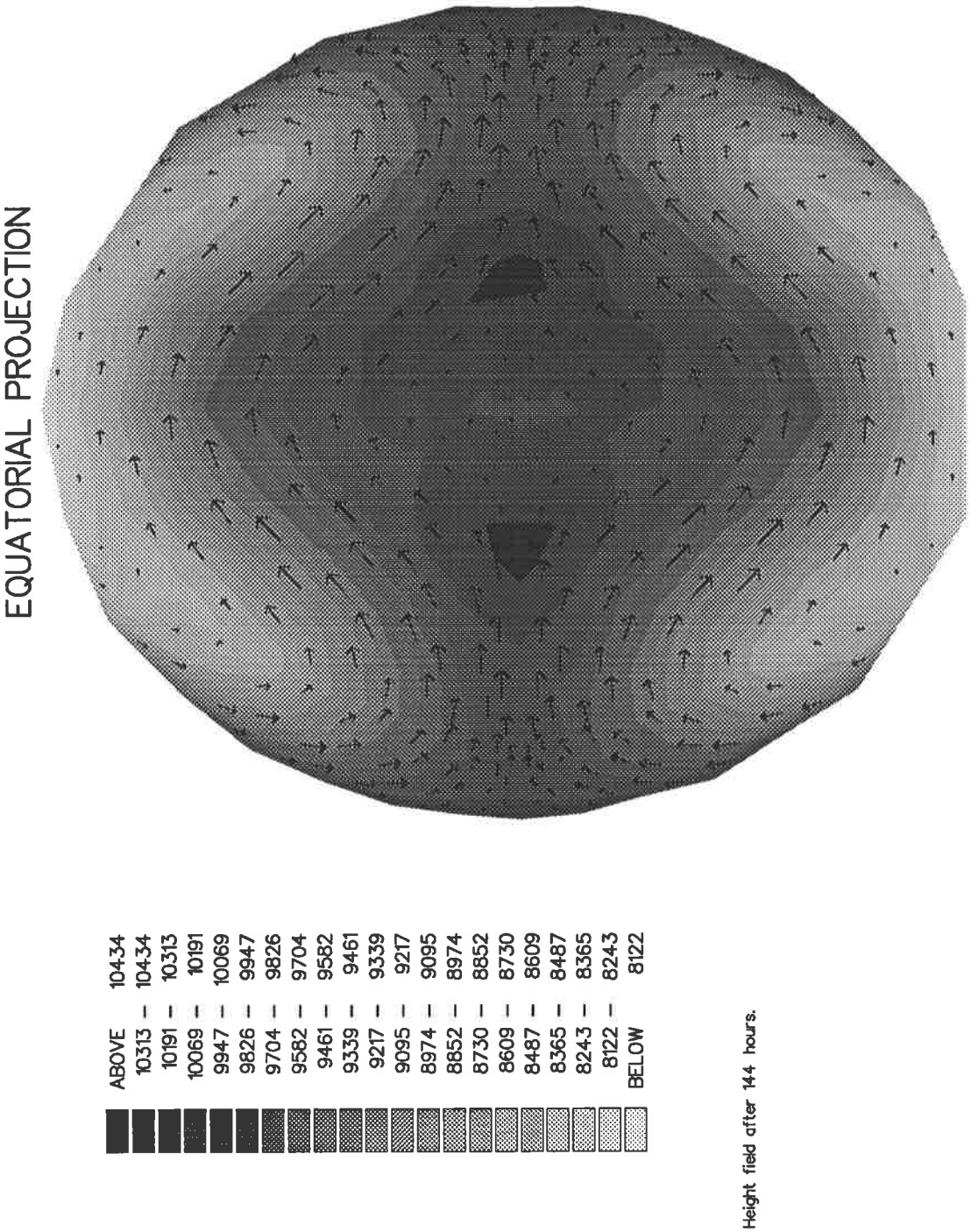

Figure 18: Equatorial projection of the height field and winds on the 3^{rd} grid after 6 days.

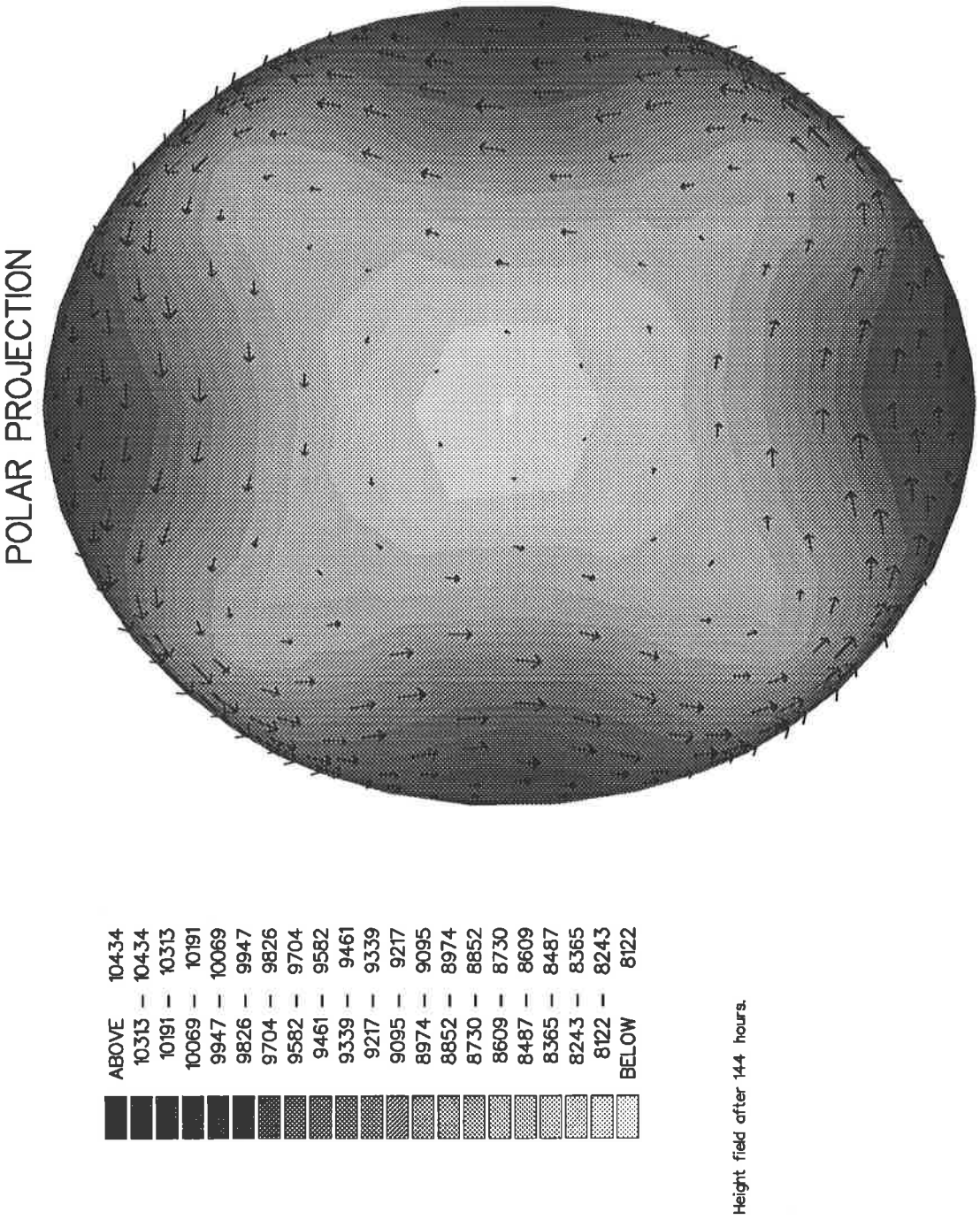

Figure 19: Polar projection of the height field and winds on the 3^{rd} grid after 6 days.

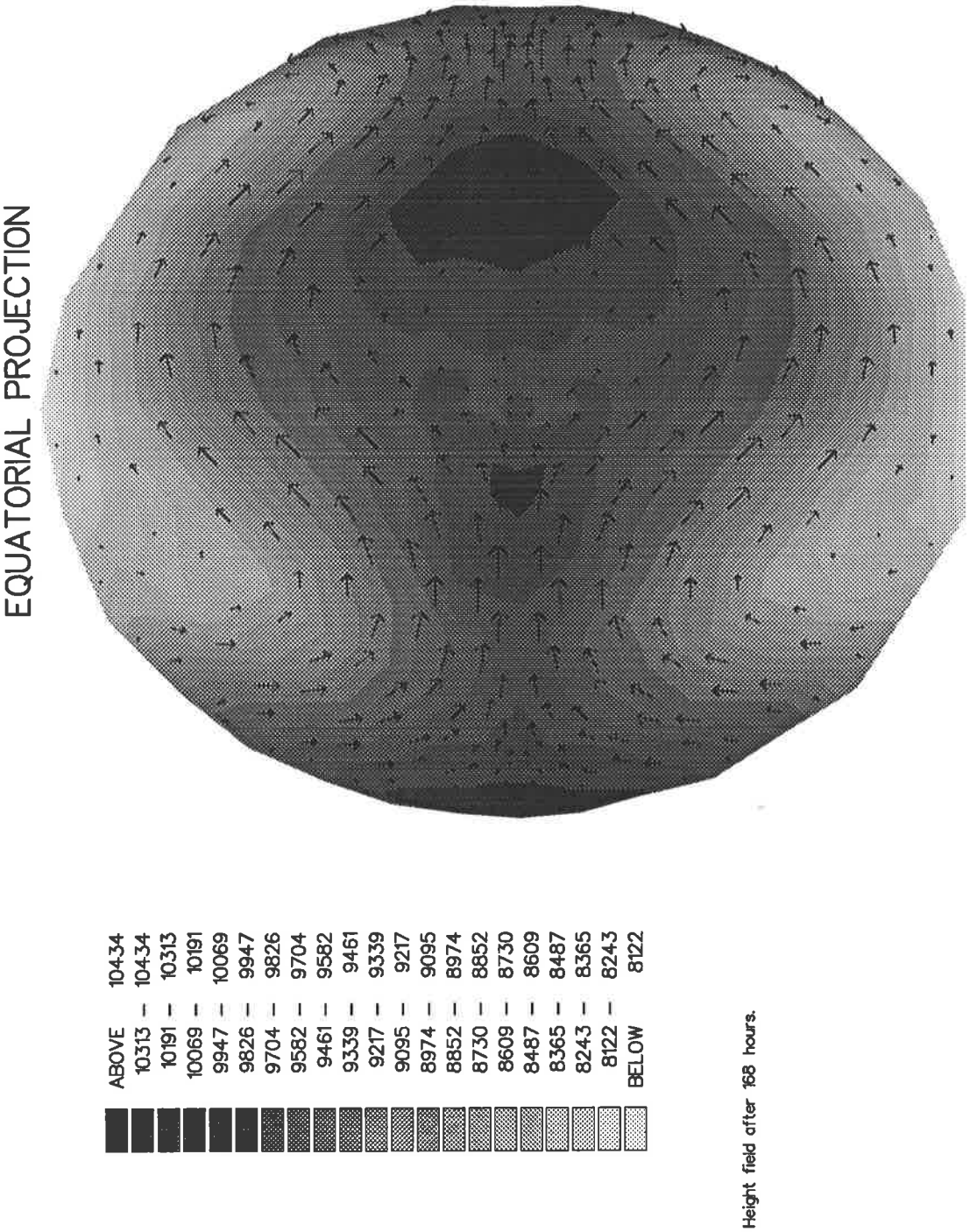

Figure 20: Equatorial projection of the height field and winds on the 3^{rd} grid after 7 days.

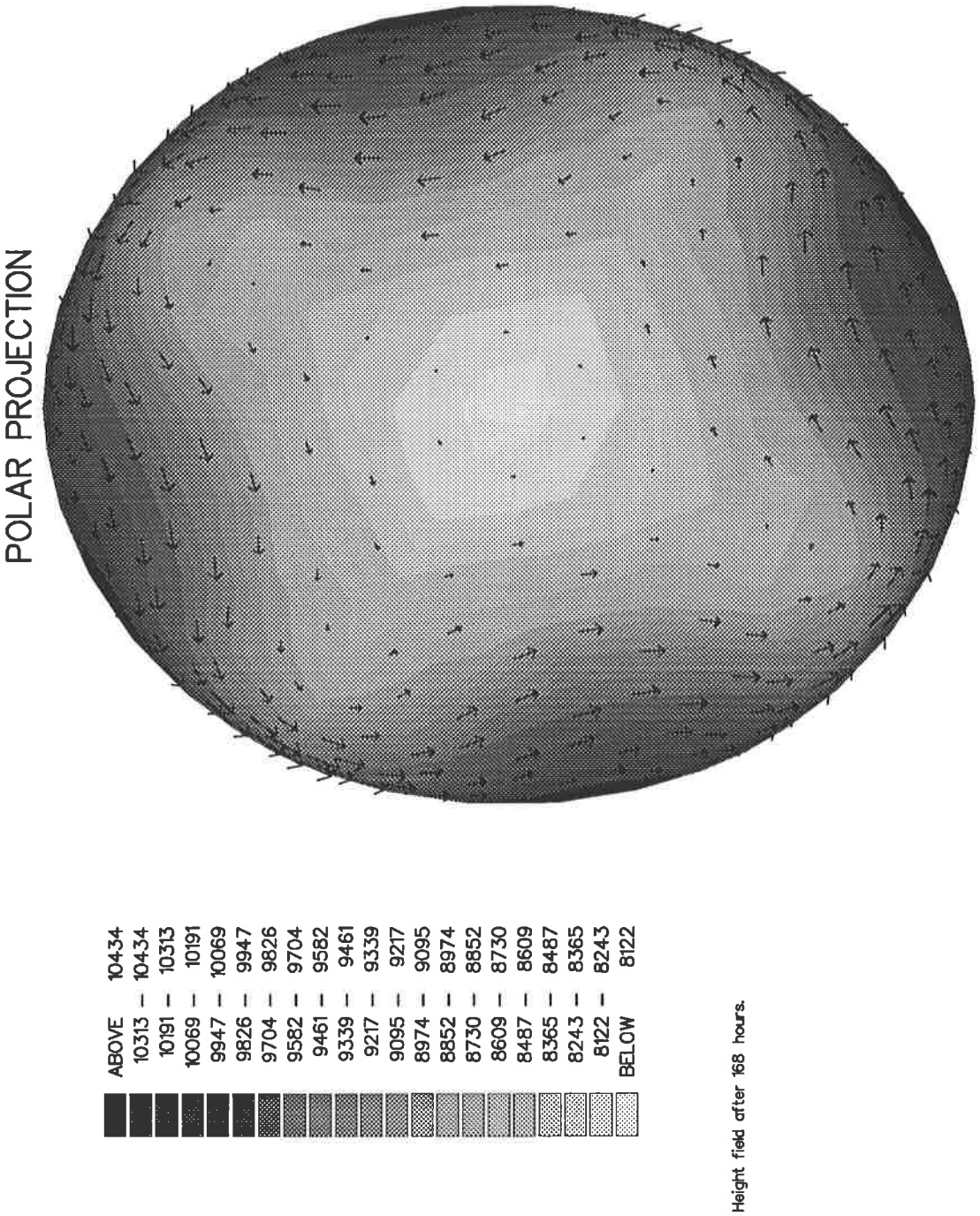

Figure 21: Polar projection of the height field and winds on the 3^{rd} grid after 7 days.

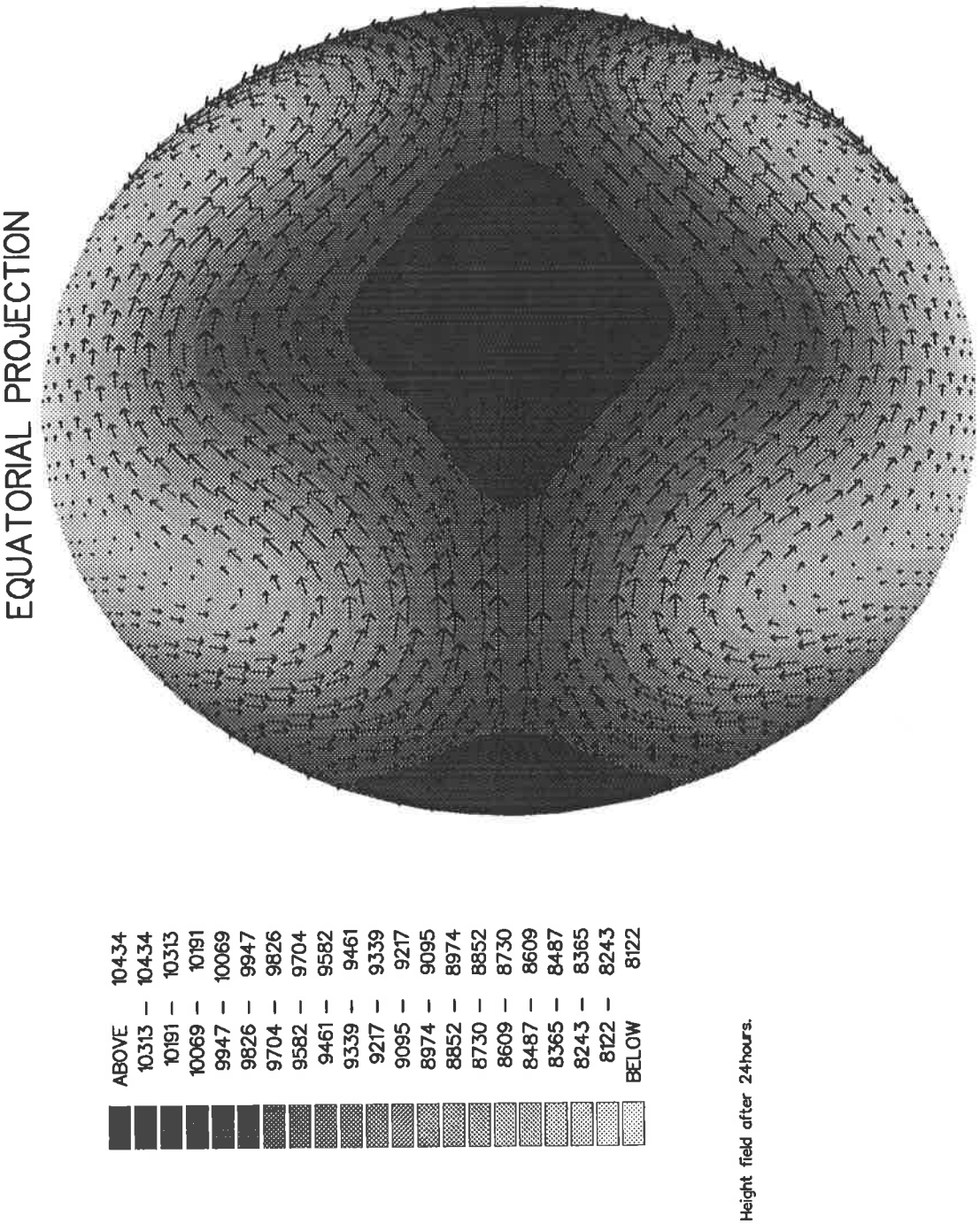

Figure 22: Equatorial projection of the height field and winds on the 4^{th} grid after 1 day.

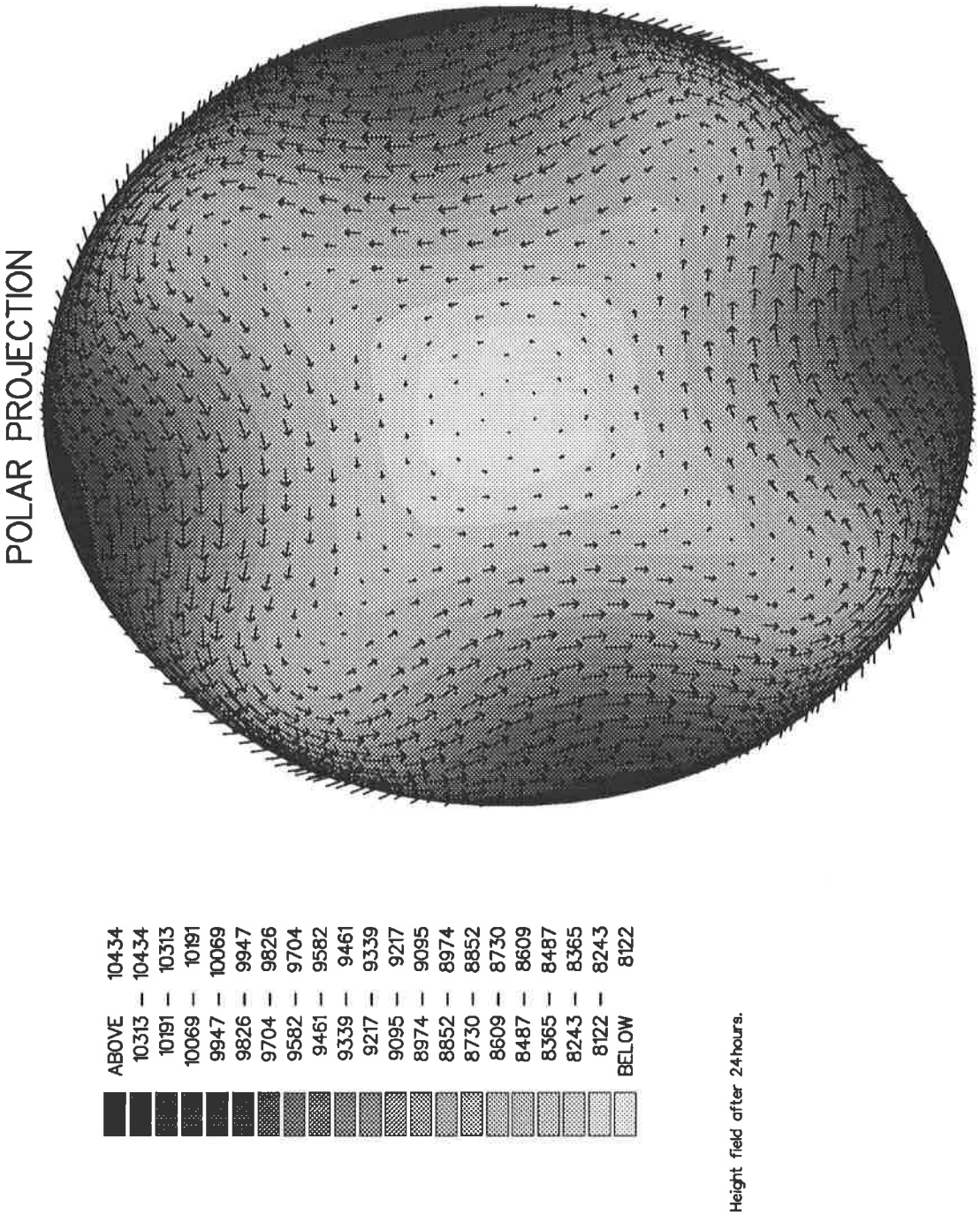

Figure 23: Polar projection of the height field and winds on the 4^{th} grid after 1 day.

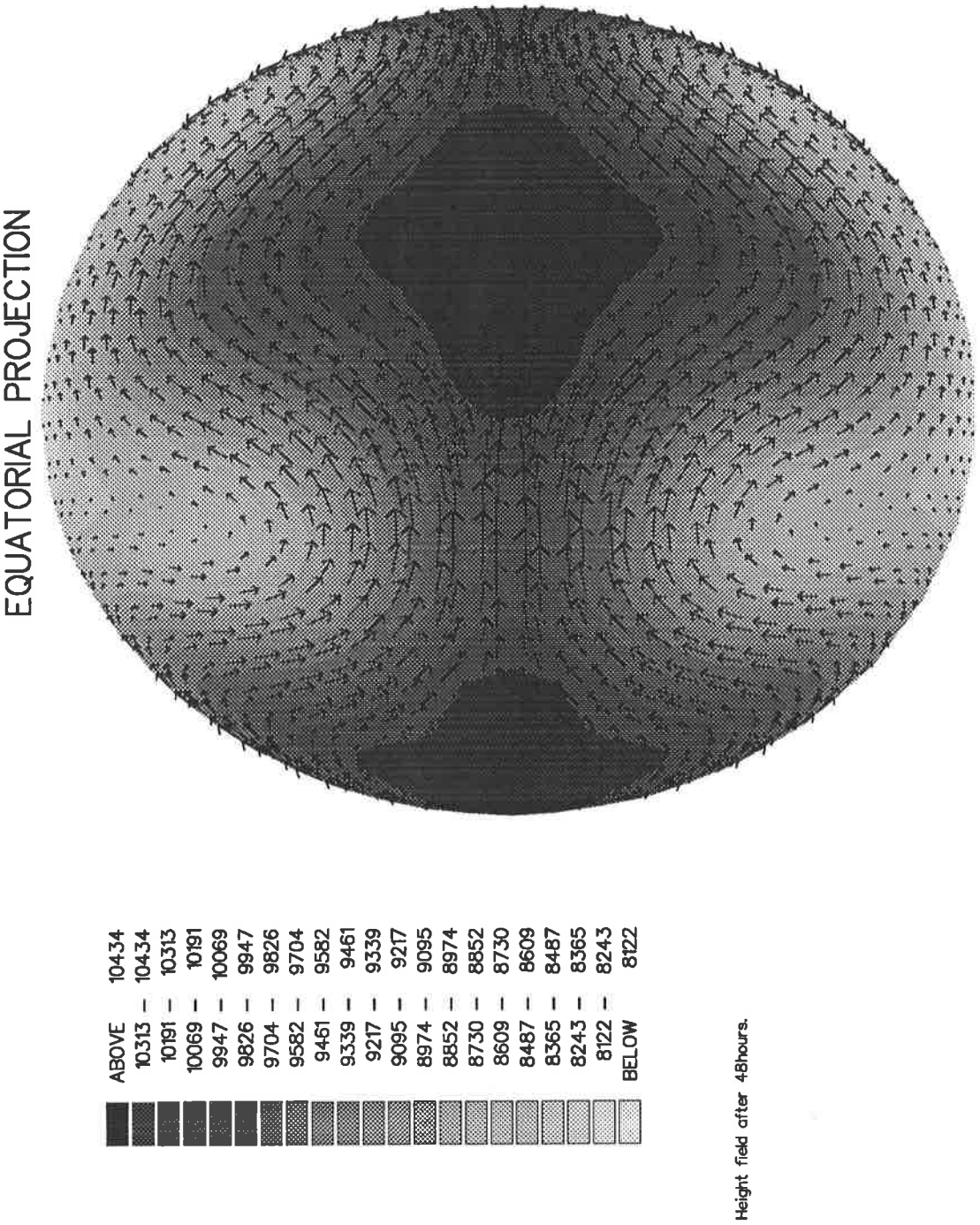

Figure 24: Equatorial projection of the height field and winds on the 4^{th} grid after 2 days.

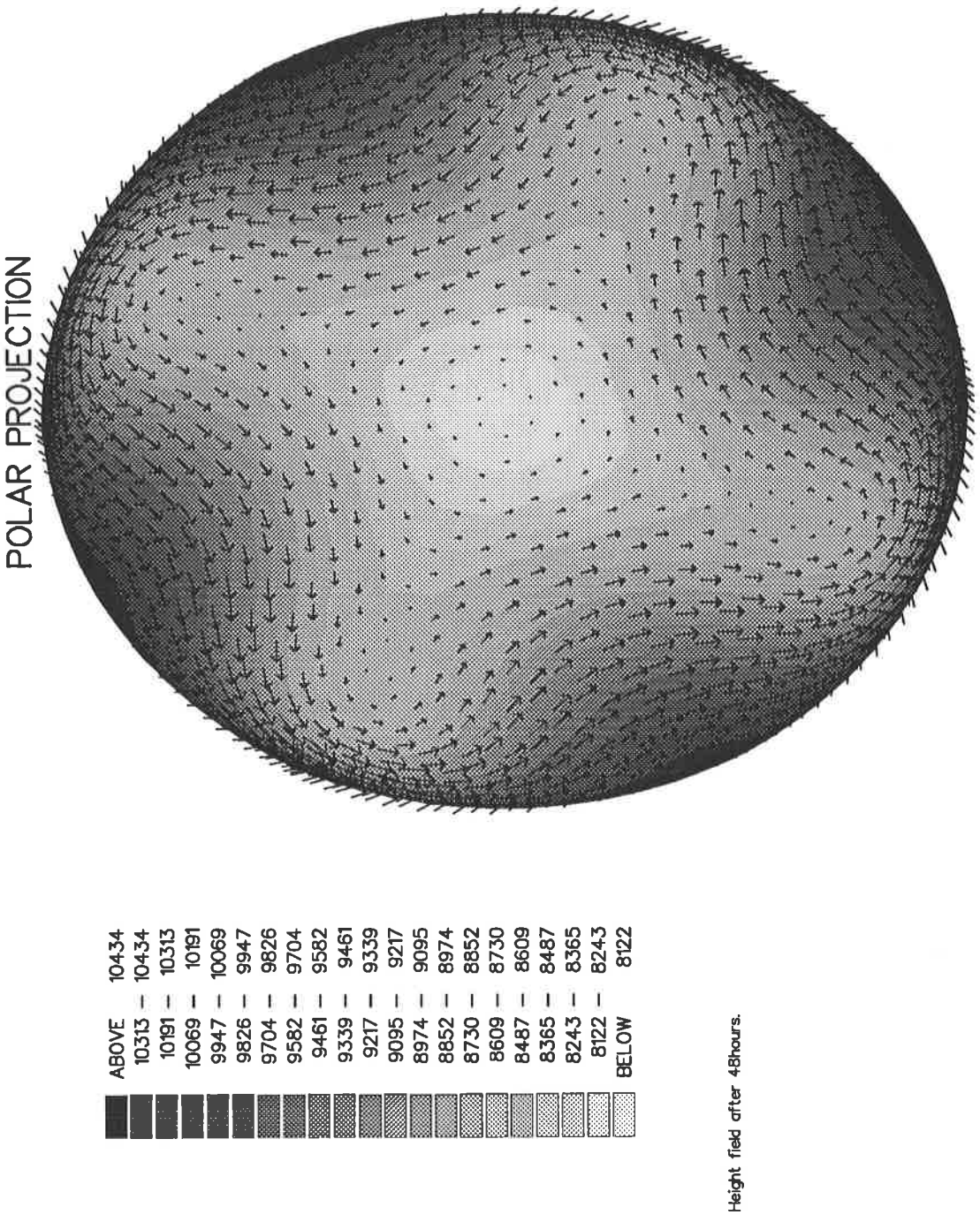

Figure 25: Polar projection of the height field and winds on the 4^{th} grid after 2 days.

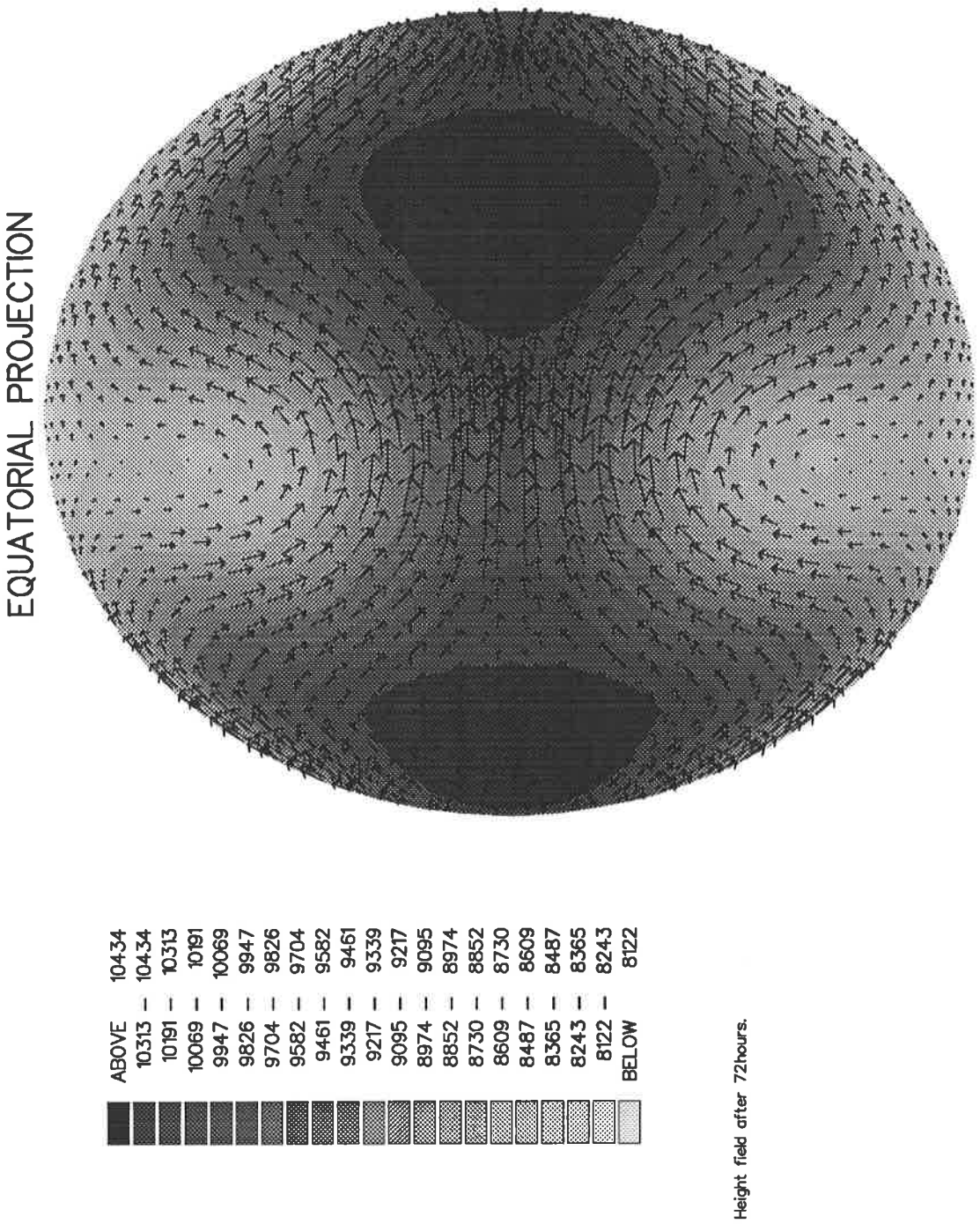

Figure 26: Equatorial projection of the height field and winds on the 4^{th} grid after 3 days.

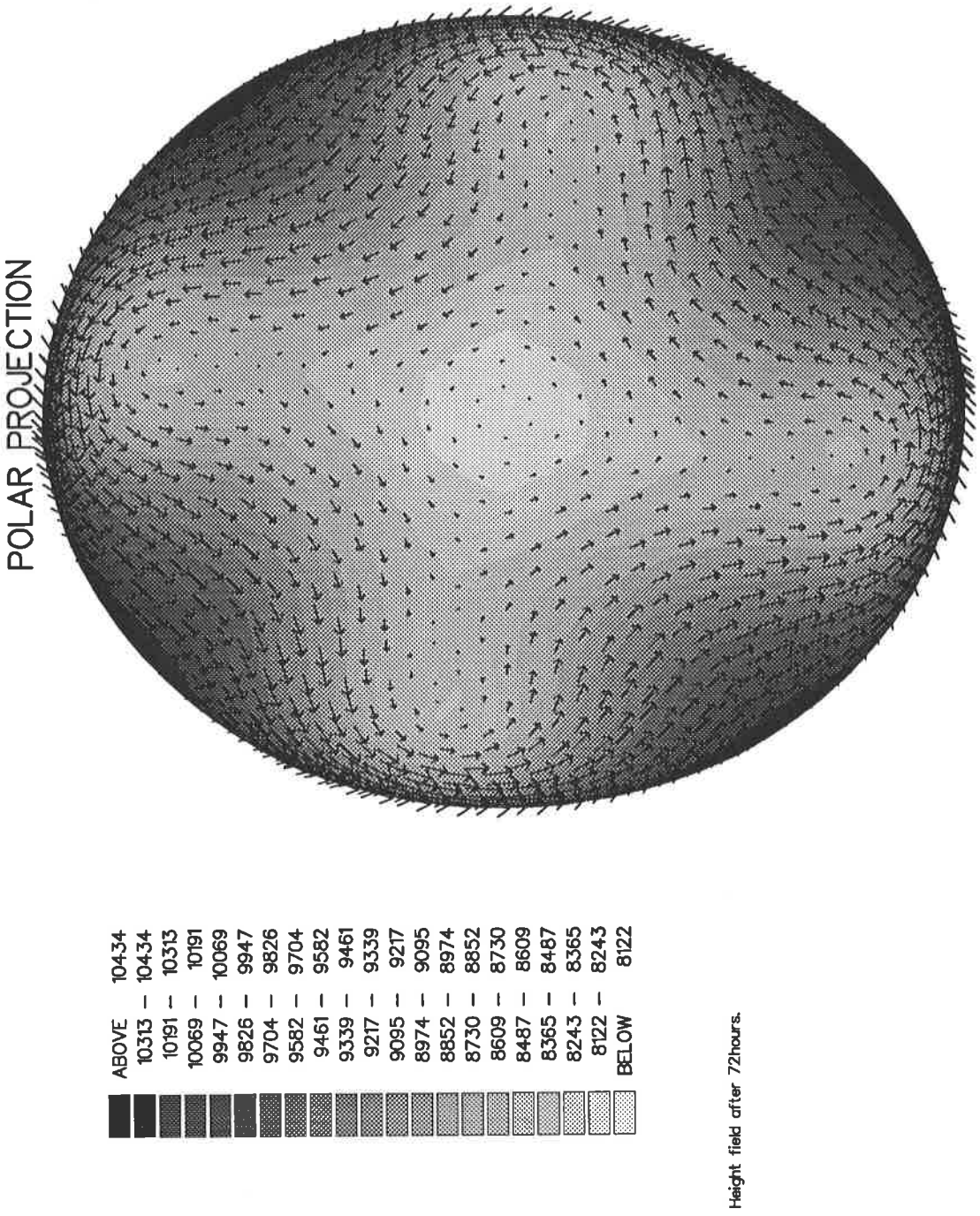

Figure 27: Polar projection of the height field and winds on the 4^{th} grid after 3 days.

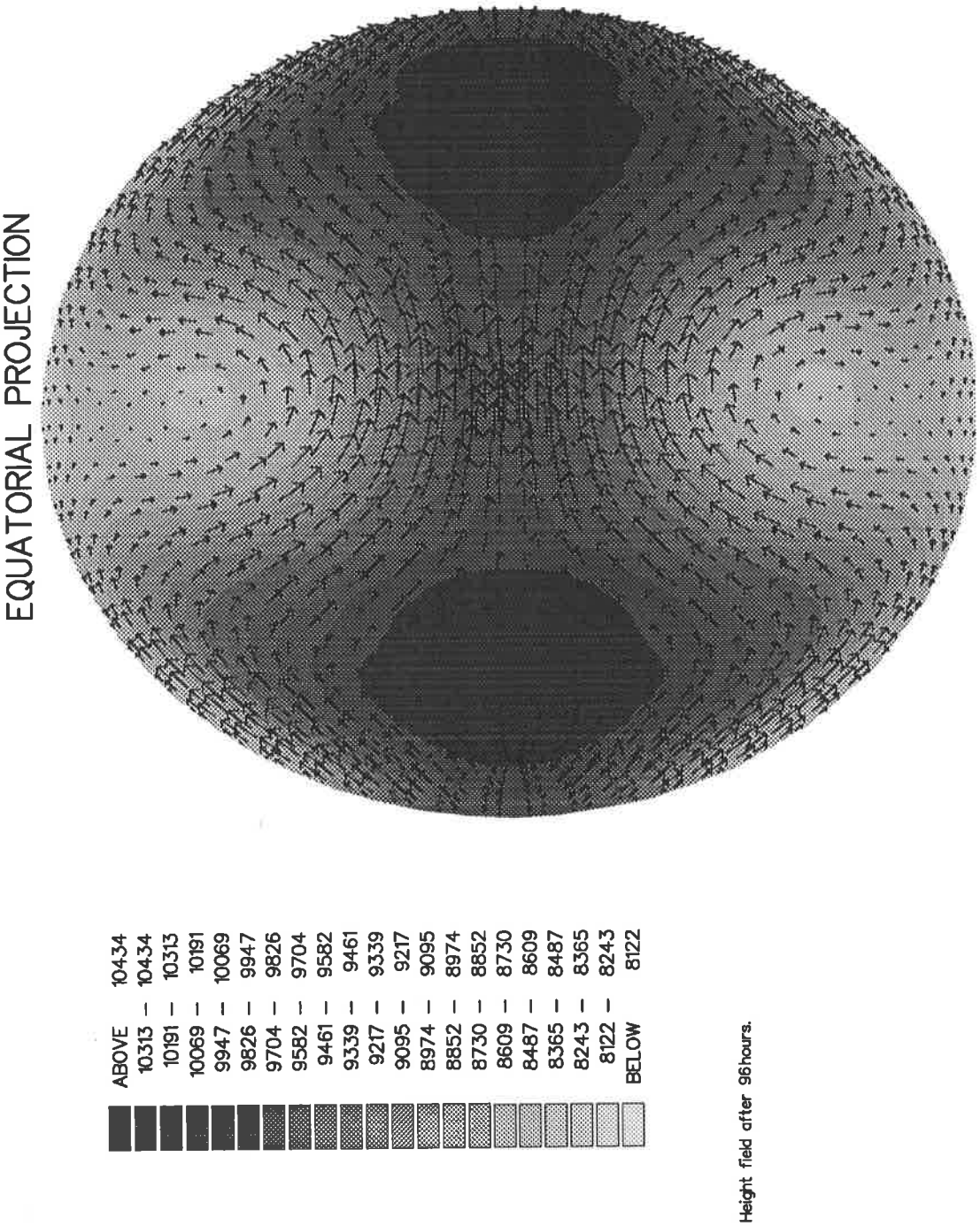

Figure 28: Equatorial projection of the height field and winds on the 4^{th} grid after 4 days.

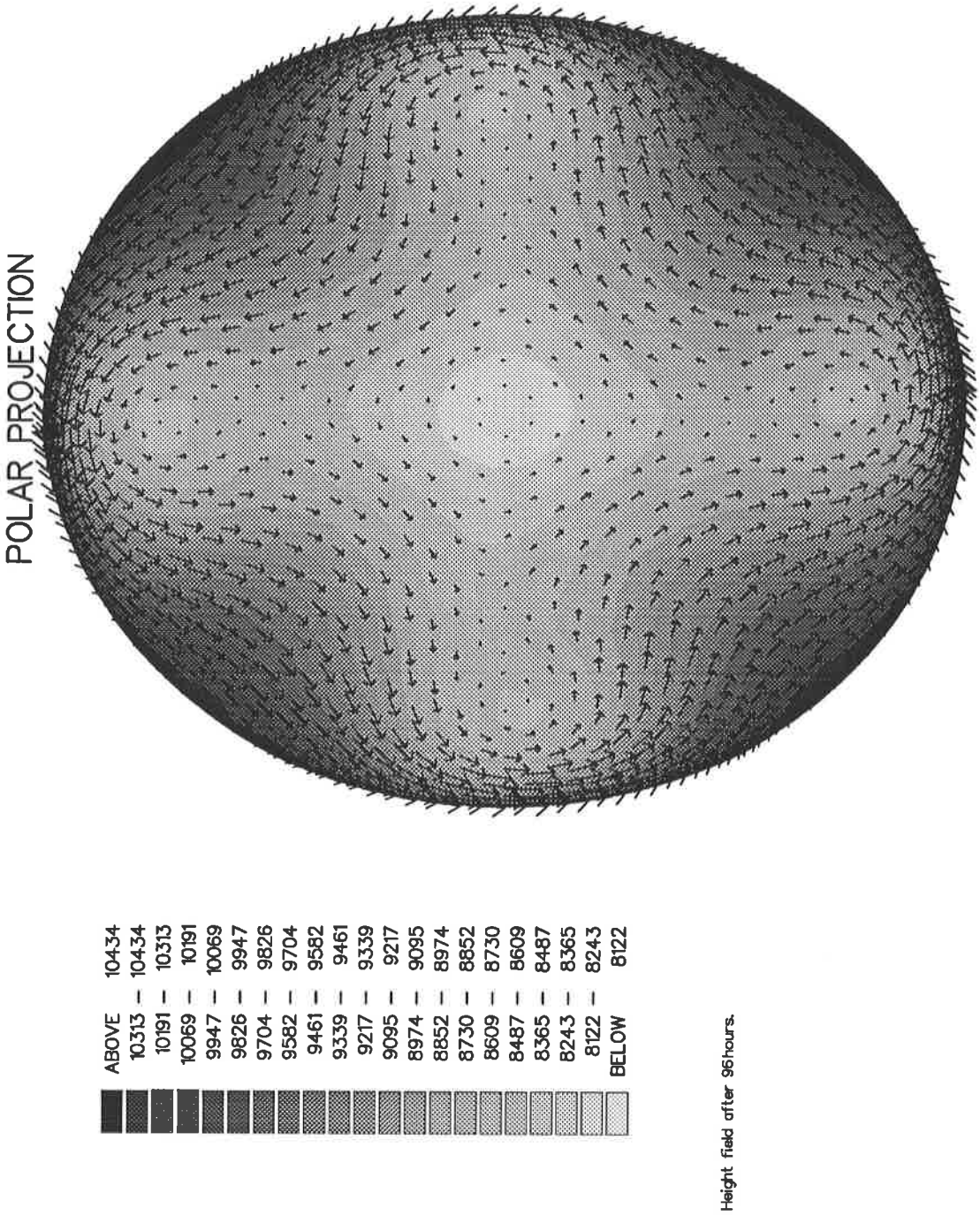

Figure 29: Polar projection of the height field and winds on the 4^{th} grid after 4 days.

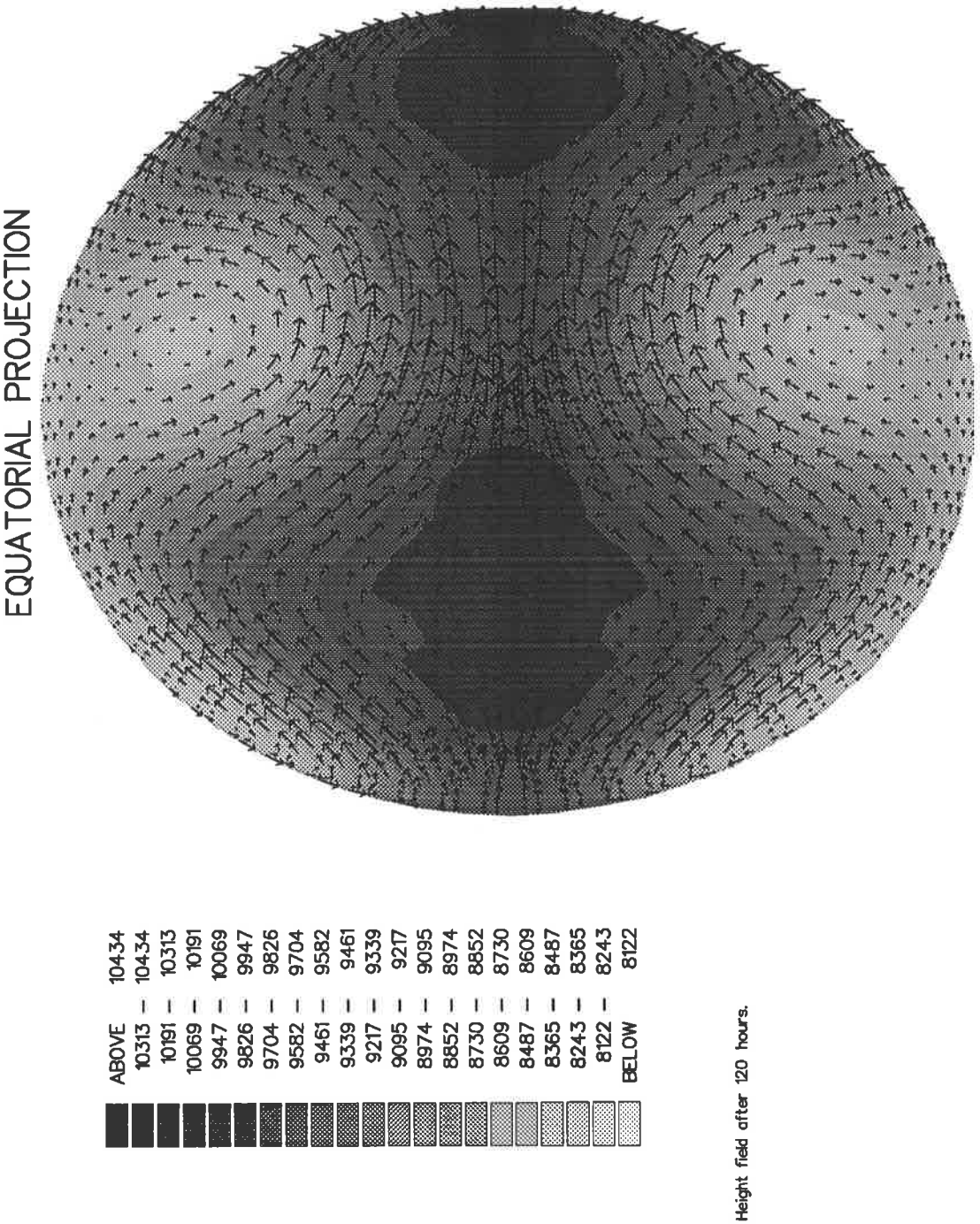

Figure 30: Equatorial projection of the height field and winds on the 4^{th} grid after 5 days.

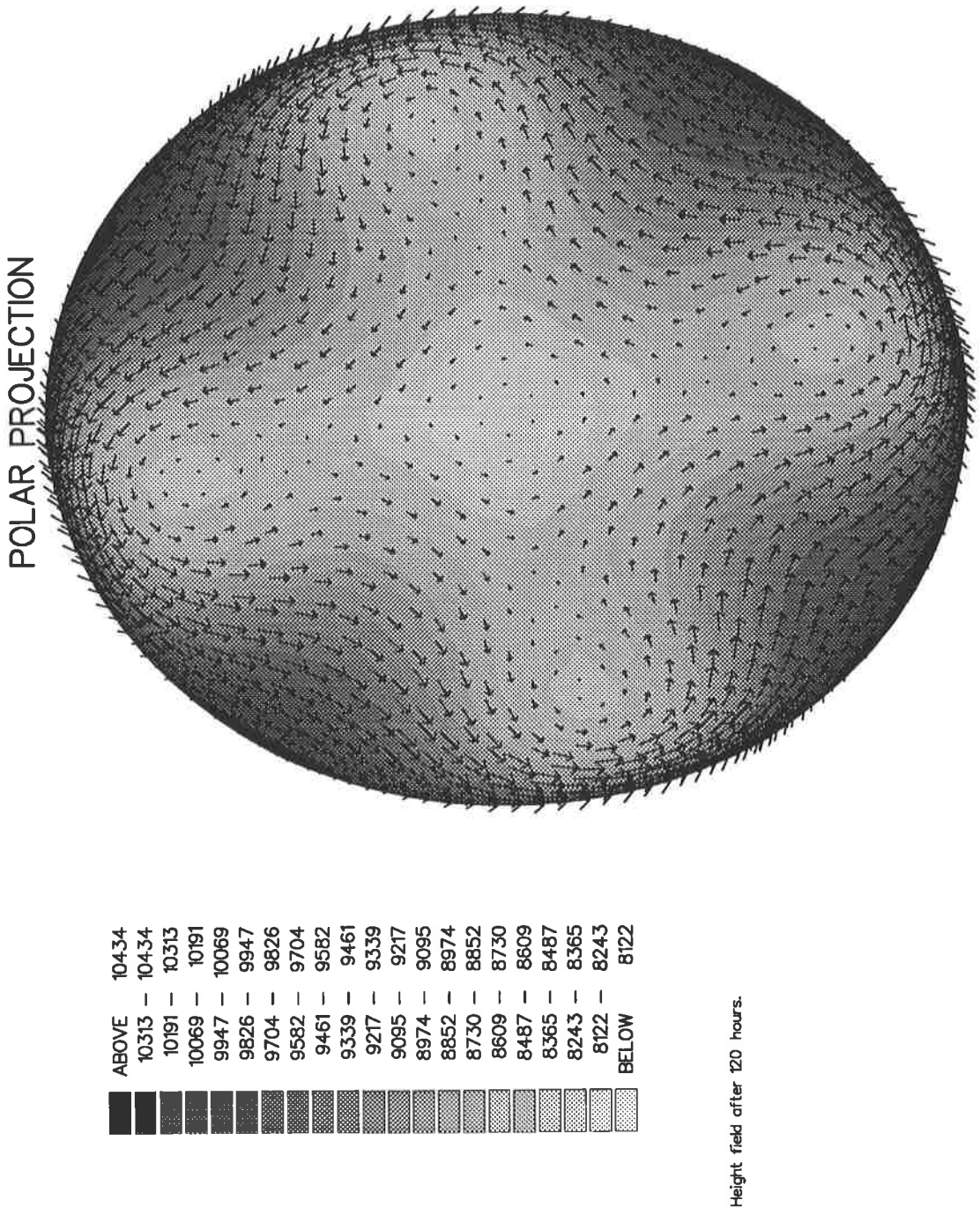

Figure 31: Polar projection of the height field and winds on the 4^{th} grid after 5 days.

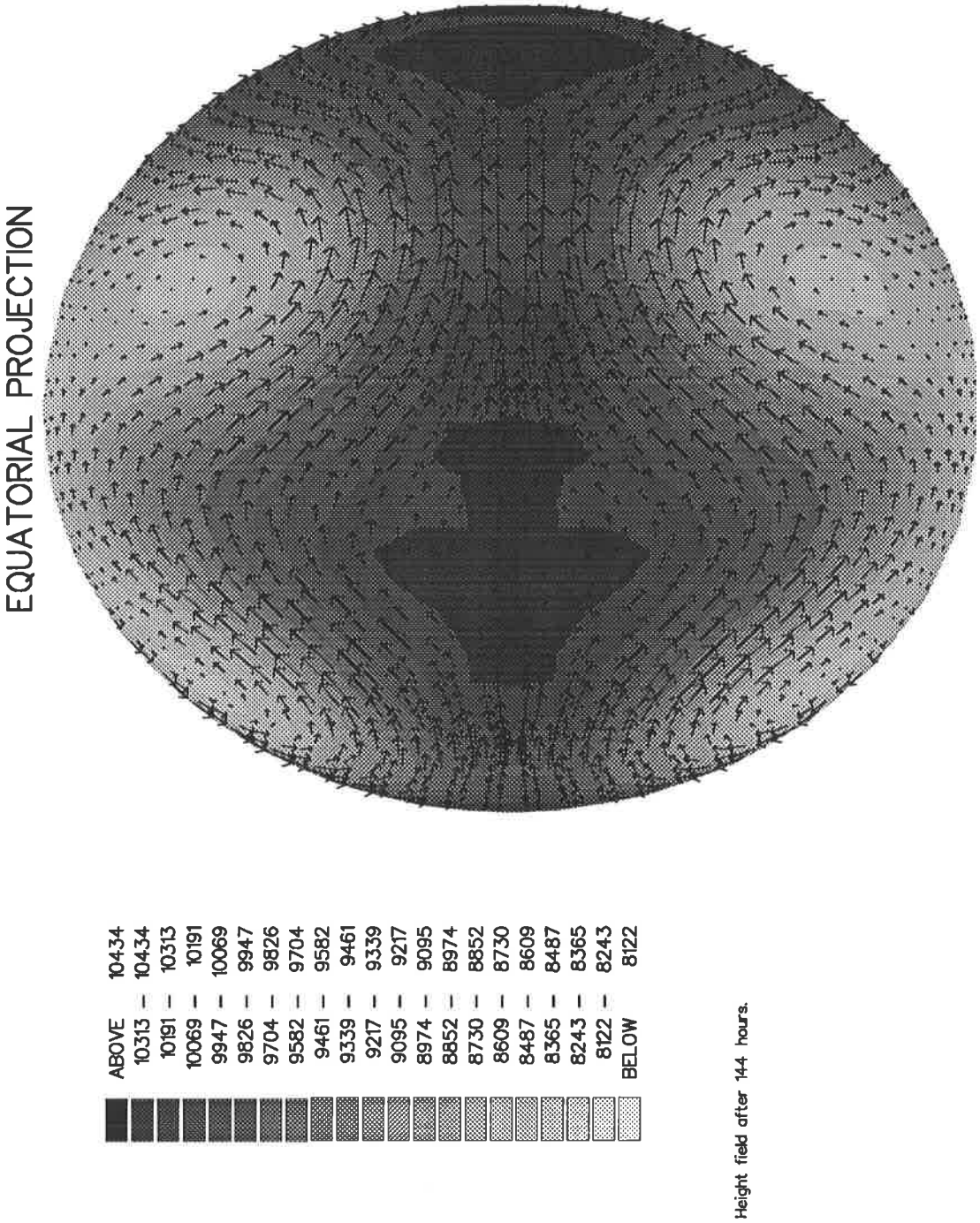

Figure 32: Equatorial projection of the height field and winds on the 4^{th} grid after 6 days.

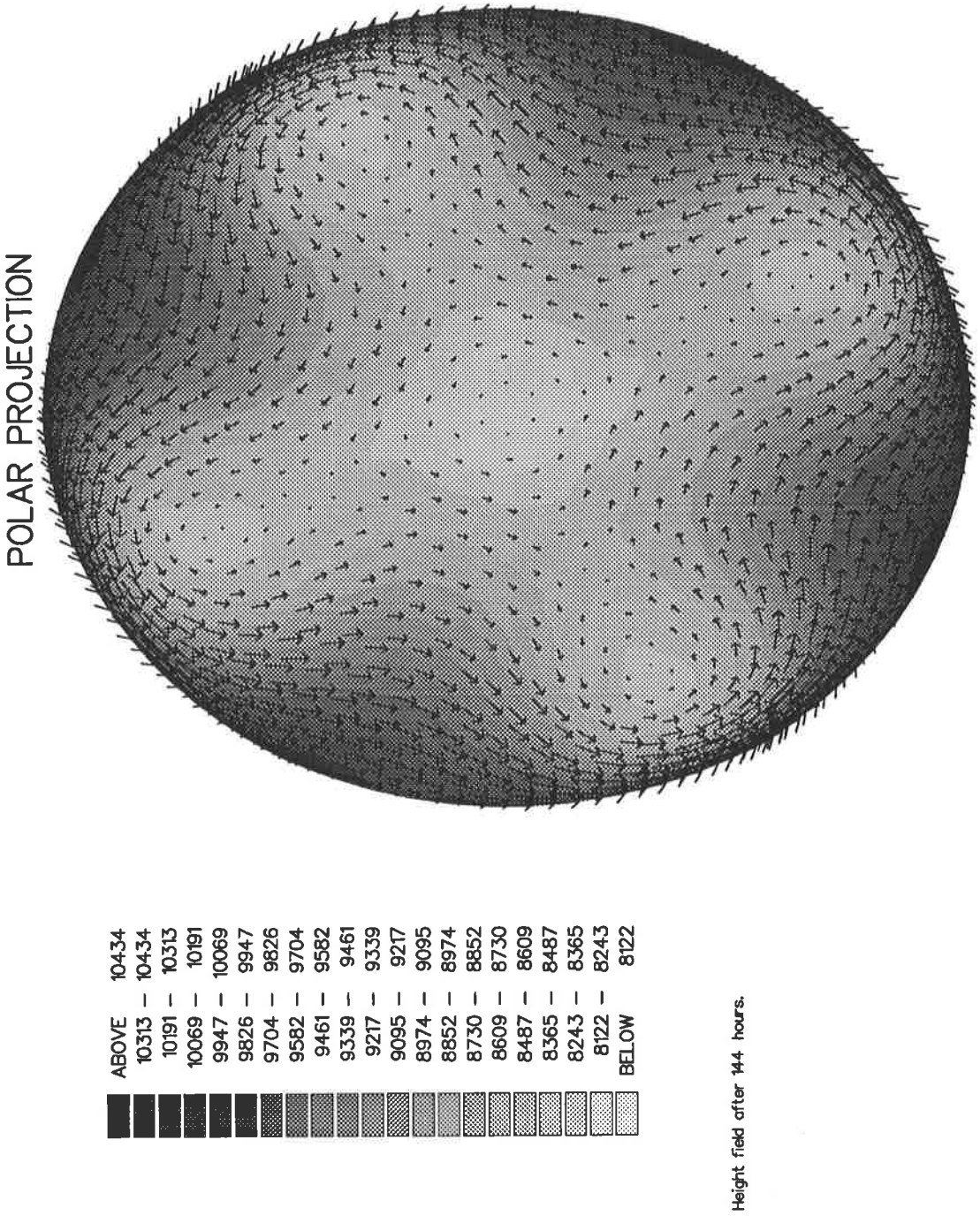

Figure 33: Polar projection of the height field and winds on the 4^{th} grid after 6 days.

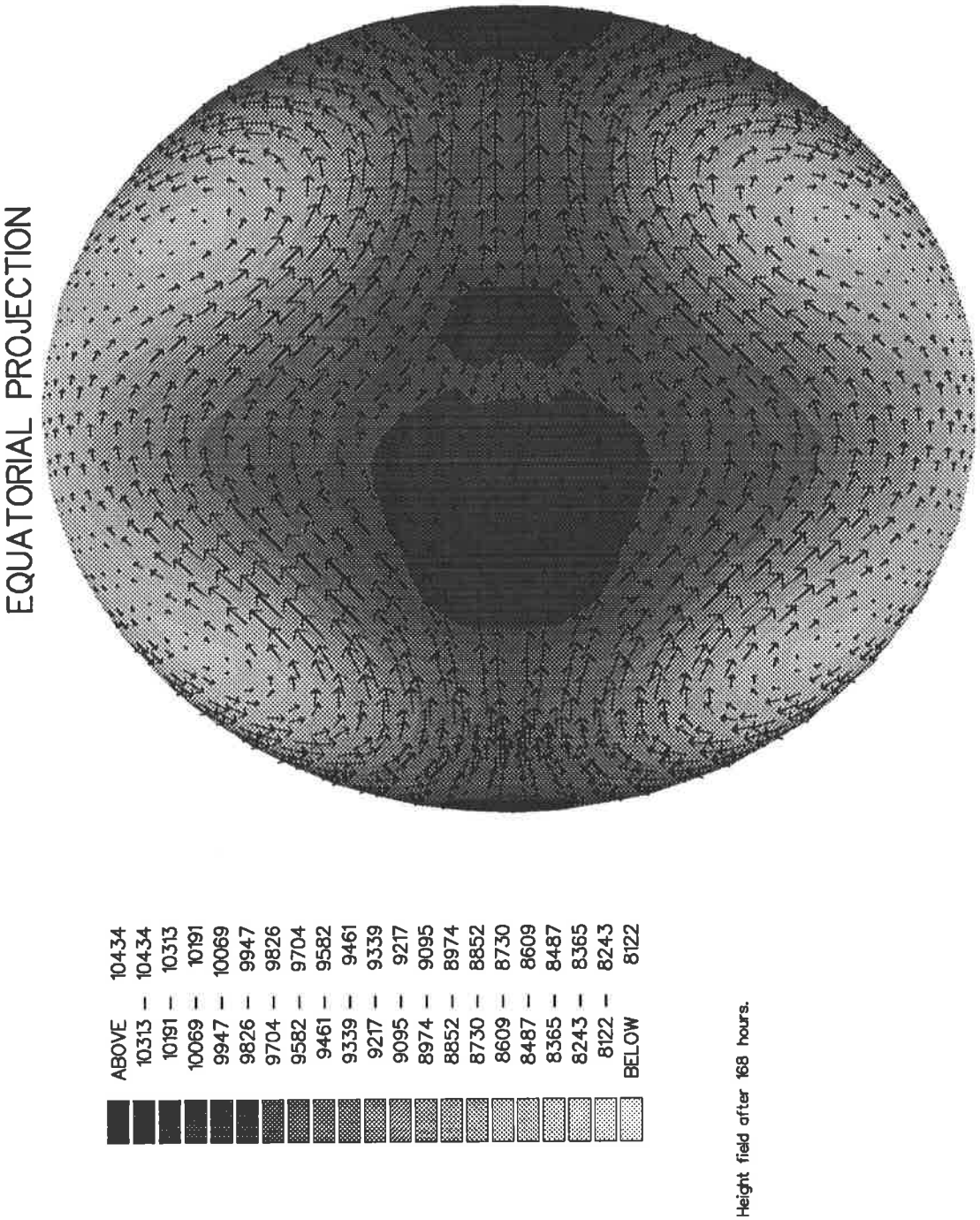

Figure 34: Equatorial projection of the height field and winds on the 4^{th} grid after 7 days.

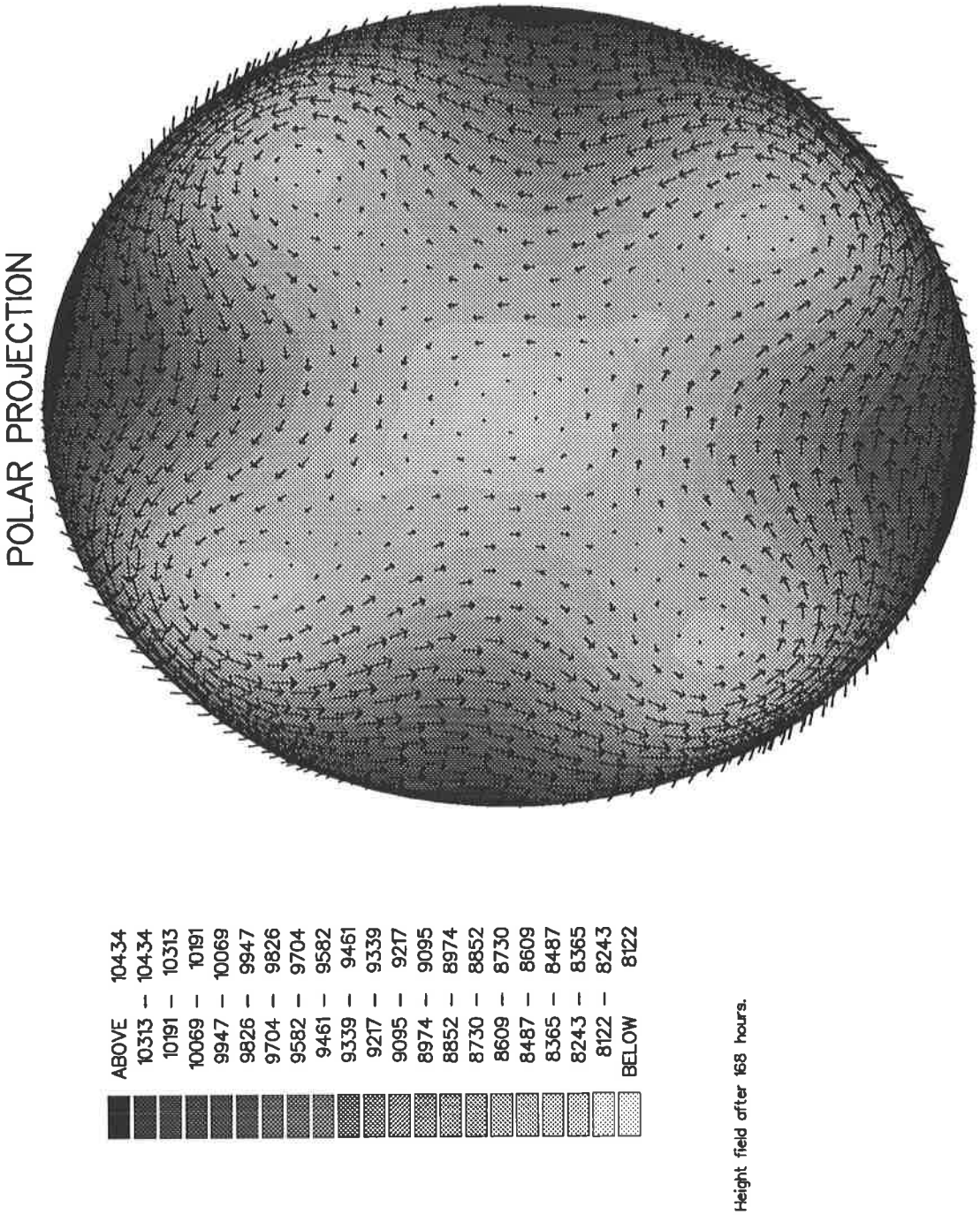

Figure 35: Polar projection of the height field and winds on the 4^{th} grid after 7 days.

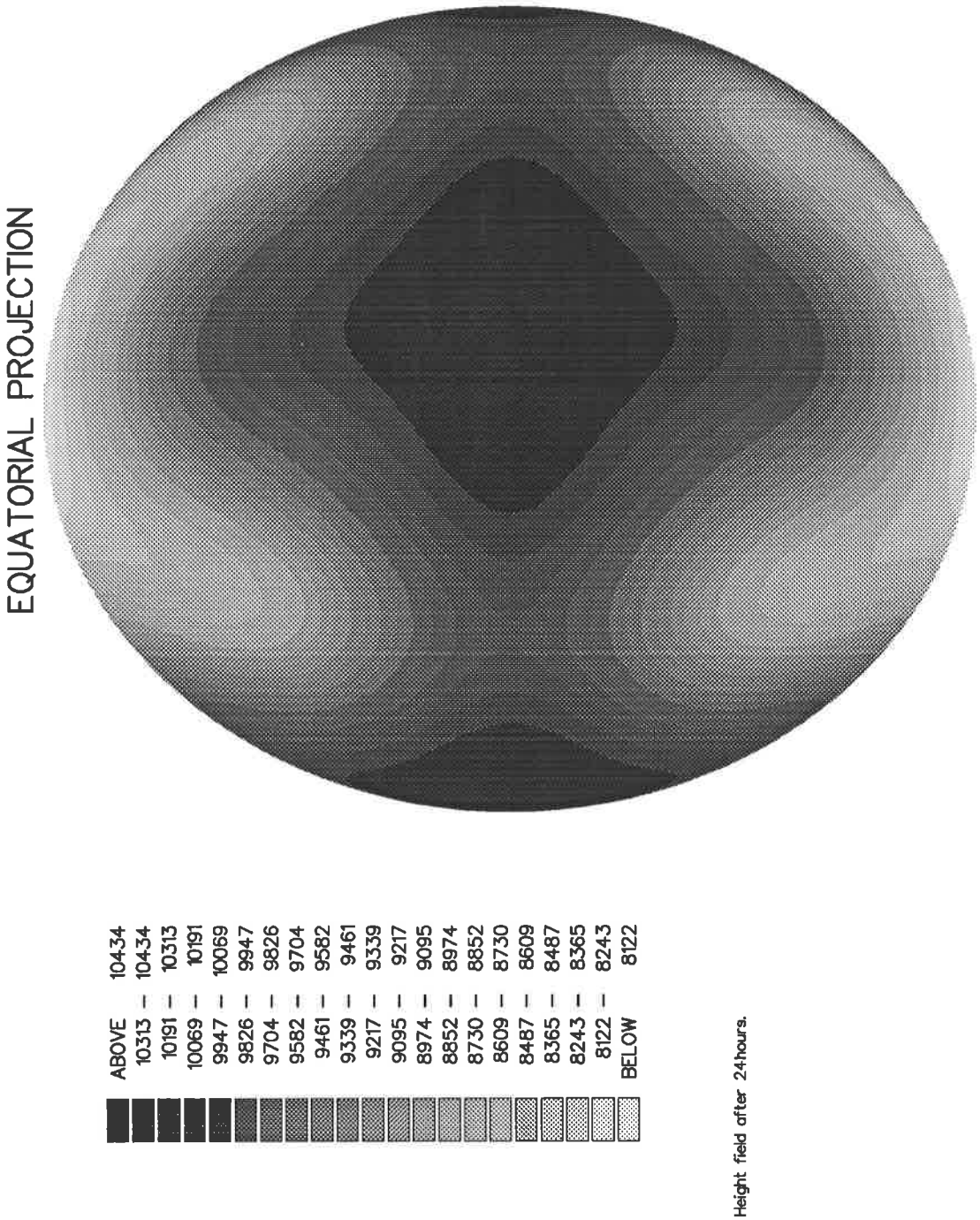

Figure 36: Equatorial projection of the height field on the 5^{th} grid after 1 day.

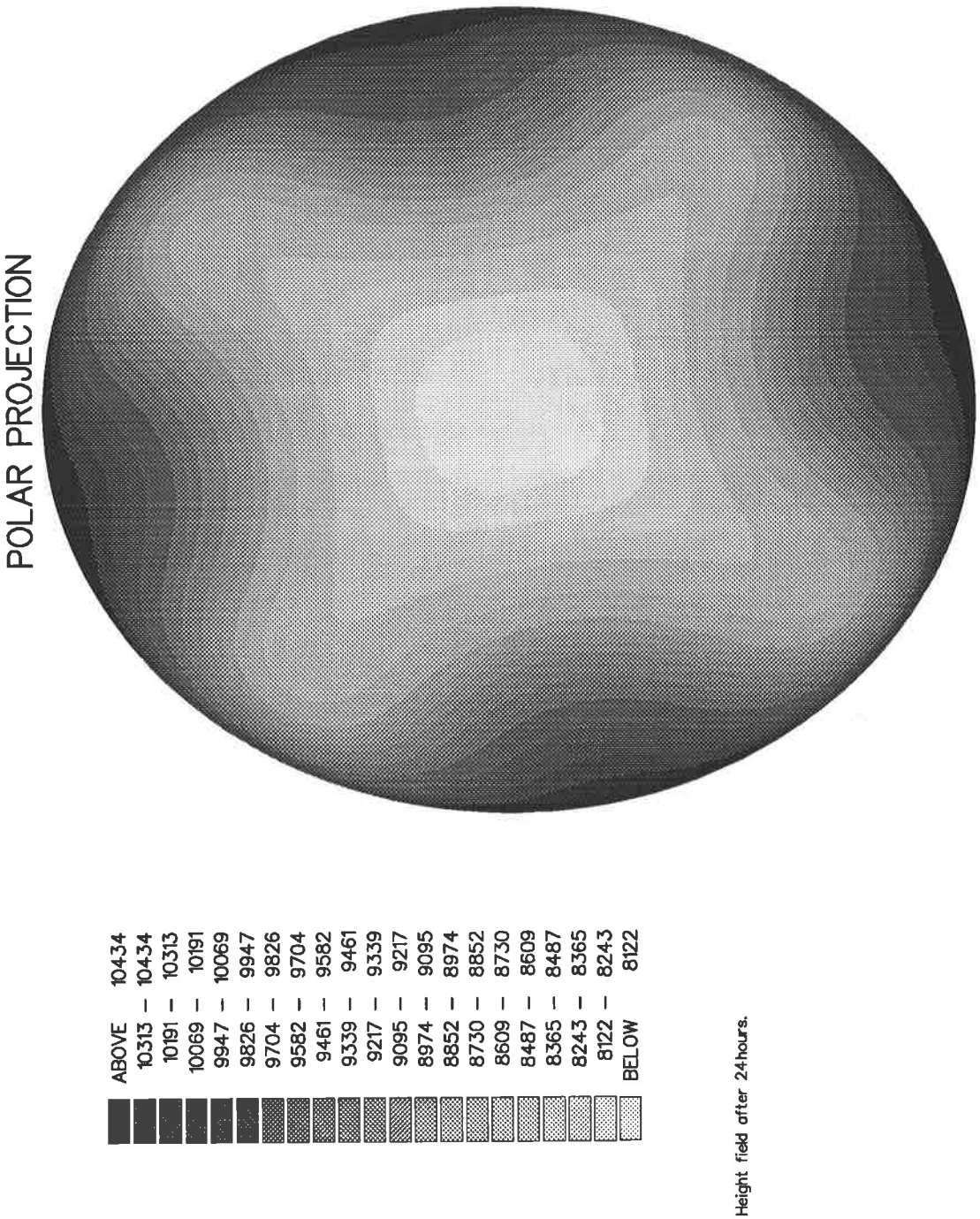

Figure 37: Polar projection of the height field on the 5^{th} grid after 1 day.

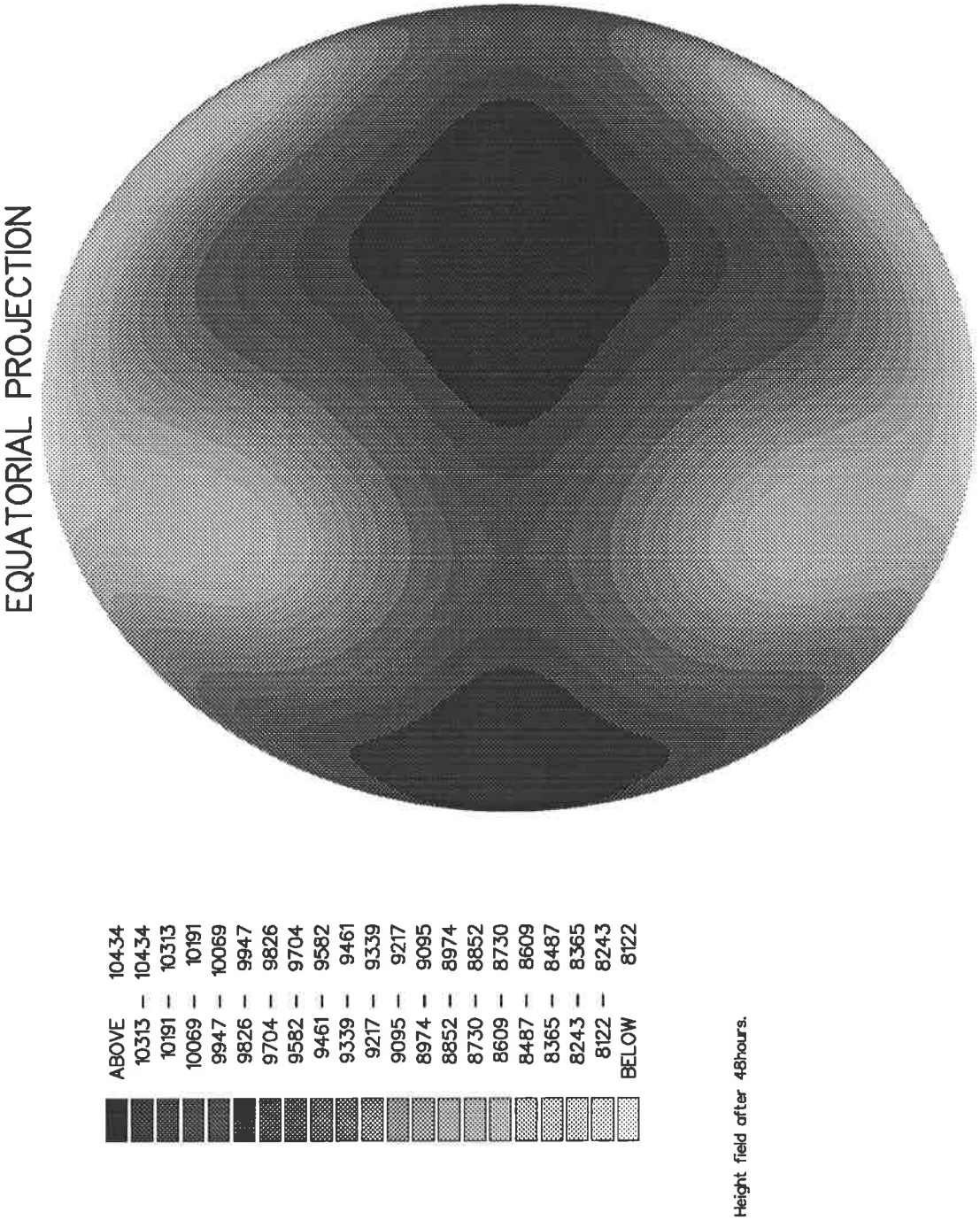

Figure 38: Equatorial projection of the height field on the 5^{th} grid after 2 days.

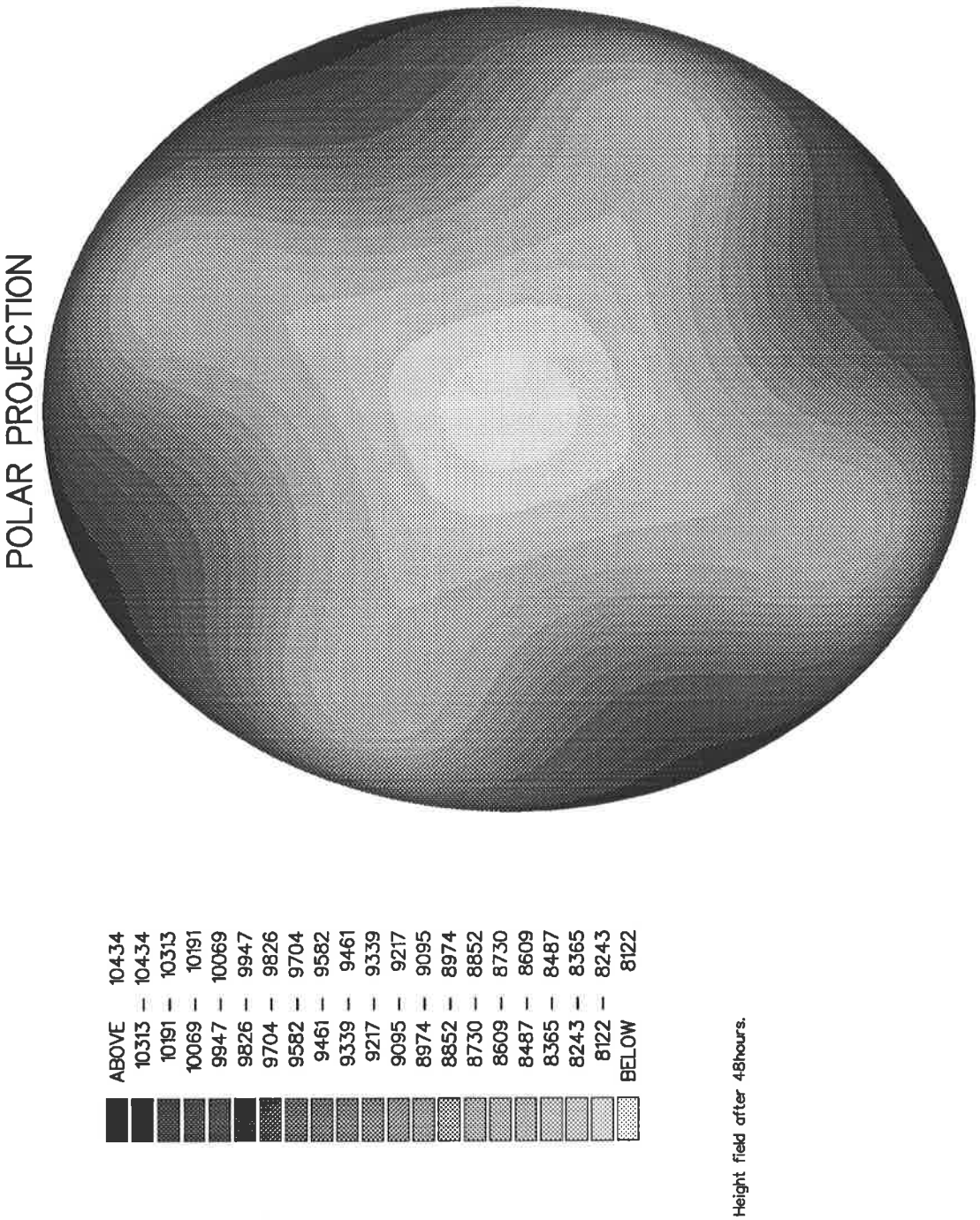

Figure 39: Polar projection of the height field on the 5^{th} grid after 2 days.

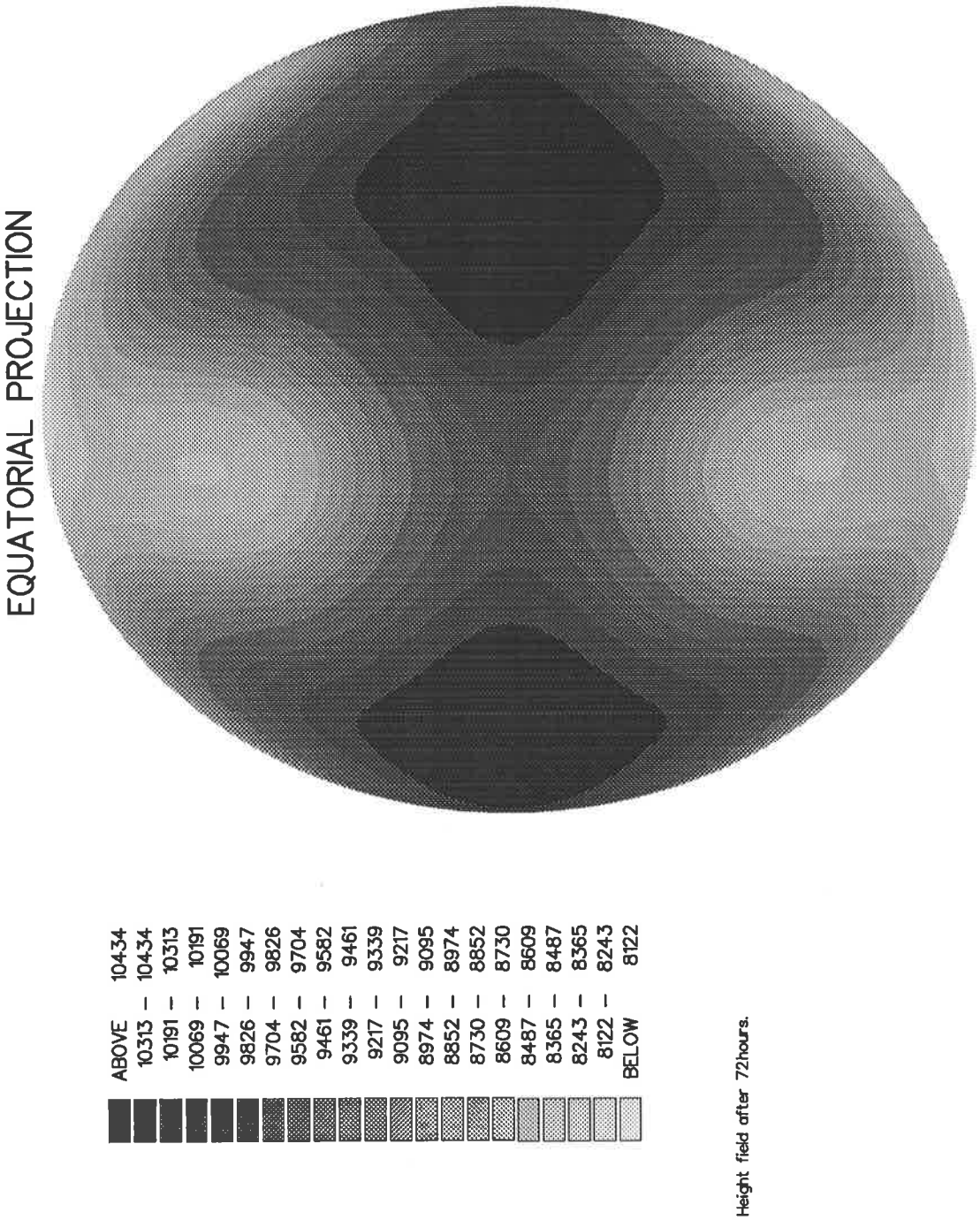

Figure 40: Equatorial projection of the height field on the 5^{th} grid after 3 days.

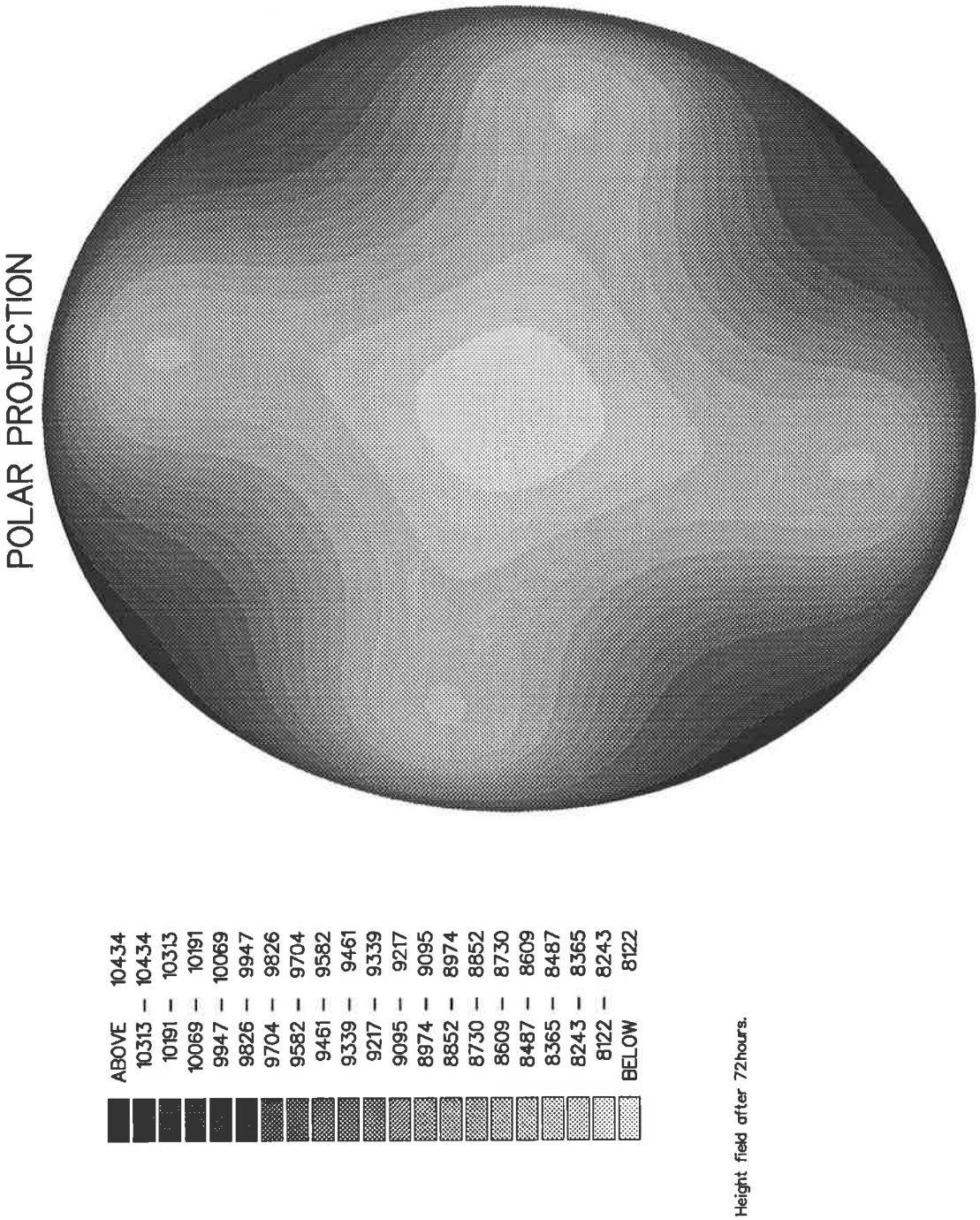

Figure 41: Polar projection of the height field on the 5^{th} grid after 3 days.

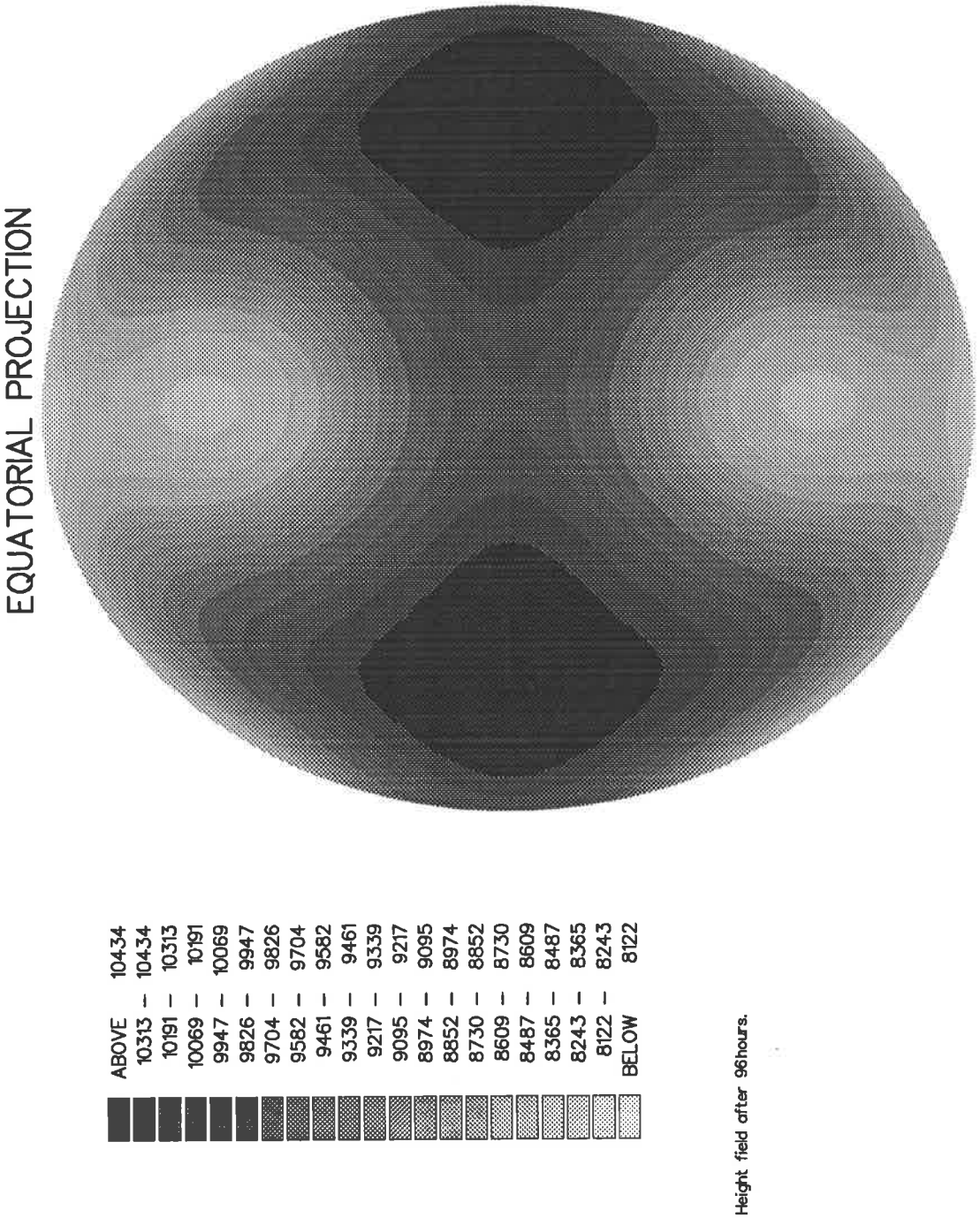

Figure 42: Equatorial projection of the height field on the 5^{th} grid after 4 days.

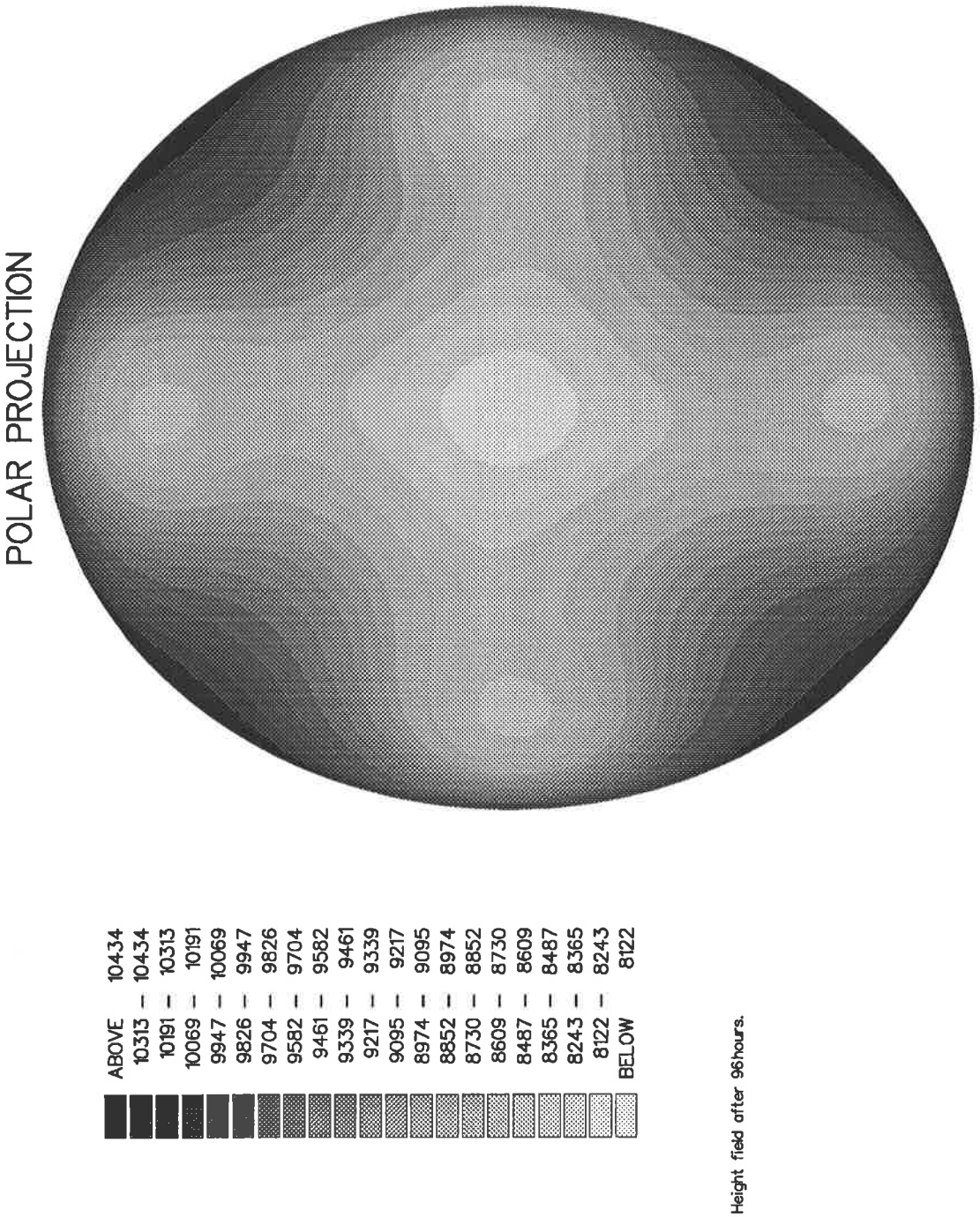

Figure 43: Polar projection of the height field on the 5^{th} grid after 4 days.

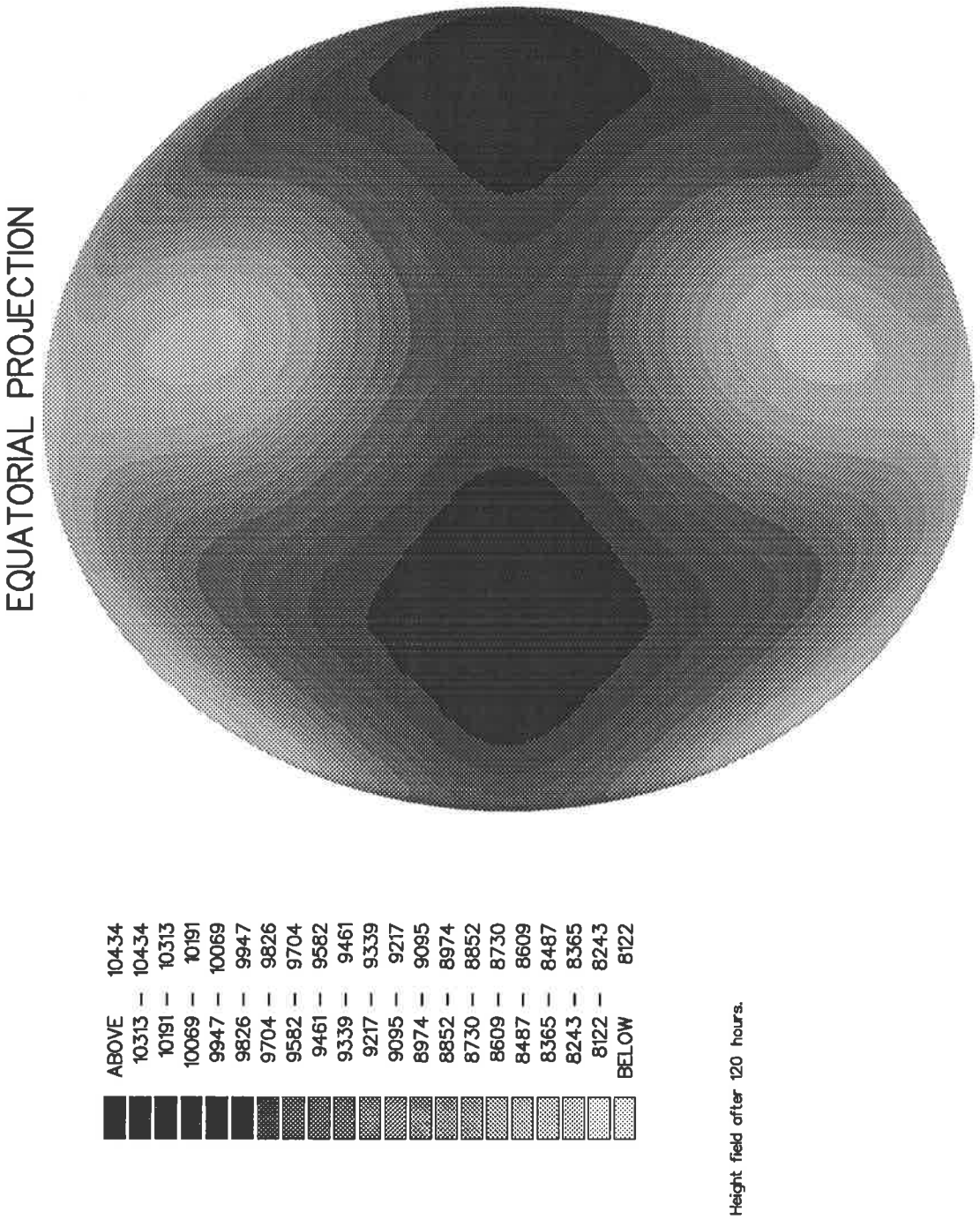

Figure 44: Equatorial projection of the height field on the 5^{th} grid after 5 days.

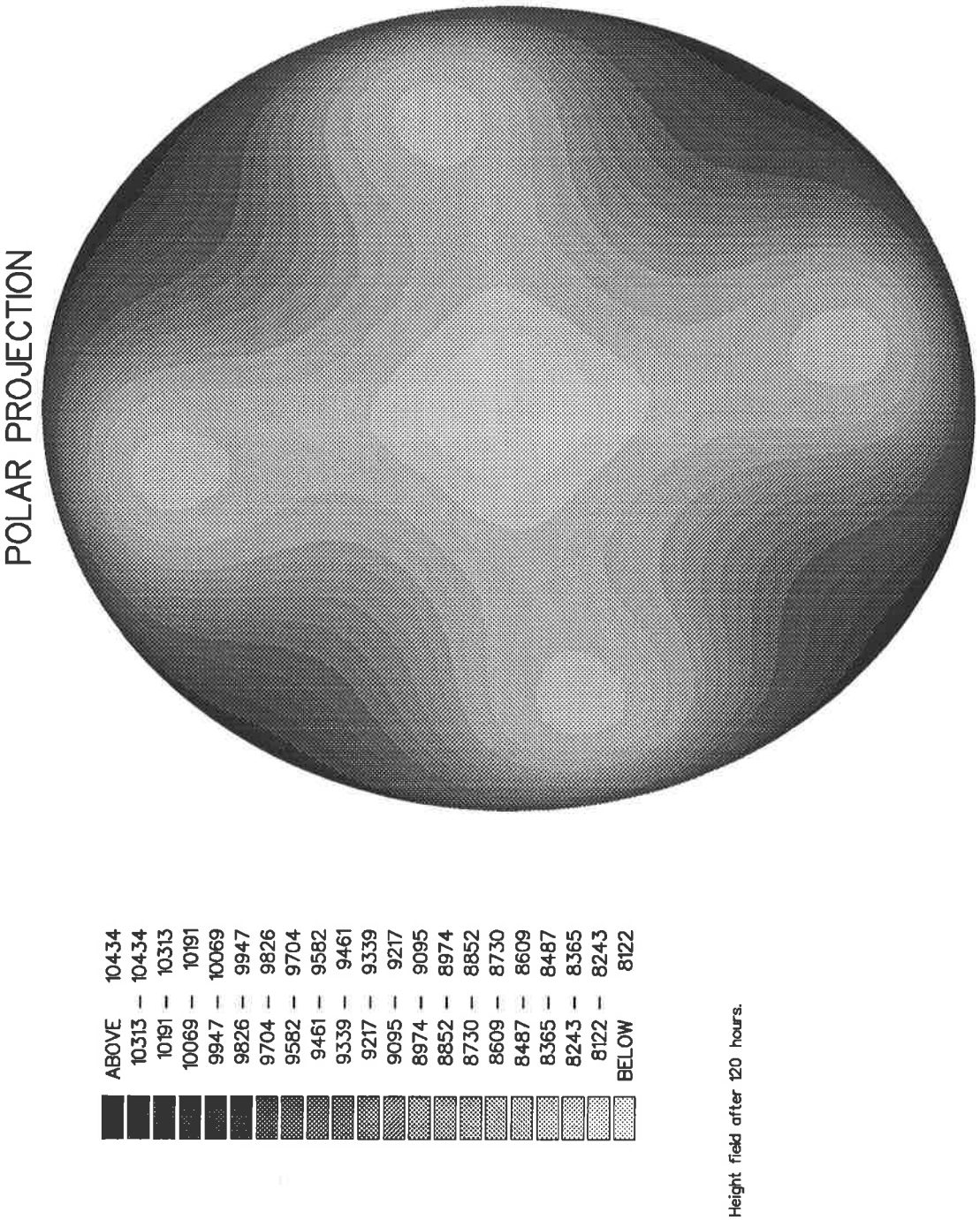

Figure 45: Polar projection of the height field on the 5^{th} grid after 5 days.

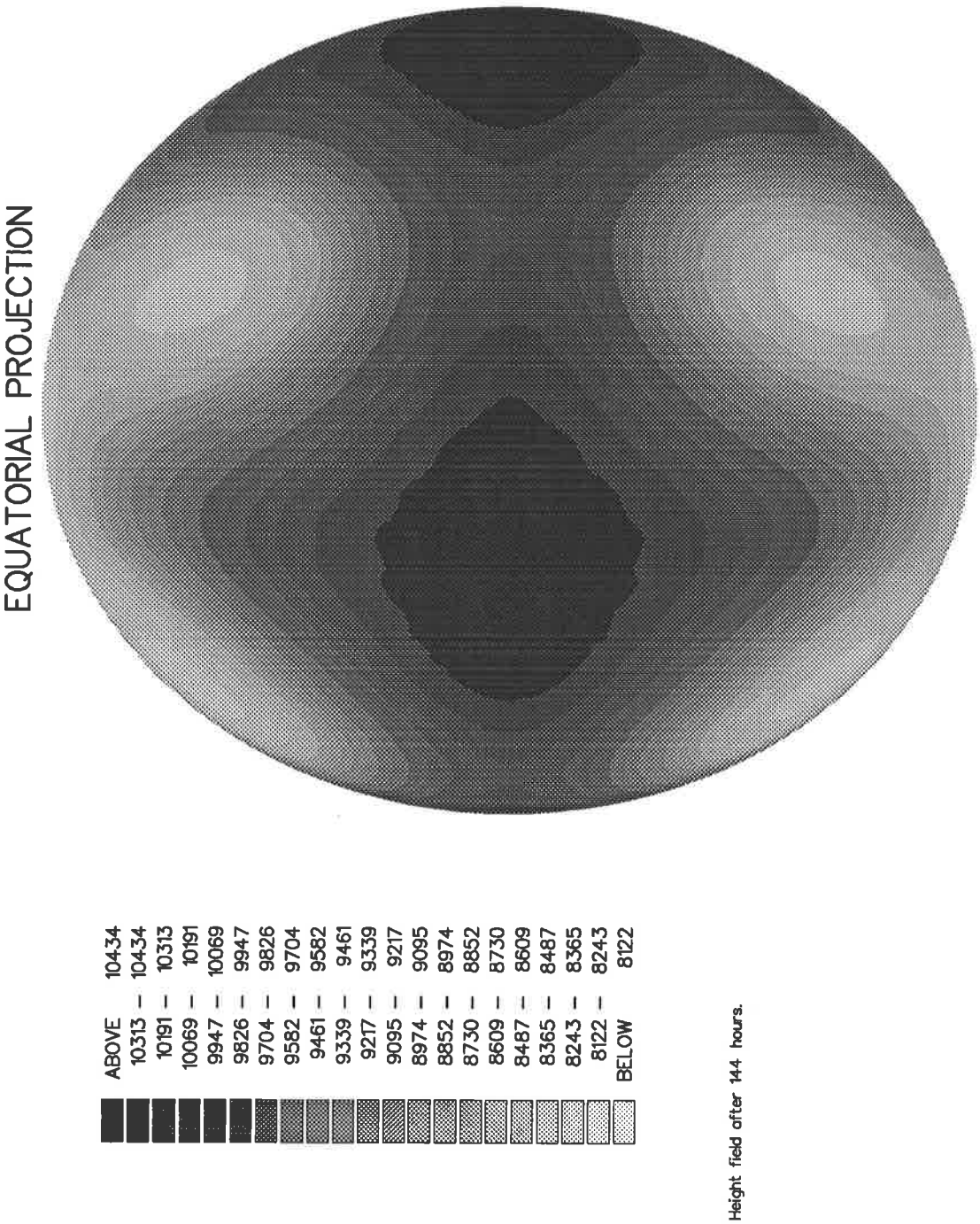

Figure 46: Equatorial projection of the height field on the 5^{th} grid after 6 days.

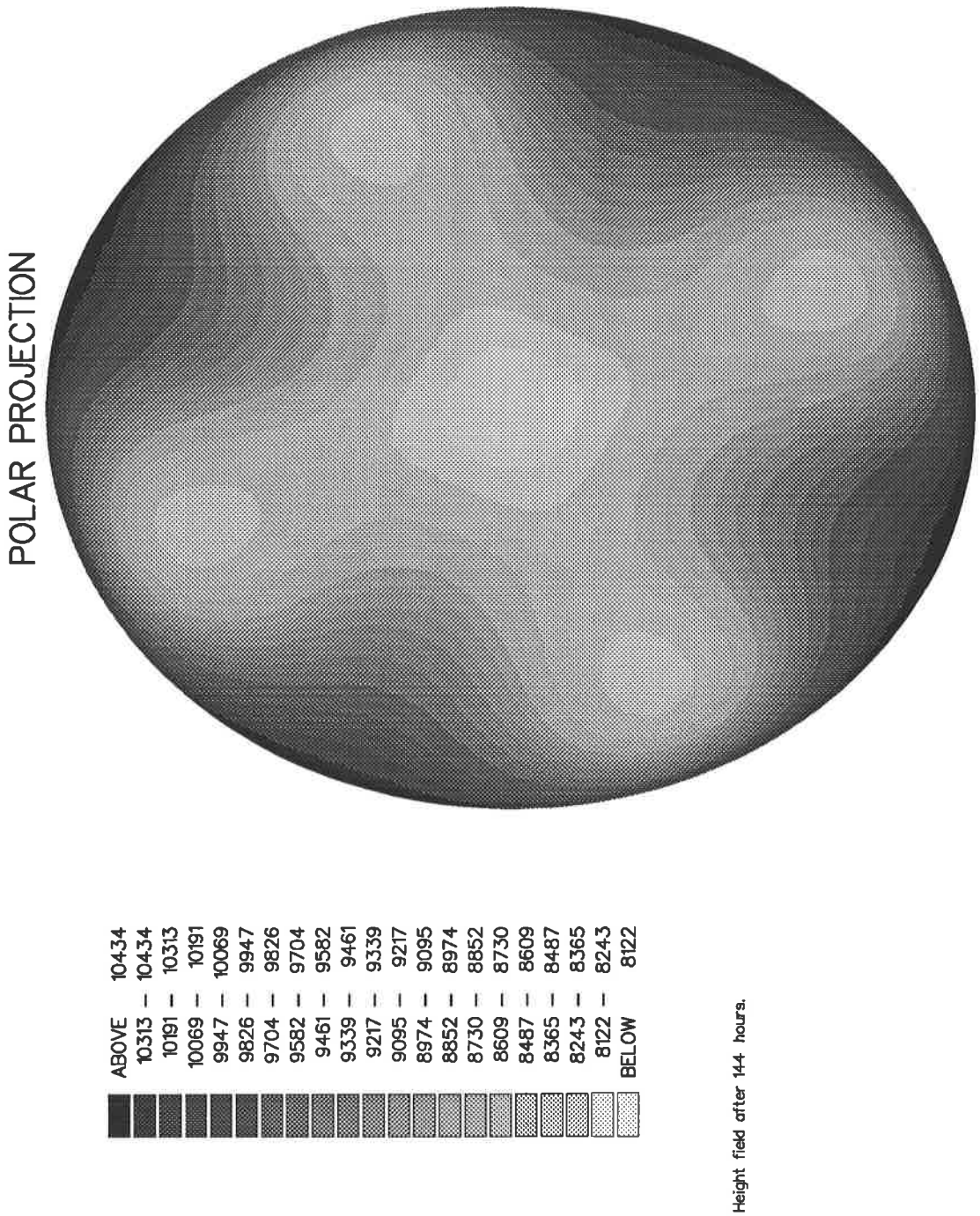

Figure 47: Polar projection of the height field on the 5^{th} grid after 6 days.

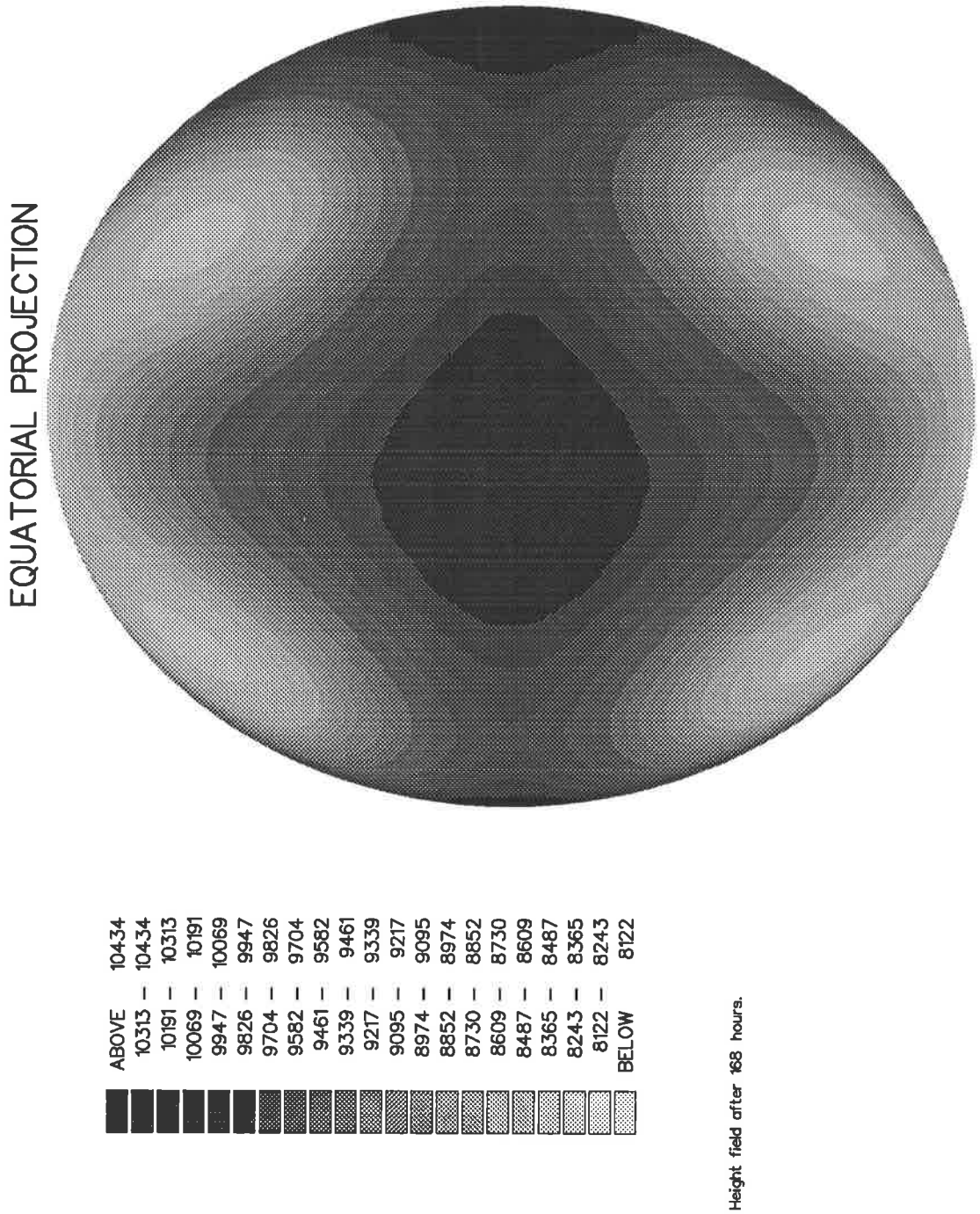

Figure 48: Equatorial projection of the height field on the 5^{th} grid after 7 days.

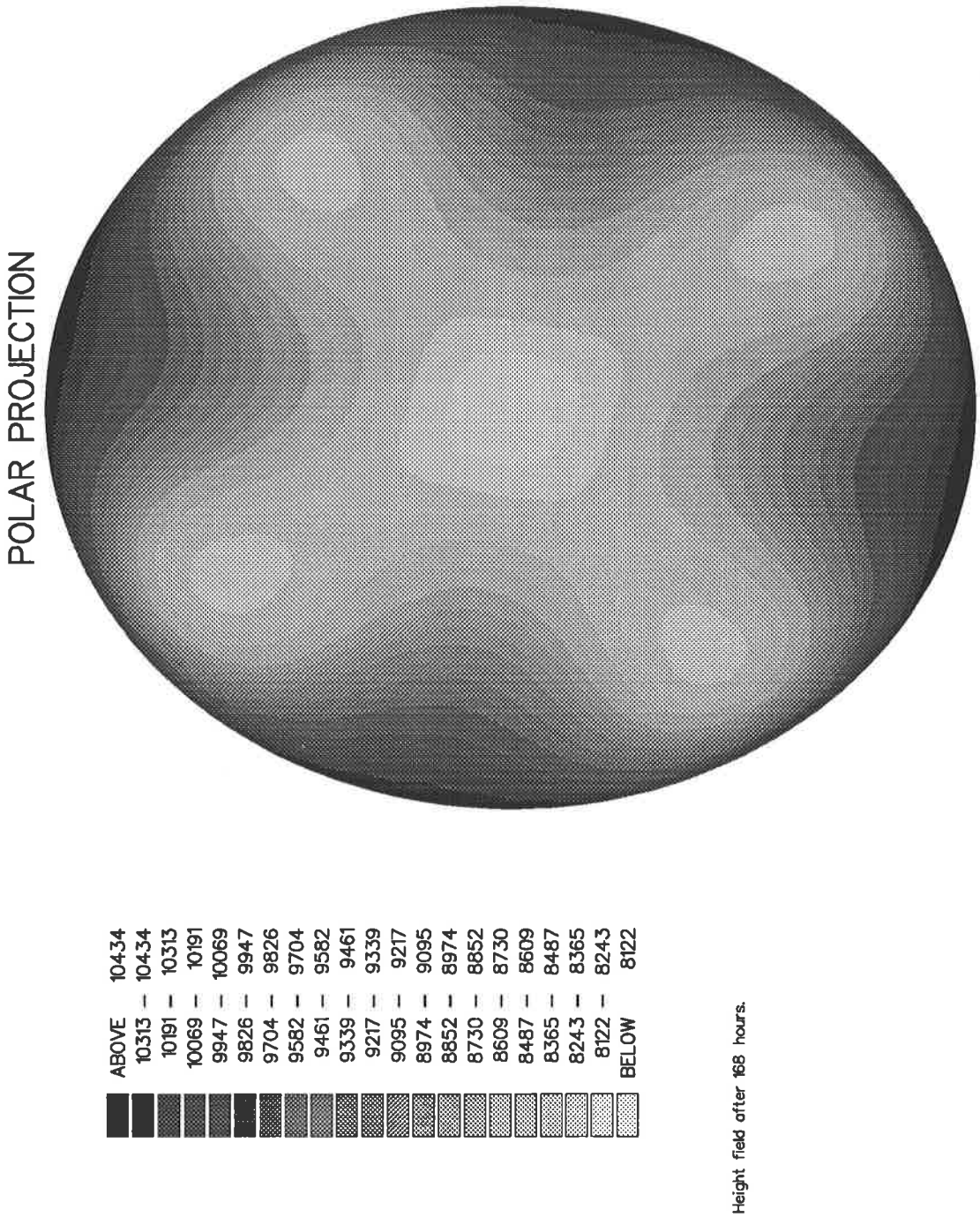

Figure 49: Polar projection of the height field on the 5^{th} grid after 7 days.